

AD-A100 751

TECHNICAL
LIBRARY

AD-A100 751

CONTRACT REPORT ARBRL-CR-00452

A TWO-DIMENSIONAL MODEL OF THE INTERIOR
BALLISTICS OF BAGGED ARTILLERY CHARGES

Prepared by

Paul Gough Associates, Inc.
P. O. Box 1614
Portsmouth, NH 03801

April 1981



US ARMY ARMAMENT RESEARCH AND DEVELOPMENT COMMAND
BALLISTIC RESEARCH LABORATORY
ABERDEEN PROVING GROUND, MARYLAND

Approved for public release; distribution unlimited.

DTIC QUALITY INSPECTED

Destroy this report when it is no longer needed.
Do not return it to the originator.

Secondary distribution of this report by originating
or sponsoring activity is prohibited.

Additional copies of this report may be obtained
from the National Technical Information Service,
U.S. Department of Commerce, Springfield, Virginia
22161.

The findings in this report are not to be construed as
an official Department of the Army position, unless
so designated by other authorized documents.

*The use of trade names or manufacturers' names in this report
does not constitute endorsement of any commercial product.*

REPORT DOCUMENTATION PAGE		READ INSTRUCTIONS BEFORE COMPLETING FORM
1. REPORT NUMBER CONTRACT REPORT ARBRL-CR-00452	2. GOVT ACCESSION NO.	3. RECIPIENT'S CATALOG NUMBER
4. TITLE (and Subtitle) A Two-Dimensional Model of the Interior Ballistics of Bagged Artillery Charges		5. TYPE OF REPORT & PERIOD COVERED Final Report June 1979 - January 1981
		6. PERFORMING ORG. REPORT NUMBER PGA-TR-81-1
7. AUTHOR(s) Paul S. Gough		8. CONTRACT OR GRANT NUMBER(s) DAAK11-79-C-0071
9. PERFORMING ORGANIZATION NAME AND ADDRESS Paul Gough Associates, Inc. P.O. Box 1614 Portsmouth, NH 03801		10. PROGRAM ELEMENT, PROJECT, TASK AREA & WORK UNIT NUMBERS
11. CONTROLLING OFFICE NAME AND ADDRESS U.S. Army Armament Research & Development Command U.S. Army Ballistic Research Laboratory ATTN: DRDAR-BLI Aberdeen Proving Ground, MD 21005		12. REPORT DATE April 1981
14. MONITORING AGENCY NAME & ADDRESS (if different from Controlling Office)		13. NUMBER OF PAGES 206
		15a. DECLASSIFICATION/DOWNGRADING SCHEDULE Unclassified
16. DISTRIBUTION STATEMENT (of this Report) Approved for public release; distribution unlimited.		
17. DISTRIBUTION STATEMENT (of the abstract entered in Block 20, if different from Report)		
18. SUPPLEMENTARY NOTES		
19. KEY WORDS (Continue on reverse side if necessary and identify by block number) Interior Ballistics TDNOVA Two-Phase Flow Solid Propellant Gun Flamespread Computer Code		
20. ABSTRACT (Continue on reverse side if necessary and identify by block number) A theoretical model is described for digital simulation of flamespreading and pressure wave propagation in a single bag artillery charge. The theory is based on a numerical solution of the balance equations for unsteady, two-dimensional, axisymmetric, heterogeneous, reacting, two-phase flow. Flamespreading through bag charges is known to be influenced strongly by details of the ullage which initially surrounds the bag and by the behavior of the bag material itself. Accordingly, an explicit representation is made of the region occupied by the		

UNCLASSIFIED

SECURITY CLASSIFICATION OF THIS PAGE(When Data Entered)

propelling charge at any time. The flow in the ullage, which surrounds the region occupied by the propellant, is represented as unsteady, inviscid and single-phase. The method of solution is illustrated by reference to the complete interior ballistic cycle of a top-tube 155-mm howitzer charge.

UNCLASSIFIED

SECURITY CLASSIFICATION OF THIS PAGE(When Data Entered)

Foreword

Technical cognizance for the subject contract
has been provided by Mr. A. W. Horst, Jr.
U. S. Army Ballistic Research Laboratory
DRDAR-BL

Summary

We describe a theoretical representation of flamespreading and pressure wave propagation in a single bag artillery charge. The theory is based on a numerical solution of the balance equations for unsteady, two-dimensional, axisymmetric, heterogeneous, reacting, two-phase flow. Flamespreading through bag charges is known to be influenced strongly by details of the ullage which initially surrounds the bag and by the behavior of the bag material itself. Accordingly, an explicit representation is made of the region occupied by the propelling charge at any time. The flow in the ullage, which surrounds the region occupied by the propellant, is represented as unsteady, inviscid and single-phase.

The ullage is divided into several disjoint regions, coupled to one another and to the two-phase flow in the propelling charge by means of finite jump conditions at all their mutual boundaries. By formulating the theory in such a manner as to use directly the jump conditions at the boundary of the bag, we provide a direct mechanism for the representation of the influence of the bag. Impermeability is reflected directly within the momentum jump condition as a quasi-steady flow loss. Similarly, the influence of exothermically reactive components, such as the basepad and centercore tube, and endothermically reactive components, such as the salt bag, are reflected by means of source terms in the mass and energy jump conditions.

The division of the ullage into several regions is based on the instantaneous configuration of the external boundaries, namely the breech, the tube, and the moving projectile, and of the configuration of the bag which predicates regions of ullage behind it, ahead of it, around it and within it. Each such region of ullage is treated as lumped parameter, quasi-one-dimensional, or as fully two-dimensional, in accordance with criteria based on its dimensions.

In addition to the representation of a basepad and centercore tube within the structure of the bag, the theory recognizes the influence of a centercore ignition charge, coaxial with the bag and moving with it, and which is represented as a quasi-one-dimensional two-phase flow. As with the ullage, the centercore is coupled to the state of the flow within the bag and, where applicable, the ullage at the ends of the chamber, by reference to finite jump conditions. The representation of the ignition train also admits the specification of an externally injected stimulus of predetermined flow rate and energy.

Each region of continuous flow properties is mapped onto a regular geometric figure, a line or a square, by means of a boundary fitted mesh transformation algorithm. The method of solution is based on an explicit two-step marching scheme which utilizes the characteristic forms of the balance equations at the external and the internal boundaries.

The method of solution is illustrated by reference to the complete interior ballistic cycle of a top zone 155mm howitzer charge. A fully two-dimensional representation of the propelling charge is maintained until flamespreading and rupture of the bag are complete. Subsequently, a quasi-two-dimensional representation is utilized which treats the propelling charge as a quasi-one-dimensional two-phase flow coupled to coaxial quasi-one-dimensional regions of radially distributed ullage and to lumped parameter regions of axially distributed ullage.

Table of Contents

	Page
Foreword	3
Summary	5
Table of Contents	7
List of Illustrations	11
1.0 INTRODUCTION	13
1.1 Background Information	13
1.2 Summary of Approach	18
2.0 GOVERNING EQUATIONS	28
2.1 Systems of Balance Equations	30
2.1.1 Two-Dimensional Two-Phase Flow	31
2.1.2 Quasi-One-Dimensional Two-Phase Flow	32
2.1.3 Two-Dimensional Single-Phase Flow	34
2.1.4 Quasi-One-Dimensional Single-Phase Flow	34
2.1.5 Lumped Parameter Single-Phase Flow	36
2.2 Constitutive Laws	36
2.2.1 Equation of State of Gas	37
2.2.2 Granular Stress Law	37
2.2.3 Propellant Form Functions	38
2.2.4 Interphase Drag	39
2.2.5 Interphase Heat Transfer	40
2.2.6 Solid Phase Surface Temperature	41
2.2.7 Ignition and Combustion	41
2.3 Initial and Boundary Conditions	43
2.3.1 External Boundary Conditions	43
2.3.2 Internal Boundary Conditions Between Regions of Ullage	44
2.3.3 Internal Boundary Conditions Involving the Mixture	48

Table of Contents (continued)

	Page
3.0 METHOD OF SOLUTION	56
3.1 The Equations in Computational Coordinates	57
3.1.1 Two-Dimensional Two-Phase Flow	59
3.1.2 Quasi-One-Dimensional Two-Phase Flow	61
3.1.3 Two-Dimensional Single-Phase Flow	62
3.1.4 Quasi-One-Dimensional Single-Phase Flow	63
3.2 Characteristic Forms of the Balance Equations	64
3.2.1 Two-Dimensional Two-Phase Flow	65
3.2.2 Quasi-One-Dimensional Two-Phase Flow	68
3.2.3 Two-Dimensional Single-Phase Flow	69
3.2.4 Quasi-One-Dimensional Single-Phase Flow	70
3.3 Discretization and Integration Algorithms	70
3.3.1 Integration at Interior Mesh Points	71
3.3.2 Integration at Boundary Points	74
3.3.2.1 The Solid-Phase	75
3.3.2.2 The Gas-Phase	79
3.3.3 Integration at Corner Points	81
3.3.3.1 Fully Attached Corner	82
3.3.3.2 Partially Separated Corner	82
3.3.3.3 Fully Separated Corner	83
3.3.4 Integration of the Quasi-Two-Dimensional Flow	84
3.4 Specification of Computational Mesh	85
3.4.1 Programming Strategy	85
3.4.1.1 Static Mesh Allocation Mode	86
3.4.1.2 Dynamic Mesh Allocation Mode	87
3.4.1.3 Transformation to Quasi-Two-Dimensional Representation	89
3.4.2 Mapping Algorithm	90

Table of Contents (continued)

	Page
3.5 Special Topics	92
3.5.1 Treatment of Tangential Velocity of Gas Entering Mixture	92
3.5.2 Treatment at Burnout	94
3.5.3 Treatment When Region Collapses	94
3.5.4 Ignition of Boundary Points	94
3.5.5 Boundary Values of Solid-Phase in Centercore Igniter	95
4.0 A COMPUTATIONAL EXAMPLE	96
4.1 Discussion of Input Data	96
4.2 Discussion of the Solution	110
References	138
Nomenclature	143
Appendix: TDNOVA--Structure and Use	147
Distribution List	201

List of Illustrations

Figure	Title	Page
1.1	Typical Bag Charge	16
1.2	Representation of Bag Charge by TDNOVA	20
1.3	Computational Regions Considered by TDNOVA	21
4.1.1	Representation of Computational Example (155mm M203)	97
4.2.1	Contours of Ignition Delay	115
4.2.2	Mesh at 0.0 msec	116
4.2.3	Mesh at 3.0 msec	116
4.2.4	Porosity at 0.0 msec	117
4.2.5	Porosity at 3.0 msec	117
4.2.6	Pressure at 0.2 msec	118
4.2.7	Pressure at 0.4 msec	118
4.2.8	Pressure at 0.6 msec	119
4.2.9	Pressure at 1.0 msec	119
4.2.10	Pressure at 1.6 msec	120
4.2.11	Pressure at 2.0 msec	120
4.2.12	Pressure at 2.8 msec	121
4.2.13	Pressure at 3.078 msec (Fully Two-Dimensional)	121
4.2.14	Pressure at 3.078 msec (Quasi-Two-Dimensional)	122
4.2.15	Pressure at 3.4 msec	122
4.2.16	Pressure at 10.0 msec	123
4.2.17	Pressure at 12.5 msec	123
4.2.18	Pressure at 16.519 msec (Muzzle Exit)	124
4.2.19	Velocity Field of Solid-Phase at 1.0 msec	124
4.2.20	Velocity Field of Solid-Phase at 2.0 msec	125
4.2.21	Velocity Field of Solid-Phase at 3.0 msec	125
4.2.22	Velocity Field of Gas-Phase at 1.0 msec	126
4.2.23	Velocity Field of Gas-Phase at 2.0 msec	126
4.2.24	Velocity Field of Gas-Phase at 3.0 msec	127

List of Illustrations (continued)

Figure	Title	Page
4.2.25	Density of Gas at 1.0 msec	127
4.2.26	Density of Gas at 2.0 msec	128
4.2.27	Density of Gas at 3.0 msec	128
4.2.28	Density of Gas at 4.0 msec	129
4.2.29	Contours of Gas-Phase Density at 1.0 msec	130
4.2.30	Contours of Gas-Phase Density at 2.0 msec	131
4.2.31	Contours of Gas-Phase Density at 3.0 msec	132
4.2.32	Temperature of Gas at 1.0 msec	133
4.2.33	Temperature of Gas at 2.0 msec	133
4.2.34	Temperature of Gas at 3.0 msec	134
4.2.35	Granular Stress at 1.0 msec	134
4.2.36	Granular Stress at 2.0 msec	135
4.2.37	Granular Stress at 3.0 msec	135
4.2.38	Surface Temperature of Solid-Phase at 1.0 msec	136
4.2.39	Surface Temperature of Solid-Phase at 2.0 msec	136
4.2.40	Surface Temperature of Solid-Phase at 3.0 msec	137

1.0 INTRODUCTION

We provide herein documentation of a digital computer program called TDNOVA which is under development for the purpose of permitting simulations of the interior ballistics of bag charges.

TDNOVA is based on a numerical solution of the balance equations which describe the macroscopic aspects of unsteady, two-dimensional two-phase reacting flow. The objective of the present work has been the development of the code to a point which permits a simulation of the complete interior ballistic cycle of a typical single bag artillery charge, taking into account the two-dimensional details of the gun chamber and projectile base, the distribution of ullage around the bag and the influence of the bag itself. A fully two-dimensional analysis of the propelling charge is maintained until flamespreading is complete and the bag is fully ruptured. Subsequently, following the establishment of radial mechanical equilibrium, the solution is continued to the point of muzzle exit by reference to a quasi-two-dimensional analysis.

This introduction contains two subsections. In section 1.1 we provide the reader with a brief summary of background material for the purpose of orientation. Section 1.2 contains a brief outline of the technical approach to our objectives and summarizes the capabilities and limitations of TDNOVA in its present form.

A complete discussion of the governing equations is given in chapter 2.0 and the method of solution is described in chapter 3.0. Chapter 4.0 presents a computational example. The code itself is documented in some detail in the appendix which describes the structure of the code and linkages of the subroutines. The appendix also contains a glossary of the principal Fortran variable names and a complete discussion of the input files.

1.1 Background Information

The work described herein is a continuation of a previous study¹ to which the reader is referred for a full discussion of background considerations. Here we simply summarize the nature of our interests.

First, with regard to interior ballistic phenomena as a whole, our interest may be described as focused on the process of flame-spreading as a hydrodynamic problem and on the influence of the path

¹Gough, P. S. "Two-Dimensional Convective Flamespreading in Packed Beds of Granular Propellant." Ballistic Research Laboratory Report ARBRL-CR-00404. July 1979 (AD #A075326)

of flamespreading on the longitudinal structure of the pressure field not only during ignition but throughout the entire interior ballistic cycle. This interest stems from the documented correlation between the existence of axial pressure waves and the incidence of gun malfunction due to overpressure² and from the experimental and theoretical evidence that the path of flamespreading can strongly influence the nature of such axial pressure waves³⁻⁹. Our investigations are not directed towards the a priori prediction of maximum gun pressure or muzzle velocity. Such an objective is precluded by the dependence of these quantities on such intractable and influential processes as heat loss and the law of resistance between the rotating band and the gun tube. Neither is our work directed towards an understanding of bore erosion and heat transfer to the gun tube, processes which require an analysis of boundary layer development and transport by diffusion.

Second, with regard to flamespreading itself, particular interest is directed towards the interplay of such elements of charge design as the venting characteristics of the ignition system, the initial distribution of free chamber volume around the charge and the impediment to flow associated with the bag material.

- ²Budka, A. J. and Knapton, J. D. "Pressure Wave Generation in Gun Systems--A Survey." Ballistic Research Laboratory Memorandum Report 2567.(AD#B008893L) 1975
- ³Kent, R. H. "Study of Ignition of 155-mm Gun." Ballistic Research Laboratory Report 22. (AD #494703) 1935
- ⁴Heddon, S. E. and Nance, G. A. "An Experimental Study of Pressure Waves in Gun Chambers." NPG Report 1534. 1957
- ⁵Horst, A. W., Jr. and Smith, T. C. "The Influence of Propelling Charge Configuration in Gun Environment Pressure-Time Anomalies." Proc. 12th JANNAF Combustion Meeting. 1975
- ⁶May, I. W., Clarke, E. V., and Hassmann, H. "A Case History: Gun Ignition Related Problems and Solutions for the XM-198 Howitzer." Ballistic Research Laboratory Interim Memorandum Report 150. 1973
- ⁷Rocchio, J., Ruth, C. and May, I. W. "Grain Geometry Effects on Wave Dynamics in Large Caliber Guns." Proc. 13th JANNAF Combustion Meeting. 1976
- ⁸Horst, A. W., Smith, T. C. and Mitchell, S. E. "Key Design Parameters in Controlling Gun-Environment Pressure Wave Phenomena--Theory versus Experiment." Proc. 13th JANNAF Combustion Meeting. 1976
- ⁹Horst, A. W. and Gough, P. S. "Influence of Propellant Packaging on Performance of Navy Case Gun Ammunition." J. Ballistics, v. 1, n. 3. 1977

To focus our discussion a little more precisely, we refer to figure 1.1, which displays a typical 155-mm bag charge of the sort with which we are presently concerned.

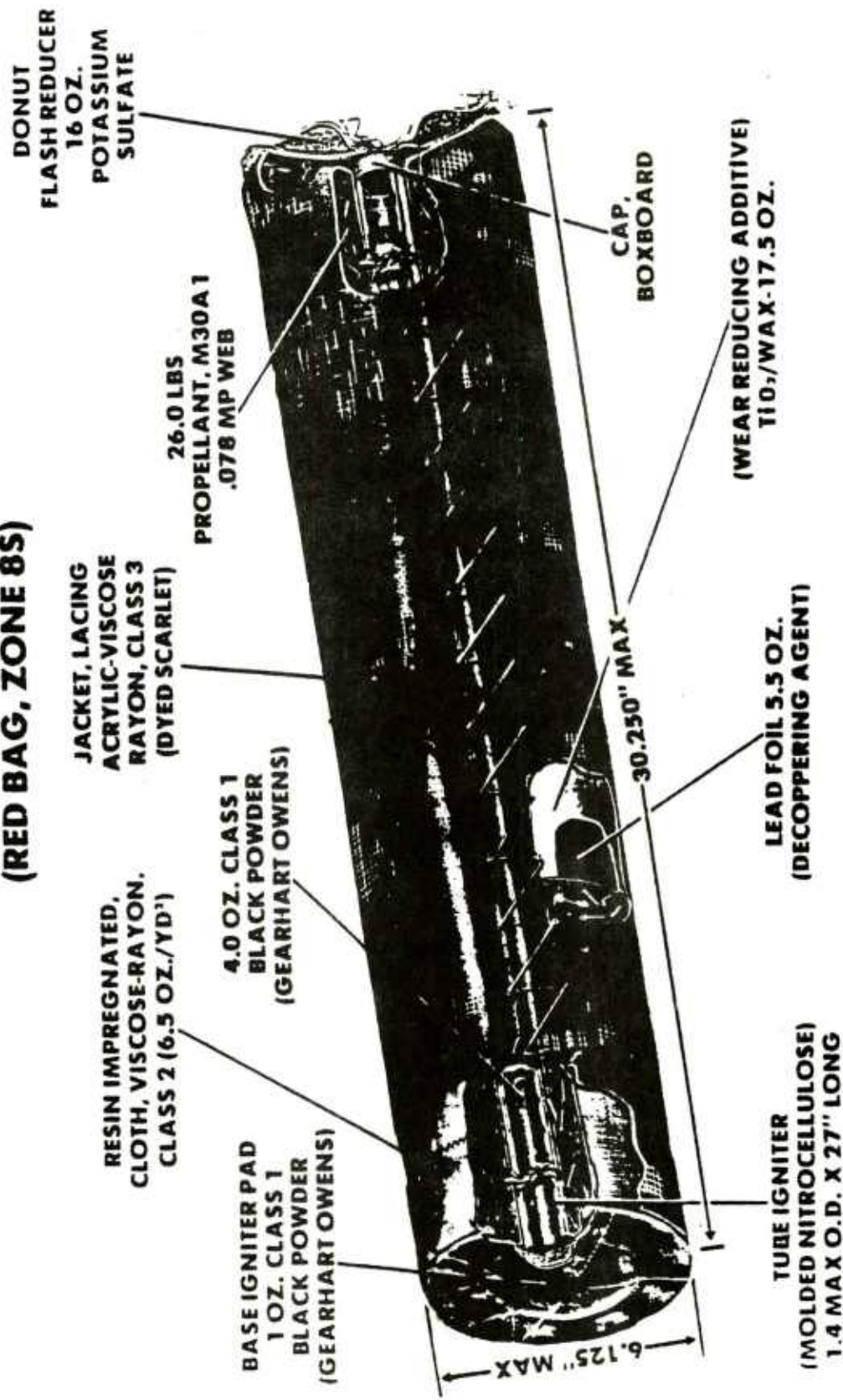
The charge is approximately 80 cm in length whereas the available length of the gun chamber is greater by approximately 10 cm, the precise figure depending on the projectile design and the state of wear of the tube. The charge is also undersized with respect to the transverse dimensions of the chamber. Its diameter of 15 cm may be contrasted with the typical values, for the tube, of 17 cm at the breech and 15.5 cm at the mouth of the tapered chamber. The free chamber volume created by the undersized dimensions of the bag is referred to as ullage, in general; we will distinguish here between axial ullage which bounds the endwalls of the bag and radial or circumferential ullage which bounds the sidewalls of the bag.

The bag is seen to be complex. In addition to providing a package for the granular propellant, the bag incorporates several components designed to minimize undesirable side effects of the propulsion cycle. Talc is included to reduce the rate of wear of the tube by thermal erosion. A lead foil is wrapped around the forward two-thirds of the sidewall. Its purpose is to reduce the rate of copper build-up on the rifling of the tube due to mechanical erosion of the projectile rotating band. An irregularly formed bag of potassium sulfate is sewn to the forward endwall. Its purpose is to reduce the likelihood of secondary flash when the fuel-rich combustion gases are vented into the atmosphere following the discharge of the projectile.

The bag also incorporates components whose purpose is to control the ignition of the charge. A basepad of black powder is sewn to the rear endwall. It overlaps part of the propelling charge and covers the rear of a centercore tube, composed of nitrocellulose, and into which is inserted a cloth tube containing black powder and extending approximately two-thirds of the length of the charge. The intended ignition sequence is as follows. A jet is discharged from a primer located in the breechblock. The jet is intended to ignite the basepad. This in turn is intended to ignite the centercore. When the centercore is burning over its length, a predominantly radial convection is established in the propelling charge which is then ignited more or less uniformly with respect to its length.

This putative sequence may be defeated in practice by the flow of gas from the basepad directly into the charge, establishing a flamespreading path which competes with that in the centercore tube. Gas will also flow around the charge and, depending on the permeability of the bag, may induce ignition near the sidewalls or even

CHARGE, PROPELLING, 155MM, M203 (RED BAG, ZONE 8S)



PM-CAWS-AM
JAN 1979

Figure 1.1 Typical Bag Charge

flow into the forward end of the charge, creating a rearward moving flame. It is in this sense that the interplay between ullage, bag and ignition system is of concern in the present investigation.

Evidently, the theoretical analysis of this interplay requires a consideration of multi-dimensional aspects of the two-phase flow consisting of the combustion gases and the granular propellant. Several models have been proposed in the past decade to consider flamespreading from a one-dimensional point of view¹⁰⁻¹⁴. Fisher¹⁵⁻¹⁸ has provided models of medium caliber weapons which have incorporated

-
- ¹⁰ East, J. L. and McClure, D. R. "Projectile Motion Predicted by a Solid/Gas Flow Interior Ballistic Model." Proc. 10th JANNAF Combustion Meeting 1973
- ¹¹ Krier, H., van Tassel, W. F., Rajan, S. and Vershaw, J. "Model of Flame Spreading and Combustion Through Packed Bed of Propellant Grains." Tech. Rept. AAE74-1, University of Illinois at Urbana-Champaign. 1974
- ¹² Kuo, K. K., Koo, J. H., Davis, T. R. and Coates, G. R. "Transient Combustion in Mobile, Gas-Permeable Propellants." Acta Astron., v. 3, n. 7-8, pp. 574-591. 1976
- ¹³ Gough, P. S. and Zwarts, F. J. "Theoretical Model for Ignition of Gun Propellant." Final Report, Part II, Contract N00174-72-C-0223 1972
- ¹⁴ Gough, P. S. "The NOVA Code: A User's Manual." Final Report, Task I, Contract N00174-79-C-0082. 1979
- ¹⁵ Fisher, E. B. and Graves, K. W. "Mathematical Model of Double Base Propellant Ignition and Combustion in the 81-mm Mortar." CAL Report No. DG-3029-D-1. 1972
- ¹⁶ Fisher, E. B. and Trippe, A. P. "A Mathematical Model of Center Core Ignition in the 175-mm Gun." Calspan Report No. VQ-5163-D-2. 1974
- ¹⁷ Fisher, E. B. "Propellant Ignition and Combustion in the 105-mm Howitzer." Calspan Report No. VQ-5524-D-1. 1975
- ¹⁸ Fisher, E. B. and Trippe, A. P. "Development of a Basis for Acceptance of Continuously Produced Propellant." Calspan Report No. VQ-5163-D-1. 1973

multi-dimensional features to a certain extent. The importance of the distribution of ullage in bag charges has been demonstrated by Gough¹⁹ using a quasi-two-dimensional model and further established by Horst and Gough²⁰ using a refinement of the earlier model. Our previous study¹ provided a basis for the development of a fully two-dimensional model by establishing a computational approach and demonstrating the feasibility of obtaining solutions to the problem of convective flamespreading in a two-dimensional packed bed bounded by an irregularly formed container.

1.2 Summary of Approach

As in the preceding section we abstract much of our discussion of our approach to the analysis of flamespreading through bag charges from our previous study¹.

The problem to be studied may be defined in general terms as involving the multi-dimensional, unsteady flow of a heterogeneous mixture consisting of the granular aggregate and its products of combustion. The analysis of such a flow taking into account details whose length scale is comparable to the scale of heterogeneity is not practical at the present time. A tractable theory can be established by reference to governing equations for the macroscopic details of the flow, equations based on averages of the microscopic state variables over a region large enough to contain many grains.

The formal development of such equations and their mathematical structure are discussed elsewhere^{21, 22, 23}. Within the framework of a macroscopic model the hydrodynamic aspects of flamespreading through a bag charge assume the following characteristics. The problem can be identified as one in which embedded discontinuities are present. These

¹⁹ Gough, P. S. "Theoretical Study of Two-Phase Flow Associated with Granular Bag Charges." Final Report, Contract DAAK11-77-C-0028. 1978

²⁰ Horst, A. W. and Gough, P.S. "Modeling Ignition and Flame-spread Phenomena in Bagged Artillery Charges." Ballistic Research Laboratory Technical Report ARBRL-TR-02263. (AD #A091790) 1980

²¹ Gough, P. S. "The Flow of a Compressible Gas Through an Aggregate of Mobile, Reacting Particles." Ph.D. Thesis, McGill University. 1974

²² Gough, P. S. and Zwarts, F. J. "Modeling Heterogeneous Two-Phase Reacting Flow." AIAA J. v. 17, n. 1, pp. 17-25. 1979

²³ Gough, P. S. "On the Closure and Character of the Balance Equations for Heterogeneous Two-Phase Flow." Dynamics and Modelling of Reactive Systems, Academic Press. 1980

discontinuities are associated with the transition of the macroscopic field variable defined by the fraction of a unit volume occupied by the gas phase--the porosity--from the value unity in the regions of ullage to a value typical of the packed bed over a length scale comparable to the scale of heterogeneity. Still within this macroscopic perspective we see the properties of the bag, including flow resistance and both exothermically reactive components, like the centercore tube and the basepad, and endothermically reactive components, like the salt bag, as having the character of surface phenomena.

Our approach may therefore be summarized as one in which the equations of macroscopic two-phase flow are solved on a time-dependent domain defined by the instantaneous configuration of the propelling charge. These equations are solved, simultaneously with balance equations for the single-phase flow in the ullage, subject to the external boundary conditions defined by the fixed tube and the moving projectile, viewed as rigid, impermeable surfaces, and subject to macroscopic jump conditions which relate the state variables on each side of the internal boundary defined by the surface of the propelling charge. Motion of the bag independently of the surface of the propelling charge is not considered. In the present model the bag is viewed as an attribute of the surface of the propelling charge. The finite boundary conditions are similar to the Rankine-Hugoniot equations which apply at a shock discontinuity in a single-phase flow. Differences arise, however, due to the presence of the source terms which reflect the addition or loss of mass, momentum and energy at the boundary of the charge as a consequence of the flow resistance and the reactive components of the bag.

Although the flow is actually three-dimensional we suppose that an adequate description of the influence of the ullage may be obtained by treating the problem as though it were two-dimensional and axisymmetric. The conceptual representation of the bag charge of figure 1.1 is presented in figure 1.2.

The computational approach may be summarized as follows. The physical domain on which the solution is to be obtained is defined by the tube, the breechblock and the base of the projectile. As shown in figure 1.3, this physical domain is broken up into several computational domains in each of which the state variables are assumed to vary sufficiently smoothly as to justify a solution by the method of finite differences. The first such region is that defined by the propelling charge itself. Four additional regions are defined by the regions of ullage, and the centercore igniter, which are contiguous with each of the four bounding surfaces of the bag. These regions are defined by projecting each side of the bag onto its respective

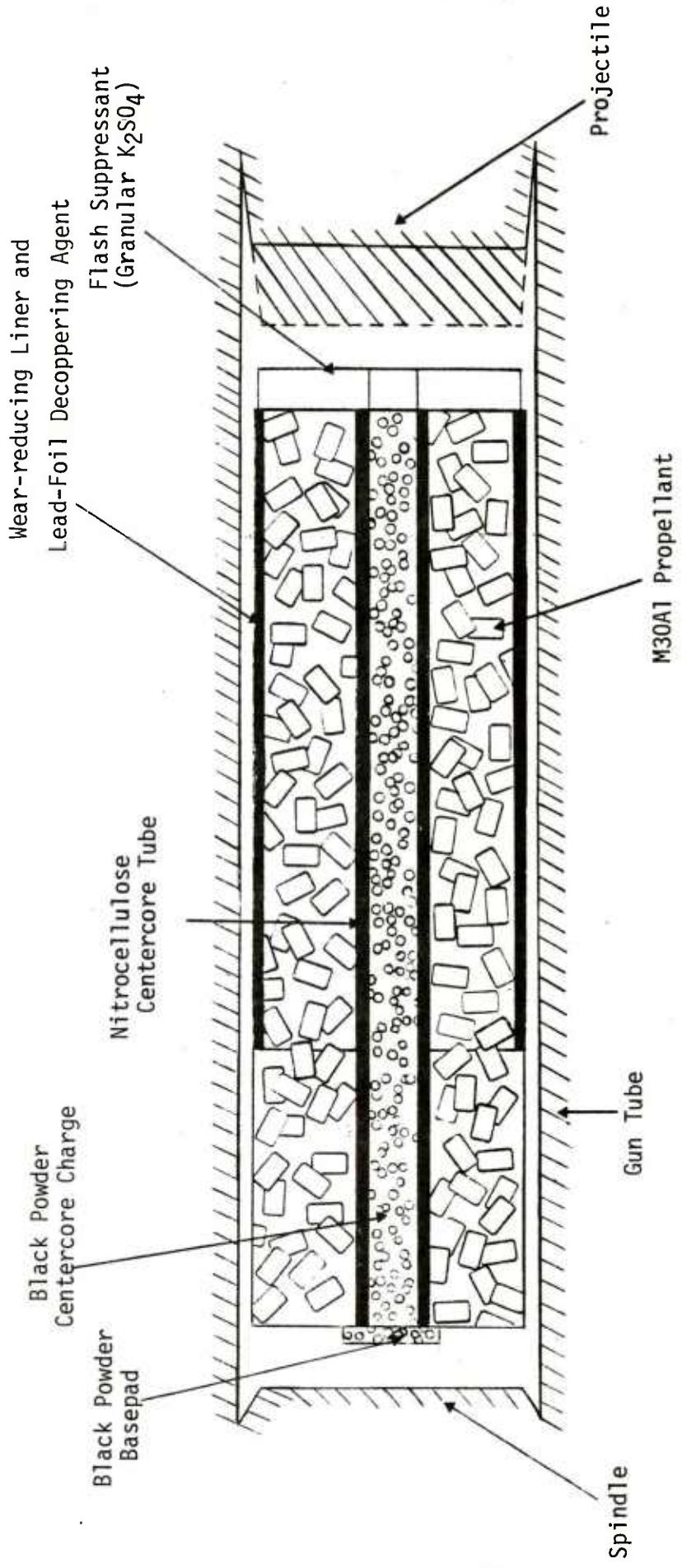


Figure 1.2 Representation of Bag Charge by TDNOVA

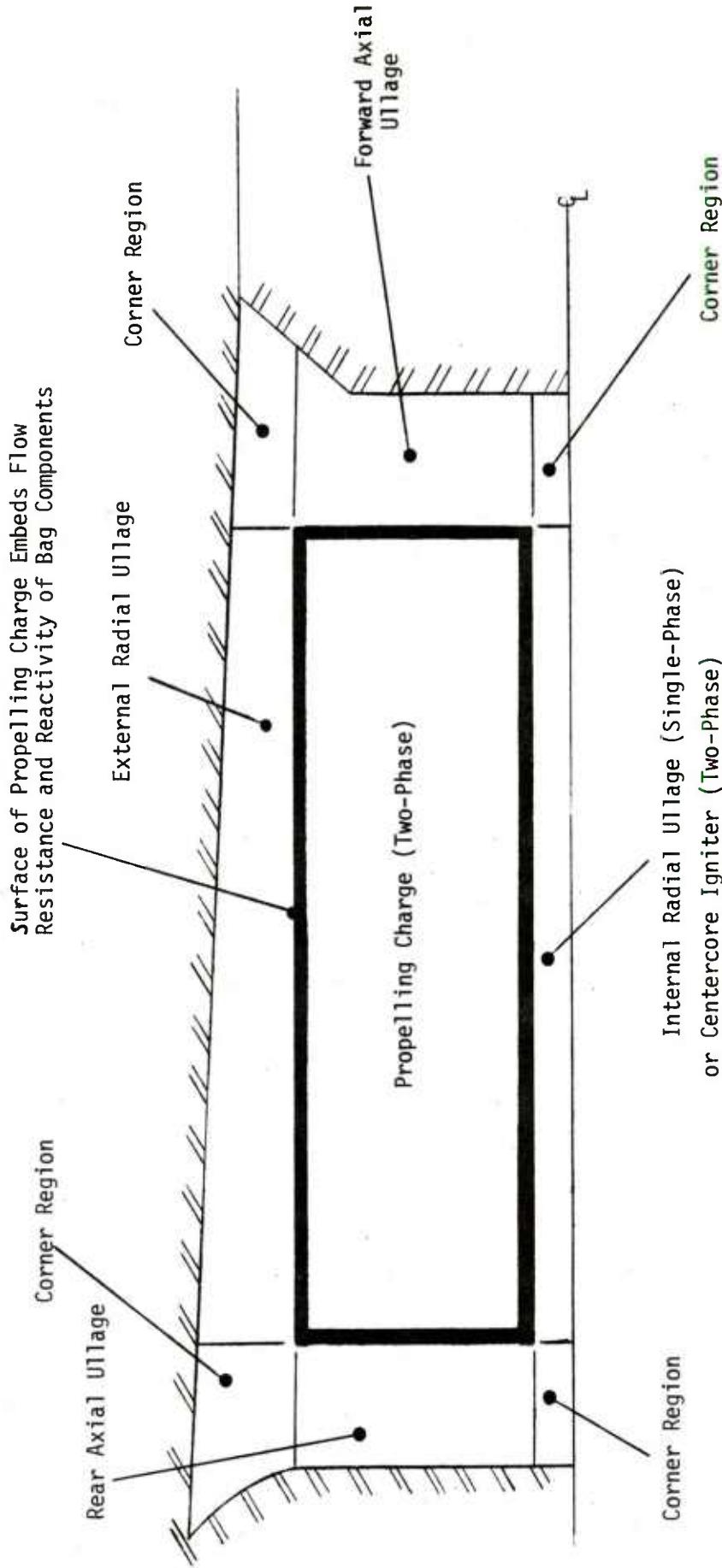


Figure 1.3 Computational Regions Considered by TDNOVA

counterpart on the external boundary, the centerline of the tube being considered an external boundary for this purpose. With this convention there are defined an additional four regions of flow, namely those in the corners of the physical domain, each of which is bounded on two sides by regions of ullage contiguous with the bag, or by the centercore, and on the two remaining sides by the external boundaries of the flow.

Two distinct modeling approaches are included in TDNOVA. Initially, and throughout the period of flamespreading and bag rupture, a fully-two-dimensional analysis is conducted. Subsequent to the completion of flamespreading and rupture of the bag, the radial structure of the pressure field is monitored until it is found to be uniform to within a user-selectable tolerance at each axial location in the chamber. When this occurs a quasi-two-dimensional approach is introduced and is used to continue the solution throughout the remainder of the interior ballistic cycle.

In regard to the fully-two-dimensional approach the user may select between two alternative methods of representation of the ullage. In both of these cases the propelling charge is treated as a fully two-dimensional two-phase flow and the centercore igniter, if present, is treated as a quasi-one-dimensional two-phase flow. In the first case, referred to as the static mesh allocation mode, the regions of ullage contiguous with each of the bounding surfaces of the bag--sidewalls and endwalls--are treated as quasi-one-dimensional, the continuum coordinate being defined by the boundary of the bag with which each region of ullage is contiguous. The corner regions of ullage are treated as lumped parameter. In the second case, referred to as the dynamic mesh allocation mode, the regions of ullage contiguous with the bag may be treated as either quasi-one-dimensional or as fully-two-dimensional in accordance with their dimensions normal to the bag boundaries. The representation of the corner regions depends on the representations of the regions of ullage with which they are contiguous. A corner region is treated as lumped parameter if it is contiguous with quasi-one-dimensional flows on two sides, as quasi-one-dimensional if it is bounded on one side by a quasi-one-dimensional flow and by a two-dimensional flow on the other, and as fully-two-dimensional when it is bounded by two-dimensional regions of ullage on both sides.

Each computational region is always mapped onto a regular figure for the purpose of defining the distribution of mesh points. Two-dimensional regions are mapped onto a unit square and one-dimensional regions are mapped onto a unit line.

An explicit finite difference scheme is used to integrate the equations of motion in each region. By explicit we mean a scheme in

which all spacewise partial derivatives are represented according to differences of values in current storage. Some implicitness, that is to say evaluation according to future level data, is introduced in respect to certain of the non-homogeneous terms, particularly the interphase drag, for the purpose of ensuring stability without unduly constraining the time step. Characteristic forms of the equations are used at all boundaries, internal and external.

The quasi-two-dimensional approach is intended to provide an economical determination of the flow following the disappearance of radial pressure gradients. In this approach, the propelling charge is treated as quasi-one-dimensional. The ullage surrounding the circumference of the charge is also quasi-one-dimensional as is that internal to the charge, if the centercore is not considered. As we have already noted, the centercore ignition charge, if present, is always treated as a quasi-one-dimensional flow.

The axial ullage at each end of the propelling charge is treated as lumped parameter in the quasi-two-dimensional approach. The radial motion of the inner and outer circumferential boundaries of the propelling charge is determined from considerations of drag associated with radial transport of gas between the coaxial one-dimensional flows and of the requirement that granular stresses satisfy certain conditions of transverse equilibrium.

The status of the program is as follows. Both the static and dynamic mesh allocation modes of the fully two-dimensional approach have been completely encoded and tested for correct linkages. However, only the static mesh allocation mode, in which the ullage contiguous with the bag is treated as quasi-one-dimensional, has been carried through a complete flamespreading calculation. The quasi-two-dimensional approach has been completely encoded, checked and used to carry the solution, obtained through flamespreading by the static two-dimensional approach, to the point of discharge of the projectile from the muzzle of the gun.

We conclude this introduction by commenting on certain of the difficulties encountered during the performance of this work and the steps taken to overcome them. We also point out some of the limitations of the code that the potential user should keep in mind.

Numerical difficulties were encountered during the development of the code in situations involving the transport of gas from a region of ullage into the mixture. The simplest transport conditions that one may propose are based on the finite jump conditions for heterogeneous two-phase flow. By analogy with the corresponding conditions for an oblique shock, the assumption that there is no loss or

gain of momentum in the macroscopically infinitesimal transition layer which separates the exterior flow from the flow interior to the mixture leads to the conclusion that the tangential component of velocity of the gas-phase is transported without alteration. In circumstances where the tangential velocity in the ullage is very much larger than that in the mixture, the imposition of a boundary value which is incompatible with the state of the interior of the mixture places a considerable strain on the numerical method whose validity depends on sufficient smoothness of the data as to justify the approximation of derivatives by finite differences.

A closer examination of the process of transport from the ullage to the mixture reveals the following characteristics. If the gas is assumed to be transported without change in the tangential velocity component it finds itself, following transport, having a velocity which is considerably different from the value which can be supported in the mixture. Under most circumstances the inertial and convective contributions to the gas-phase momentum equation in the mixture are small by comparison with the pressure gradient and flow resistance terms. Accordingly, the gas-phase momentum equation may be thought of as expressing, to a first approximation, a balance between pressure gradient and flow resistance or interphase drag. Thus, following transport, the velocity of the gas rapidly decays to a value typical of the equilibrium between pressure gradient and drag. The rate of damping is extremely high. It is found that the tangential velocity decays to a value close to equilibrium during the interval of time required for the normal transport of the gas over a fraction of a diameter of a grain.

This picture of the normal transport of gas from the ullage into the mixture creates the image of a velocity profile which has a boundary layer type of structure. The tangential velocity in the mixture is comparable to that in the ullage only in a thin layer near the interface and this layer is so thin as to lie outside the resolving power of the balance equations themselves which are only validly applied to features of the flow which are characterized by length scales greater than the scale of heterogeneity.

We have developed our response to this problem by modifying the physical formulation of the conditions of transfer at the interface. Certainly, a numerical algorithm can be developed to capture the structure of the tangential velocity field as we have described it in the preceding paragraphs. However, it is the case that the governing equations themselves are incompetent to describe this level of structure of the flow so that the refinement of the method of solution to accommodate such a structure is, in our view, an exercise in self-deception.

Since the tangential velocity approaches an equilibrium value in a layer which is sub-scale-of-heterogeneity, we modify the jump conditions to incorporate a loss of tangential momentum. At the present time such a formulation must necessarily incorporate some essentially ad hoc or speculative features. We deduce the momentum loss by obtaining an approximate integral of the equation of motion of the gas-phase during normal transport over a layer equal in thickness to the initial diameter of a propellant grain. It is not thought that the solutions so generated will be especially sensitive to the details of this approach, at least at the macroscopic level. It will, however, be useful in future work to confirm this assumption by performing calculations in which the layer thickness is varied with respect to the current value and noting the influence of this variation on the path of flamespreading and the structure of the pressure field.

A second numerical difficulty is closely related to the first. The constitutive laws for the granular aggregate treat it as a quasi-fluid with no resistance to shear deformation under any circumstances and with non-zero normal stress due to intergranular forces only when the aggregate is sufficiently packed. The lack of resistance to shear deformation can result in significant distortion of the aggregate near the boundaries if the interphase drag on the boundary is significantly different from that in the interior of the aggregate. With the use of a loss in the tangential component of the gas-phase momentum, this difficulty is also circumvented, at least in the limited computational studies performed to date. However, the use of discontinuously distributed reactive components in the specification of the properties of the bag can introduce sufficient convection on the boundary of the aggregate as to introduce a significant and highly localized degree of deformation. An obvious remedy to such a difficulty is to require that the user specify the distribution of reactivity of the bag so as to satisfy conditions of smoothness. We have chosen, however, to address this problem by incorporating into the method of solution a crude expression of the inability of the aggregate to exhibit significant shear over a length scale less than the typical dimensions of a grain. The tangential component of velocity of the solid-phase at a boundary mesh point is taken to be equal to that of its neighbor in the interior rather than being deduced from the local equation of motion.

It is thought that the increase in utilitarian value of having the code accept discontinuously distributed reactive components is worth the loss in accuracy associated with the determination of the tangential component of velocity of the solid-phase. The present approach can be interpreted physically as an expression of the requirement that the shear deformation vanish at the surface. A more satisfactory approach, deferred for future work, would be to modify the

constitutive law for the granular aggregate, possibly to reflect the macroscopic shear modulus, and certainly to filter out deformations which are sub-scale-of-heterogeneity.

We turn now to some comments on the limitations of the code as presently formulated. First, the user should continually bear in mind the limitation of the code to the description of macroscopic details of the flow. The computational difficulties we have described above have been circumvented by the deliberate introduction of procedures to filter out details of the numerical solution which are, in our view, outside the resolving power of the equations. From this perspective, any of the predicted details of the radial structure of the flow should be regarded with some caution as the radial dimensions of the tube are not much larger than the scale of heterogeneity of the mixture.

In respect to the details of the base of the projectile it should be noted that the radial gap between the boattail and the tube is particularly small in most cases involving howitzer charges. In fact, the space may be smaller than the typical dimensions of a grain so that intrusion of the granular aggregate into the space around the boattail while admissible by the treatment of the aggregate as a quasi-fluid, may not be realizable in practice.

With regard to the treatment of regions of ullage according to a quasi-one-dimensional formulation it should be kept in mind that details of the modeled velocity component are only described with any accuracy when the cross-sectional area varies slowly with respect to the non-trivial spatial coordinate and, moreover, when the curvature of the flow channel is small.

On the other hand, the use of a fully-two-dimensional treatment of the ullage according to the inviscid equations may not necessarily offer any real improvement. Indeed, such solutions may not be as good as the quasi-one-dimensional solutions. Certain details of the two-dimensional flow may be inherently outside the scope of the inviscid flow equations due to the presence of shear layers and shocks in the vicinity of the corners of the mixture and the potential for flow separation at the corners of the projectile base. To obtain significantly better results than those offered by the quasi-one-dimensional treatment will require that the Navier-Stokes equations be solved in the ullage. But the determination of such solutions in the neighborhood of the reacting mixture raises formidable theoretical obstacles in respect to either the formulation of boundary conditions at the mixture interface or the continuation of the turbulence laws into the region occupied by the mixture. Even granting the satisfactory hurdling of these obstacles, there remain the facts that the distribution of ullage is three-dimensional, since the bag initially rests against the

bottom of the tube rather than being located axisymmetrically, and that the bag material is blown away from the propellant, following rupture, so that the detailed analysis of the flow in the ullage must somehow account for the influence of the bag components.

It should be kept in mind that at present no account is taken of the independent motion of the bag. It is, at all times, an attribute of the surface of the propelling charge and its influence is felt in terms of flow resistance, of mechanical constraint and of mass production due to reactive substrates.

Finally, we comment on the treatment of the centercore igniter. The igniter, which normally consists of black powder, is modeled as a quasi-one-dimensional two-phase flow. This model admits the simulation of flamespreading through the igniter as driven by a convective thermal stimulus. However, it is known that²⁴, at low pressure, at least, flamespreading in black powder is strongly influenced by the discharge of hot molten salts which, traveling from an ignited grain to a neighboring inert grain, may represent the principal thermal stimulus. Such a process is not modeled in the code at present. Thus, a priori calculations of flamespreading through the black powder cannot yet be performed.

The user should understand that our motive in treating the black powder as a two-phase continuum is presently based solely on the desire to capture the resistance to flow through the centercore since this represents a potentially important path for the equilibration of longitudinal pressure gradients.

We also note that the centercore tube is presently treated as rigid until locally ruptured and that the rupture pressure is assumed to be the same for bursting as for crushing.

²⁴Williams, F. A. "The Role of Black Powder in Propelling Charges." Picatinny Arsenal Technical Report 4770. 1975

2.0 GOVERNING EQUATIONS

The analytical approach described in chapter 1.0 may be summarized as follows. The propelling charge is always represented as a two-phase, reacting, heterogeneous mixture. Initially, the propelling charge is described by fully two-dimensional, axisymmetric, balance equations. Such a representation is expected to be continued at least until flamespreading and bag rupture are complete. Subsequently, a quasi-one-dimensional representation, which retains explicitly only the axial structure of the flow, may be sufficient to continue the analysis to the point of muzzle exit. In both cases we require constitutive laws, not only to describe the state of each phase but also to characterize certain of the microscopic interactions between them.

The ullage which is defined by the external boundaries--breech, tube, centerline and projectile base--and by the boundaries of the propelling charge, is always represented as containing an inviscid single-phase flow. The ullage is subdivided into several regions. The representation of each such region may be lumped parameter, quasi-one-dimensional or fully two-dimensional. Only the equation of state of the gas is required to support these balance equations.

The ignition train may be represented as comprising several elements--a basepad, a centercore tube, a centercore charge and an external stimulus. The external stimulus is represented as predetermined and is defined by tabular data. The contents of the centercore ignition charge, however, are represented as a quasi-one-dimensional two-phase flow which requires balance and constitutive equations similar to those of the propelling charge.

The basepad and centercore tube, when present, are represented as attributes of the bag which in turn are assumed to be amenable to description within the boundary conditions which couple the flow within the propelling charge to that in each of the contiguous regions of ullage.

Internal boundary conditions are also required to describe the coupling of regions of ullage to one another at their mutual interfaces. External boundary conditions, reflecting the impermeability of the breech, tube and projectile base are required, together with the equation of motion of the projectile. Finally, of course, one requires a statement of the initial conditions.

The order of presentation of these governing equations is as follows. In section 2.1 we summarize all the balance equations for the various types of flow, noting the circumstances in which they are to be used. In section 2.2 we summarize the constitutive laws which govern the state of each of the phases as well as those which govern certain microscopic interactions between them. In section 2.3 we discuss the initial and boundary conditions. The discussion of the behavior of the bag, including the influence of reactive components, is also addressed in section 2.3.

2.1 Systems of Balance Equations

We first state the fully two-dimensional equations of two-phase flow and subsequently the quasi-one-dimensional equations. The balance equations for two-phase flow are derived elsewhere according to both formal averaging techniques^{22,23} and, in the case of quasi-one-dimensional flow, according to a more intuitive control volume approach²⁵. In both cases we state the balance equations for each of the two phases. However, as the solid phase is assumed to consist of individually incompressible, but deformable grains, an energy balance is required only for the gas phase. The balance equations have the formal interpretation as governing equations for macroscopic properties of each of the phases, the state variables being understood to represent averages formed over a region which is large compared with the scale of heterogeneity. As in all our previous work, the complex boundary layer phenomena--drag, heat transfer, combustion rate--all appear as nonhomogeneous terms or algebraic entities in the balance equations. Closure requires that these complex microscopic interactions be related to the macroscopic variables in some fashion. In the present work we assume that such relationships are furnished as empirical correlations as discussed in section 2.2.

The quasi-one-dimensional formulation of the two-phase flow equations contains a provision for transverse mass exchange with neighboring regions. Both the quasi-one-dimensional and the two-dimensional systems incorporate a source term to reflect an ignition stimulus. However, heat loss to the gun tube is neglected and the stress tensor is taken to be isotropic for both species so that resistance to shearing is not considered for either the gas or the solid phase.

We assume the single phase continuum flow to be inviscid and non-heat conducting. However, we do retain the source terms which may embed either an ignition stimulus or transverse mass transfer from a neighboring region.

The statements of the balance equations given in the present section are based on cylindrical coordinates, except in the case of quasi-one-dimensional single-phase flow. It should be noted that the method of solution is based on a curvilinear coordinate scheme in which the region boundaries are characterized by a constant value of one of the curvilinear coordinates. The computational form of the equations is given in chapter 3.0.

²⁵Gough, P. S. "Modeling of Two-Phase Flow in Guns"
Progress in Astronautics and Aeronautics v. 66,
edited by H. Krier and M. Summerfield. 1979

2.1.1 Two-Dimensional Two-Phase Flow

These equations are used to describe the flow within the region occupied by the granular propellant at least until flame-spreading and bag rupture are complete.

In cylindrical coordinates such that z is the axial coordinate, r is the radial coordinate and t is the time, the balance equations take the forms:

Balance of Mass of Gas Phase

$$\frac{D\varepsilon\rho}{Dt} + \varepsilon\rho \left[\frac{\partial u}{\partial z} + \frac{\partial v}{\partial r} \right] = \dot{m} + \psi - \frac{\varepsilon\rho v}{r} \quad 2.1.1.1$$

The notation conforms with that used previously¹. We have ρ , the density of the gas, ε the porosity, u and v the z - and r - components of gas phase velocity, D/Dt the convective derivative along the gas phase streamline, ψ the source term associated with a stimulus, \dot{m} the rate of production of gas due to combustion of the solid phase.

We recall:

$$\frac{D}{Dt} \equiv \frac{\partial}{\partial t} + u \frac{\partial}{\partial z} + v \frac{\partial}{\partial r} \quad 2.1.1.2$$

$$\dot{m} = (1 - \varepsilon) \frac{s_p}{V_p} \dot{d}\rho_p = s_p \dot{d}\rho_p \quad 2.1.1.3$$

Here s_p , V_p are the surface area and volume of an individual grain and d is the rate of surface regression. We have introduced s_p as the surface area per unit volume.

Balance of Momentum of Gas Phase

$$\varepsilon\rho \frac{D\vec{u}}{Dt} + \varepsilon g_o \nabla p = -\vec{f} + \dot{m}(\vec{u}_p - \vec{u}) - \psi \vec{u} \quad 2.1.1.4$$

Here \vec{u} is the velocity with components u and v , and \vec{f} represents the velocity dependent interphase drag.

Balance of Energy of Gas Phase

$$\begin{aligned} \varepsilon p \frac{De}{Dt} + \varepsilon p \left[\frac{\partial u}{\partial z} + \frac{\partial v}{\partial r} \right] + p \frac{D\varepsilon}{Dt} &= \vec{f} \cdot (\vec{u} - \vec{u}_p) - s_p q \quad 2.1.1.5 \\ &+ \dot{m} \left(e_p - e + \frac{p}{\rho_p} + \frac{|u - u_p|^2}{2g_o} \right) \\ &+ \psi \left(e_{IG} - e + \frac{\vec{u} \cdot \vec{u}}{2g_o} \right) - \varepsilon p \frac{v}{r} \end{aligned}$$

Here $e = e(p, \rho)$ is the internal energy of the gas phase and q is the interphase heat transfer per unit surface area of the solid phase.

Balance of Mass of Solid Phase

$$\frac{D\varepsilon}{Dt_p} - (1 - \varepsilon) \left[\frac{\partial u}{\partial z} + \frac{\partial v}{\partial r} \right] = \frac{\dot{m}}{\rho_p} + (1 - \varepsilon) \frac{v_p}{r} \quad 2.1.1.6$$

The subscript p denotes properties of the solid phase and D/Dt_p is defined by analogy with 2.1.1.2.

Balance of Momentum of Solid Phase

$$(1 - \varepsilon) \rho_p \frac{Du}{Dt_p} + (1 - \varepsilon) g_o \nabla p + g_o \nabla \sigma = \vec{f} \quad 2.1.1.7$$

The vector form of this equation should be noted. We have $\sigma = (1 - \varepsilon) R(\varepsilon, \dot{\varepsilon})$ where R is the average stress due to contacts between particles and is assumed to depend upon porosity according to a viscoplastic law.

2.1.2 Quasi-One-Dimensional Two-Phase Flow

These equations are always used to represent the behavior of a centercore ignition charge. They are used, moreover, to represent the behavior of the propelling charge as a whole, following flame-spreading and bag rupture and provided that radial gradients of pressure have subsided within the mixture.

Thus, in the applications of interest to us, the non-trivial spacewise coordinate is aligned with the axis of the tube so that u , u_p are the non-trivial components of gas and solid phase velocity respectively. The cross sectional area of the annulus through which the flow occurs is taken to be $A(z,t)$ and therefore depends upon both position and time. It is supposed that the circumferential boundaries are permeable to the gas phase and that mass transfers must be considered. We use R_i and R_o to denote respectively the radii of circumferential surfaces on which influx (\dot{m}_i) or efflux (\dot{m}_o) occur. Attention should be paid to this convention. The subscripts i and o do not refer to the interior and exterior surfaces, only to the direction of mass transfer. We understand \dot{m}_i and \dot{m}_o to represent rates of transfer per unit surface area. Moreover, we will also denote the properties transported with \dot{m}_i by the subscript i . Thus u_i will be the axial velocity associated with the incoming gas. The exiting properties are, of course, those of the gas in the quasi-one-dimensional region presently under consideration.

Balance of Mass of Gas Phase

$$\frac{\partial}{\partial t} \varepsilon A \rho + \frac{\partial}{\partial z} \varepsilon A \rho u = A \dot{m} + A \psi + 2\pi [\sum R_i \dot{m}_i - \sum R_o \dot{m}_o] \quad 2.1.2.1$$

The summations are over all entering and all exiting fluxes.

Balance of Momentum of Gas Phase

$$\varepsilon \rho \frac{Du}{Dt} + \varepsilon g_o \frac{\partial p}{\partial z} = - f - \psi u + \dot{m}(u_p - u) + \frac{2\pi}{A} \sum R_i \dot{m}_i (u_i - u) \quad 2.1.2.2$$

Balance of Energy of Gas Phase

$$\begin{aligned} \varepsilon \rho \frac{De}{Dt} + \frac{p}{A} \frac{D\varepsilon A}{Dt} + \varepsilon p \frac{\partial u}{\partial z} &= \frac{f}{g_o} (u - u_p) - s_p q \\ &+ \psi [e_{IG} - e + \frac{u^2}{2g_o}] \\ &+ \dot{m} [e_p - e + \frac{p}{\rho_p} + \frac{(u - u_p)^2}{2g_o}] \\ &+ \frac{2\pi}{A} \sum \dot{m}_i R_i [e_i + \frac{p_i}{\rho_i} + \frac{(u - u_i)^2}{2g_o} - e] \\ &- \frac{2\pi}{A} \frac{p}{\rho} \sum \dot{m}_o R_o \end{aligned} \quad 2.1.2.3$$

Balance of Mass of Solid Phase

$$\frac{1}{A} \frac{D}{Dt} \frac{p}{\rho_p} (1 - \varepsilon) A + (1 - \varepsilon) \frac{\partial u_p}{\partial z} = - \frac{\dot{m}}{\rho_p} \quad 2.1.2.4$$

Balance of Momentum of Solid Phase

$$\rho_p (1 - \varepsilon) \frac{Du_p}{Dt} + (1 - \varepsilon) g_o \frac{\partial p}{\partial z} + g_o \frac{\partial \sigma}{\partial z} = f \quad 2.1.2.5$$

2.1.3 Two-Dimensional Single-Phase Flow

These familiar equations represent the limiting forms of 2.1.1.1, 2.1.1.4 and 2.1.1.5 as $\varepsilon \rightarrow 1$, bearing in mind that f , \dot{m} and $q \rightarrow 0$. They are used to describe the flow in sufficiently large regions of ullage.

Balance of Mass

$$\frac{D\rho}{Dt} + \rho \left[\frac{\partial u}{\partial z} + \frac{\partial v}{\partial r} \right] = \psi - \frac{\rho v}{r} \quad 2.1.3.1$$

Balance of Momentum

$$\rho \frac{D\vec{u}}{Dt} + g_o \nabla p = - \vec{\psi} \cdot \vec{u} \quad 2.1.3.2$$

Balance of Energy

$$\rho \frac{De}{Dt} + p \left[\frac{\partial u}{\partial z} + \frac{\partial v}{\partial r} \right] = \psi [e_{IG} + \frac{\vec{u} \cdot \vec{u}}{2g_o} - e] - p \frac{v}{r} \quad 2.1.3.3$$

2.1.4 Quasi-One-Dimensional Single-Phase Flow

A quasi-one-dimensional representation is made of regions of ullage which have significant extension in one direction but which are relatively thin in the perpendicular direction. In contrast to the situation in section 2.1.2, we cannot assume that the non-trivial direction is axial. The flow will be directed according to the configuration of the boundary of the propelling charge with which it is contiguous. In recognition of this fact we designate

the nontrivial coordinate by s and the corresponding component of velocity by u_T , to be interpreted as a velocity tangential to the contiguous mixture boundary.

Using the same conventions as in section 2.1.2 to describe entering and exiting mass fluxes we have the balance equations of quasi-one-dimensional flow as follows:

Balance of Mass

$$\frac{\partial}{\partial t} A\rho + \frac{\partial}{\partial s} A\rho u_T = A\psi + 2\pi[\sum R_i \dot{m}_i - \sum R_o \dot{m}_o] \quad 2.1.4.1$$

Balance of Momentum

$$\rho \frac{Du_T}{Dt} + g_o \frac{\partial p}{\partial s} = -\psi u + \frac{2\pi}{A} \sum R_i \dot{m}_i (u_i - u_T) \quad 2.1.4.2$$

Balance of Energy

$$\begin{aligned} \rho \frac{De}{Dt} + p \frac{DA}{Dt} + p \frac{\partial u_T}{\partial s} &= \psi [e_{IG} - e + \frac{u_T^2}{2g_o}] \\ &+ \frac{2\pi}{A} \sum \dot{m}_i R_i [e_i + \frac{p_i}{\rho_i} + \frac{(u_T - u_i)^2}{2g_o} - e] \\ &- \frac{2\pi}{A} \frac{p}{\rho} \sum \dot{m}_o R_o \end{aligned} \quad 2.1.4.3$$

It is worth emphasizing the assumptions according to which these equations are expected to represent the flow reliably. First, the cross-sectional area A is assumed to vary only weakly with respect to the streamwise coordinate s so that the flow may be essentially parallel. Second, the centerline of the flow is assumed to have only a small curvature so that variations of pressure within the cross-section, due to centrifugal effects, may be neglected. Thus, we must expect that equations 2.1.4.1-2.1.4.3 will be incapable of representing with any accuracy the flow in the neighborhood of a sharp bend or a sudden change of flow area.

2.1.5 Lumped Parameter Single-Phase Flow

As in previous work we provide balance equations only for mass and energy. It is assumed that the velocity of the gas in the lumped parameter region can be deduced from the boundary values by interpolation. Using V to denote the volume of the region and S the bounding surface we have:

$$\frac{dV}{dt} = \int_S \vec{w} \cdot \vec{n} da \quad 2.1.5.1$$

where \vec{w} is the boundary velocity and \vec{n} is the outward facing normal. The mass balance is:

$$\frac{d}{dt} \rho V = \int_V \psi dv + \dot{\Sigma m}_i - \dot{\Sigma m}_o \quad 2.1.5.2$$

where the \dot{m}_i and \dot{m}_o now refer to the total fluxes rather than the fluxes per unit area used previously.

The energy balance is:

$$\begin{aligned} \frac{d}{dt} \rho EV = & \int_V \psi e_{IG} dv + \dot{\Sigma m}_i (e_i + \frac{p_i}{\rho_i} + \frac{u_i^2}{2g_o}) - p \int_S \vec{w} \cdot \vec{n} da \\ & - \dot{\Sigma m}_o (E + \frac{p}{\rho}) \end{aligned} \quad 2.1.5.3$$

where E is the total energy $e + u^2/2g_o$.

2.2 Constitutive Laws

We describe, in the present section, both the equations of state for the solid and gas phases as well as the relationships between the interphase transfer processes--drag, heat transfer and combustion--and the macroscopic state variables. The relationships governing mass transfer from one region to another are, however, viewed as boundary conditions, as are the properties of the bag, and these topics are addressed in the next section.

2.2.1 Equation of State of Gas

It is assumed that the gas obeys the covolume equation of state:

$$e = c_v T = \frac{p(1 - b\rho)}{(\gamma - 1)\rho} \quad 2.2.1.1$$

where b is the covolume, γ is the ratio of specific heats and c_v is the specific heat at constant volume.

The molecular weight and the ratio of specific heats are assumed to be constant and are given values appropriate to the fully reacted propellant.

2.2.2 Granular Stress Law

The granular stress is taken to depend on porosity and also on the direction of loading. We embed the constitutive law into the formula for the rate of propagation of intergranular disturbances:

$$a(\varepsilon) = \left[-\frac{g_o}{\rho_p} \frac{d\sigma}{d\varepsilon} \right]^{1/2} \quad 2.2.2.1$$

We may recast 2.2.2.1 into a form more suitable for numerical integration, namely:

$$\frac{D\sigma}{Dt_p} = -\rho_p \frac{a^2}{g_o} \frac{D\varepsilon}{Dt_p} \quad 2.2.2.2$$

In order to formulate the functional behavior of $a(\varepsilon)$ we introduce ε_o , the settling porosity of the bed, and values of $a(\varepsilon)$ equal to a_1 and a_2 which respectively correspond to loading at ε_o and to unloading/reloading. The nominal loading curve, corresponding to monotonic compaction of the bed from ε_o to a smaller value of the porosity ε is given by:

$$\sigma = \sigma_{\text{nom}}(\varepsilon) = \rho_p \frac{a_1^2}{g_o} \varepsilon_o^2 \left(\frac{1}{\varepsilon} - \frac{1}{\varepsilon_o} \right) \quad 2.2.2.3$$

The functional dependence of $a(\varepsilon)$ may now be stated as:

$$a(\dot{\varepsilon}) = \begin{cases} a_1 \dot{\varepsilon}_o / \dot{\varepsilon} & \text{if } \dot{\varepsilon} \leq 0, \sigma = \sigma_{\text{nom}}, \dot{\varepsilon} \leq \dot{\varepsilon}_o \\ a_2 & \text{if } 0 \leq \sigma < \sigma_{\text{nom}}, \dot{\varepsilon} \leq \dot{\varepsilon}_o \\ & \text{or if } \dot{\varepsilon} > 0, \sigma = \sigma_{\text{nom}}, \dot{\varepsilon} \leq \dot{\varepsilon}_o \\ 0 & \text{if } \sigma = 0 \text{ and } \dot{\varepsilon} > 0 \text{ or if } \dot{\varepsilon} > \dot{\varepsilon}_o \end{cases} \quad 2.2.2.4$$

where we understand $\dot{\varepsilon}$ to mean $D\varepsilon/Dt_p$.

Equation 2.2.2.4 is assumed to govern the behavior of not only the granular propellant but also the black powder within the center-core igniter. However, the values of a_1 , a_2 and $\dot{\varepsilon}_o$ are not assumed to be the same for the two granular media.

2.2.3 Propellant Form Functions

It is assumed, in the present study, that the propellant grains are multi-perforated cylinders having initial length L_o , external diameter D_o and perforation diameter d_o . The surface area per unit volume is related to the individual surface area S_p and volume V_p of each particle according to:

$$S_p = (1 - \varepsilon) S_p / V_p \quad 2.2.3.1$$

Until such time as slivering occurs, that is to say the time at which the regressing perforation surfaces intersect, the surface area and volume are given by:

$$S_p = \pi(L_o - 2d)[(D_o - 2d) + N(d_o + 2d)] \quad 2.2.3.2$$

$$+ \pi/2[(D_o - 2d)^2 - N(d_o + 2d)^2]$$

$$V_p = \pi(L_o - 2d)[(D_o - 2d)^2 - N(d_o + 2d)^2]/4 \quad 2.2.3.3$$

where N is the number of perforations and d is the total linear surface regression, assumed uniform over all the surfaces of a grain.

Once slivering occurs, the form functions become rather

complicated for $N > 1$. Formulae for the form functions following the slivering of seven-perforation grains may be found in Krier et al²⁶. The present version of the code supports single-, seven- and nineteen-perforations grains in the propelling charge, the form functions for the latter in the slivering phase being calculated by means of a subroutine furnished by the Naval Ordnance Station, Indian Head, MD²⁷.

At present it is assumed that the grains of black powder in the centercore igniter are spherical.

2.2.4 Interphase Drag

The interphase drag is assumed to be governed by the relationship

$$\vec{f} = \frac{1 - \epsilon}{D_p} \rho |\vec{u} - \vec{u}_p| (\vec{u} - \vec{u}_p) \hat{f}_s \quad 2.2.4.1$$

where D_p is the effective particle diameter given by:

$$D_p = \frac{6V}{S_p} \quad 2.2.4.2$$

and \hat{f}_s is governed by the high Reynolds number limit of the empirical correlation of Ergun²⁸, for packed beds, extended into the fluidized regime by the tortuosity factor of Anderssen²⁹:

²⁶ Krier, H., Shimp, S. A. and Adams, M. J. "Interior Ballistic Predictions Using Data From Closed and Variable Volume Simulators." Univ. of Illinois at Urbana-Champaign. TR-AAE-73-6 1973

²⁷ Horst, A. Private communication.

²⁸ Ergun, S. "Fluid Flow Through Packed Columns." Chem. Eng. Progr. v. 48, p. 89. 1952

²⁹ Anderssen, K. E. B. "Pressure Drop in Ideal Fluidization." Chem. Eng. Sci. v. 15, pp. 276-297. 1961

$$\hat{f}_s = \begin{cases} 1.75 & \varepsilon \leq \varepsilon_o \\ 1.75 \left[\frac{1 - \varepsilon}{\varepsilon} \frac{\varepsilon_o}{1 - \varepsilon_o} \right]^{0.45} & \varepsilon_o \leq \varepsilon \leq \varepsilon_1 \\ 0.3 & \varepsilon_1 \leq \varepsilon \leq 1 \end{cases} \quad 2.2.4.3$$

where

$$\varepsilon_1 = [1 + 0.02 \left(\frac{1 - \varepsilon_o}{\varepsilon_o} \right)]^{-1} \quad 2.2.4.4$$

Some discussion of the validity of 2.2.4.3 in the case of packed beds is given in the previous final report¹. The present incorporation of the Anderssen tortuosity factor recognizes our intention to carry solutions through the completion of burnout of the propelling charge.

Equation 2.2.4.3 is assumed to govern the flow resistance in both the propelling charge and in the centercore ignition charge.

2.2.5 Interphase Heat Transfer

The interphase heat transfer, in both the propelling charge and the centercore ignition charge is assumed to be governed by the empirical correlation of Gelperin and Einstein³⁰. We express the heat transfer in the form

$$Nu_p = 0.4 Pr^{1/3} Re_p^{2/3} \quad 2.2.5.1$$

where

$$Nu_p = h D_p / k_f$$

$$Re_p = \rho_f |\vec{u} - \vec{u}_p| D_p / \mu_f$$

$$h = q / (T - T_p)$$

³⁰Gelperin, N. I. and Einstein, V. G. "Heat Transfer in Fluidized Beds." *Fluidization*, edited by Davidson, J. F. and Harrison, D. Academic Press, NY

1971

The subscript f denotes an evaluation of properties at the film temperature $(T + T_p)/2$ where T and T_p are respectively the gas bulk average temperature and the particle surface average temperature. The viscosity is taken to have a Sutherland-type dependence on temperature:

$$\mu = 0.134064 \frac{(T/298)^{1.5}}{T + 110} \quad 2.2.5.2$$

The thermal conductivity follows from the Prandtl number which is assumed to satisfy:

$$Pr = \frac{C_p \mu}{k} = \frac{4\gamma}{9\gamma - 5} \quad 2.2.5.3$$

2.2.6 Solid Phase Surface Temperature

Assuming that ignition is an essentially uniform event with respect to the surface of each grain of either the propelling charge or the centercore ignition charge and supposing that the temperature distribution within the solid phase can be captured by a cubic profile, leads to the following expression for the surface temperature

$$T_p = T_{p_0} - \frac{2}{3} \frac{hH}{k_p^2} + \left[\left(T_{p_0} - \frac{2}{3} \frac{hH}{k_p^2} \right)^2 + \frac{4}{3} \frac{hTH}{k_p^2} - T_{p_0} \right]^{1/2} \quad 2.2.6.1$$

where T_{p_0} is the initial surface temperature and H satisfies:

$$\frac{DH}{Dt_p} = \alpha_p q \quad 2.2.6.2$$

2.2.7 Ignition and Combustion

Ignition is assumed to occur when the surface temperature exceeds a predetermined value. The rate of surface regression is given by:

$$\frac{Dd}{Dt_p} = B_1 + B_2 p^n$$

2.2.7.1

It should be noted that only one of 2.2.6.2 and 2.2.7.1 has to be solved at each point according as the temperature is less than or equal to the ignition temperature.

2.3 Initial and Boundary Conditions

The initial conditions are straightforward and require minimal attention. For the problems of interest to us we may suppose that both phases are at rest and at atmospheric pressure. The propellant bed is packed within a bag and may be assumed to be at the settling porosity, obtained without irreversible compaction. The intergranular stress may be assumed to be zero throughout the bed. The temperatures of the two phases may differ initially but are uniform throughout each of the respective media. The porosity is piecewise continuous, the discontinuities being defined by the boundaries of the bed.

Our subsequent discussion addresses the boundary conditions. In section 2.3.1 we discuss the external boundary conditions, including the motion of the projectile. In section 2.3.2 we discuss the conditions which apply at boundaries between regions of ullage. In section 2.3.3 we consider the boundary conditions at the interfaces between the propelling charge and the neighboring regions of flow. The discussion of section 2.3.3 considers the influence of the bag and addresses both the case when the neighboring region contains only gas and the case when it corresponds to the center-core igniter.

2.3.1 External Boundary Conditions

We do not consider the possibility of flow of either phase through any external boundary. Since both phases are assumed to be inviscid at the macroscopic level, slip boundary conditions apply not only to the gas but also to the solid phase whenever it is in contact with an external boundary. The breech, the tube and the centerline constitute stationary boundaries on which the conditions of kinematic compatibility are simply

$$\vec{u} \cdot \vec{n} = \vec{u}_p \cdot \vec{n} = 0$$

2.3.1.1

where \vec{n} is a vector normal to the external boundary. We will take the convention that \vec{n} is positive when directed out of the combustion chamber.

Now let S_{PROJ} be the surface of the projectile which intrudes into the combustion chamber. Let n_z be the z-component of \vec{n} . Let the axial speed of the projectile be u_{PROJ} . Then the boundary conditions at the projectile surface are:

$$\vec{u} \cdot \vec{n} = \vec{u}_p \cdot \vec{n} = n_z u_{\text{PROJ}}$$

2.3.1.2

Of course, the condition on the solid phase applies only in a region of two-phase flow.

The projectile motion is assumed to be governed by:

$$\frac{M}{g_o} \frac{d}{dt} u_{\text{PROJ}} = \int_{S_{\text{PROJ}}} (p + \sigma) n_z da - F_{\text{res}} \quad 2.3.1.3$$

where M is the projectile mass and F_{res} is the bore resistance, assumed to be available from an empirical correlation.

2.3.2 Internal Boundary Conditions Between Regions of Ullage

In the present work, a region of ullage may be represented as lumped parameter, quasi-one-dimensional or fully two-dimensional. These alternative representations require that we consider the possibilities of the following types of region interfaces or internal boundaries. A fully two-dimensional region may be bounded by another fully two-dimensional region or by a quasi-one-dimensional region. A quasi-one-dimensional region may share a boundary with any other type of region, fully two-dimensional, quasi-one-dimensional, or lumped parameter.

With regard to the interpretation of the boundary conditions, it should be borne in mind that when we are concerned with an interface between a two-dimensional and a quasi-one-dimensional flow, only the component of velocity tangential to the interface is modeled explicitly in the quasi-one-dimensional region. A boundary between a quasi-one-dimensional region and either a lumped parameter region or another quasi-one-dimensional region is always oriented so as to be perpendicular to the non-trivial flow component in the quasi-one-dimensional region in question. When the interface involves a lumped parameter region it should be borne in mind that the normal flow component is modeled explicitly only on the quasi-one-dimensional side.

Let us distinguish properties on each side of an arbitrary interface by the subscripts 1 and 2 and let us use the subscripts n and t to distinguish velocity components normal and tangential to the interface respectively. Then the finite continuity equation may be stated as:

$$j = \rho_1 u_{n_1} = \rho_2 u_{n_2}$$

2.3.2.1

and we understand u_n to mean $(\vec{u} - \vec{u}_s) \cdot \vec{n}$ where \vec{u}_s is the velocity of the interface at the point in question.

We assume all transfers to be adiabatic so that:

$$j(e_1 + \frac{p_1}{\rho_1} + \frac{u_{n_1}^2}{2g_o}) = j(e_2 + \frac{p_2}{\rho_2} + \frac{u_{n_2}^2}{2g_o}) \quad 2.3.2.2$$

Here we have incorporated the mass flux j as a multiplier so as to imply the possibility of a slip discontinuity or a contact discontinuity on which j may be zero and the enthalpy may be discontinuous. We express the tangential momentum jump analogously:

$$ju_{t_1} = ju_{t_2} \quad 2.3.2.3$$

thereby admitting the possibility of a slip discontinuity.

In general we may impose one more physical boundary condition which will be tantamount to a finite balance equation for the normal momentum flux. However, the form in which we express this remaining physical condition varies not only with the nature of the internal boundary but also with the state of the flow, particularly the Mach number.

In the present work the location and motion of the interface are controlled by computational considerations and may be regarded as determined in the present discussion. Evidently, we have in general eight boundary values to consider, namely $p_1, \rho_1, u_{n_1}, u_{t_1}, p_2, \rho_2, u_{n_2}, u_{t_2}$, when we assume that the equation of state $e = e(p, \rho)$ is also given. Since we have described a total of no more than four physical boundary conditions we must suppose that the remaining conditions are provided by the governing equations themselves. It is well known that the equations of unsteady, inviscid, compressible flow are of the hyperbolic type and that there exist surfaces on which the equations reduce in such a fashion as to limit the arbitrariness of initial data. Such surfaces are called characteristic and the constraints on the data are called conditions of compatibility. As we describe further in chapter 3.0, we make explicit use of the conditions of compatibility in determining the state of the flow on both external and internal boundaries.

We now proceed to discuss the boundary conditions relevant to each type of interface with particular attention to the interpretation of 2.3.2.1 through 2.3.2.3 in each case. We also provide a discussion of the influence of the state of flow, considering both subsonic and supersonic transfers. However, it should be noted that the coding to date admits transfers which are at most sonic.

Boundary Between Two Two-Dimensional Regions

In this case equations 2.3.2.1, 2.3.2.2 and 2.3.2.3 involve the values of the state variables on each side of the interface, all quantities being represented explicitly.

The remaining physical boundary condition may be expressed in the simple form

$$p_1 = p_2 \quad 2.3.2.4$$

which is valid whether or not $j = 0$. Moreover, excluding the possibility that the boundary fortuitously coincides with a shock, 2.3.2.4 remains valid independently of the Mach number of the flow.

Boundary Between Two-Dimensional Region and Quasi-One-Dimensional Region

Let us take the subscript 1 to refer to the two-dimensional flow and let 2 refer to the quasi-one-dimensional flow. The value of u_{n_2} is not modeled explicitly but may be assumed equal to the normal velocity of the neighboring external boundary from which the two-dimensional region is presumably separated by the quasi-one-dimensional region. The mass flux j then refers to boundary values for the two-dimensional region and to a rate of mass addition or loss in so far as the quasi-one-dimensional region is concerned. With regard to the overall interpretation of equations 2.3.2.1, 2.3.2.2 and 2.3.2.3, it must be understood that ρ_2 , p_2 , e_2 , u_{t_2} can only be identified with the state of the quasi-one-dimensional flow in the event that the flow corresponds to a mass transfer directed into the two-dimensional region. When the direction of the flow is such as to correspond to mass addition to the quasi-one-dimensional region, the quantities ρ_2 , p_2 , e_2 , u_{t_2} may be thought of as describing the state of transferred gas prior to irreversible mixing. In particular, 2.3.2.2 may be understood to determine the total enthalpy of the fluid added to the quasi-one-dimensional flow.

The remaining physical condition must express the nature of the forces acting on a fluid particle during transfer. Consider first the case of transfer from the quasi-one-dimensional region to the two-dimensional region. The transfer may be thought of as an expansion of the fluid in the quasi-one-dimensional region and induced by the action of normal pressure forces. Then we may suppose the transfer to be isentropic as expressed by

$$p_1 = p_2 (T_1/T_2)^{\frac{\gamma}{\gamma-1}} \quad 2.3.2.5$$

and p_2 , T_2 may be identified with the state of the quasi-one-dimensional flow. Equation 2.3.2.5 may be used as long as the transfer is subsonic based on the value of $|u_{n_1}|$ and $c_1(p_1, \rho_1)$ where c is the isentropic speed of sound given by

$$c = \sqrt{\frac{g_o \gamma p}{\rho(1 - b\rho)}} \quad 2.3.2.6$$

for the covolume equation of state. If the use of 2.3.2.5 leads to a value of $|u_{n_1}| > c$ we replace 2.3.2.5 with the condition that the transfer is sonic as expressed by

$$|u_{n_1}| = c_1(p_1, \rho_1) \quad 2.3.2.7$$

When the direction of transfer is such as to represent mass addition to the quasi-one-dimensional flow we replace 2.3.2.5 with the condition

$$p_1 = p_2 \quad 2.3.2.8$$

where p_2 is to be understood to be the instantaneous pressure in the quasi-one-dimensional region. Equation 2.3.2.8 may be interpreted to mean that fluid added to the quasi-one-dimensional flow is subjected to a rapid equilibration of pressure on crossing the region interface. The process of addition and mixing is, however, irreversible and the equilibration of u_{t_1} to the value u_{t_2} in the quasi-one-dimensional flow is achieved through dissipative mechanisms.

Equation 2.3.2.8 is used to describe the mass transfer to the

quasi-one-dimensional region unless it yields a value $|u_{n_1}| > c_1$ in which case we use 2.3.2.7. We note that when the direction of transfer is such as to correspond to efflux from the two-dimensional region, it is not actually necessary to limit the Mach number to unity. The hyperbolic structure of the equations admits supersonic efflux and a mechanical boundary condition is not required at all. The state 1 is determined entirely by the equations of motion and equations 2.3.2.1, 2.3.2.2, 2.3.2.3 are required only to characterize the properties of the gas added to the quasi-one-dimensional flow.

Boundary Between Two Quasi-One-Dimensional Flows

In this instance the quasi-one-dimensional regions are to be thought of as placed end-to-end. The quantity u_t is modeled in neither region and only 2.3.2.1 and 2.3.2.2 are applicable. The quantities in these two equations correspond with explicitly represented state variables and the remaining physical condition is 2.3.2.4 independently of the state of the flow.

Boundary Between Quasi-One-Dimensional Region and Lumped Parameter Region

The lumped parameter region is to be thought of as terminating the quasi-one-dimensional region. Again, u_t is modeled in neither region and only 2.3.2.1 and 2.3.2.2 are applicable. If we now identify the subscript 1 with the state of the quasi-one-dimensional flow and 2 with the lumped parameter side of the interface, the discussion of the remaining physical condition and the interpretation of the terms in 2.3.2.1 and 2.3.2.2 parallels that for the interface between the two-dimensional and the quasi-one-dimensional regions. The mechanical condition is therefore 2.3.2.5 for transfer from the lumped parameter region and 2.3.2.8 for transfer to the lumped parameter region, both being replaced by 2.3.2.7 if they yield sonic or supersonic flow.

2.3.3 Internal Boundary Conditions Involving the Mixture

We consider first the conditions which apply to the boundaries of the mixture when the bag is locally ruptured, or absent altogether, and when the solid phase is not in contact with an external boundary. We assume for the moment that the mixture is represented as two-dimensional. Subsequently we will reinterpret our results in the case of quasi-one-dimensional two-phase flow. Finally we will consider the influence of the bag, introducing suitable modifications into the boundary conditions to reflect impermeability, mechanical constraint due to material integrity and mass addition due to the action of combustible elements of the bag viewed as surface phenomena.

Neglecting the bag, for the moment, we have to consider that the boundary separates the propelling charge either from a region of ullage or from another mixture region, namely the centercore ignition charge. Since a basic feature of our approach is the assumption that discontinuities in porosity be modeled explicitly, it is the case that the boundary follows the motion of the solid phase and we need consider it as permeable to the gas phase alone.

Using $u_s = \vec{u}_p \cdot \vec{n}$ as the normal component of velocity of the boundary, the jump conditions at the discontinuity in porosity may be expressed in a macroscopic form as:

$$j_1 = \varepsilon_1 \rho_1 (u_{n_1} - u_s) = j_2 = \varepsilon_2 \rho_2 (u_{n_2} - u_s) \quad 2.3.3.1$$

$$p_1 + \sigma_1 + \frac{\varepsilon_1 \rho_1}{g_o} (u_{n_1} - u_s)^2 = p_2 + \sigma_2 + \frac{\varepsilon_2 \rho_2}{g_o} (u_{n_2} - u_s)^2 \quad 2.3.3.2$$

$$j_1 [e_1 + \frac{p_1}{\rho_1} + \frac{(u_{n_1} - u_s)^2}{2g_o}] = j_2 [e_2 + \frac{p_2}{\rho_2} + \frac{(u_{n_2} - u_s)^2}{2g_o}] \quad 2.3.3.3$$

$$j_1 u_{t_1} = j_2 u_{t_2} \quad 2.3.3.4$$

where u_n , u_t are, as in 2.3.2, normal and tangential components of the gas velocity respectively.

Equation 2.3.3.4 expresses the assumption that there is no surface source of momentum of the gas phase. In fact, this assumption may be difficult to support when it is considered that the jump conditions are only meaningfully applied to points separated by a distance which is large by comparison with the scale of heterogeneity of the mixture. As we shall discuss further in chapter 3.0, a significant loss of tangential momentum can be experienced by gas entering the mixture as it penetrates a depth equal to a typical particle diameter. However, a priori criteria are not presently available for the determination of such losses and their representation as surface effects within the macroscopic formulation. Accordingly, we defer this topic to chapter 3.0 in which a loss is postulated, on an essentially ad hoc basis, mainly with a view to providing a better-posed computational problem.

It is noted that the finite momentum balance 2.3.3.2 is expressed only for the mixture and cannot be split with respect to the two phases without a constitutive assumption which essentially determines the exchange of momentum between the phases at the discontinuity.

As in previous work¹⁴ we postulate that 2.3.3.2 can be split as:

$$\sigma_1 = \sigma_2 \quad 2.3.3.5$$

$$p_1 + \frac{\varepsilon_1 \rho_1}{g_o} (u_{n_1} - u_s)^2 = p_2 + \frac{\varepsilon_2 \rho_2}{g_o} (u_{n_2} - u_s)^2 \quad 2.3.3.6$$

When the mixture is contiguous with a region of ullage, the boundary condition 2.3.3.5 reduces to $\sigma_1 = 0$ where side 1 is supposed to correspond with the propellant bed. If side 2 is not ullage, but corresponds to the centercore igniter, then 2.3.3.5 expresses a condition of mechanical equilibrium of the boundary value σ_1 in the propelling charge with the stress σ_2 , assumed isotropic, in the quasi-one-dimensional two-phase flow used to represent the centercore igniter.

It is convenient to recast 2.3.3.6 as:

$$p_1 - p_2 = \frac{j^2}{g_o} \left[\frac{1}{\varepsilon_2 \rho_2} - \frac{1}{\varepsilon_1 \rho_1} \right] \quad 2.3.3.7$$

When region 2 does not contain an explicit representation of u_n , 2.3.3.7 may be used provided that it is kept in mind that ρ_2 is the explicitly modeled state variable in region 2 only when the direction of mass transfer is from 2 to 1. When the direction of mass transfer is from 1 to 2, a value ρ_2 may be computed but it does not necessarily coincide with the state on side 2. The quantity ρ_2 is to be interpreted, in such a case, as the density following transfer but prior to mixing.

Following the completion of flamespreading and bag rupture, the propelling charge may be represented as a quasi-one-dimensional two-phase flow. In the event of radial transfer of gas, the normal velocity component will be modeled explicitly in neither the propelling charge nor the coaxial region of ullage. Equation 2.3.3.7 may still be used subject to the interpretation of the preceding

paragraph whether the direction of flow is from 1 to 2 or vice versa.

However, computational experience shows the pressure jump to be almost always negligible during the quasi-two-dimensional phase of the calculation. Accordingly, the present version of the code simply assumes continuity of pressure across the interface, an assumption which may easily be relaxed in future work, if necessary.

We now consider the influence of the bag in which the propelling charge is initially loaded and show how the behavior of the bag can be represented within the internal boundary conditions. The attributes of the behavior of the bag which we wish to incorporate into our model are its impermeability to the gas phase, a characteristic which may result in a first order level of interaction with the ignition stimulus, its impediment also to the motion of the solid phase, and finally, the reactivity of certain sections of its surface, particularly the rear endwall to which is attached the basepad igniter. It should be understood throughout this section that we use the word bag in a general sense to refer to the boundaries of the propelling charge and in particular, that the centercore igniter tube is viewed as a part of the bag.

Effects of Flow Resistance and Strength of Bag

Consider first the impermeability of the bag with respect to the gas phase. In anticipation of the acquisition of appropriate empirical data, we suppose that the impermeability of the bag can be represented by means of a dimensionless friction factor K . Assuming as before that side 1 corresponds to the mixture within the bag, we revise equation 2.3.3.6 to become

$$p_1 + \frac{\epsilon_1 \rho_1}{g_o} u_{n_1}^2 - \frac{K \rho_1}{g_o} u_{n_1} |u_{n_1}| = p_2 + \frac{\epsilon_2 \rho_2}{g_o} u_{n_2}^2 \quad 2.3.3.8$$

In order to achieve an overall momentum balance, further considerations are necessary. If the direction of flow is such that the gas is entering the mixture, we suppose that the pressure drop associated with the friction factor K cannot be supported by the flexible sections of the bag, such as the endwalls and the outer sidewall, and is transmitted into the solid phase. In such a case we must revise 2.3.3.5 so that the condition on the granular stress becomes

$$\sigma_1 = \sigma_2 - K\rho_1 u_{n_1} |u_{n_1}|$$

2.3.3.9

If, however, the direction of flow is reversed, $u_{n_1} > 0$, corresponding to transfer from the mixture, we may assume the existence of stresses in the bag which are sufficient to balance the pressure loss due to impermeability. Then 2.3.3.5 is unchanged but we introduce

$$F_{\text{bag}} = K\rho u_{n_1} |u_{n_1}|$$

2.3.3.10

as the pressure difference to be supported by the flexible bag material.

An additional mechanical boundary condition to be considered when the bag is unruptured arises when the material on the sidewall is fully dilated. In such a case the bag acts as a direct impediment to the radial motion of the propellant bed. In the present model we do not attempt to analyze the stress field in the bag according to a fundamental theory of deformation in which the stress tensor is defined everywhere by reference to the state of strain of the bag. We assume simply that if the bag is unruptured it cannot be dilated locally beyond its original diameter. In such a case the mechanical boundary condition appropriate to the solid phase is simply that the normal component of velocity must vanish. The state of stress must then follow from the equations of motion. Since, in this case, equation 2.3.3.5 is not satisfied, the right hand side of 2.3.3.10 must be augmented by the difference $\sigma_1 - \sigma_2$.

A similar condition applies in regard to the centercore tube which is viewed as rigid until it is ruptured. In contradistinction to the flexible sections of the bag, we assume 2.3.3.10 to apply to the centercore tube, independently of the direction of flow, so that the possibility of rupture due either to crushing or to local bursting is admitted.

With regard to the endwalls of the bag, however, we simply neglect the possible confinement of the charge due to inextensibility of the bag. In contrast to the sidewalls, the endwalls are initially planar. Since the material behaves like a membrane, when loaded, its resistance to normal motion is negligible in its initial condition. Only when local curvature has been established in the endwalls can the tensile stresses in the constituent fibers develop components of force in the axial direction. Whereas the

confinement imposed by the sidewall can be evaluated from a simple consideration of the local diameter of the bag, that due to the endwall requires a consideration of the state of deformation of the entire bag. For, if we suppose the existence of stresses within the surface of the endwall, these must be transferred to the sidewall and then communicated over the length of the bag to the opposing endwall.

We have, in the foregoing discussion, assumed the inertia of the bag to be everywhere negligible. Nor do we consider the finite thickness of the bag. Both of these simplifications are, however, easy to relax in the context of the present representation of the bag.

On the other hand, our treatment of the bag as an attribute of the boundary of the propelling charge involves certain assumptions which we must keep in mind. First, it is clear that slip of the solid phase relative to the bag is not considered. Second, if the bag is locally compressed and then, due to changes in the local pressure, begins to dilate, we do not consider the possible separation of the cloth from the propelling charge: the diameter of the bag remains equal to the local diameter of the bed. To be useful, the present model should only be applied to cases in which the bag properties vary relatively weakly by comparison with typical relative displacements of the propellant bed prior to rupture. Moreover, the potential flow channel induced by bag separation prior to rupture must not be extensive.

As with the analysis of direct confinement of the solid phase by the endwalls, the effects of relative slip and of normal separation require a detailed representation of the displacement field of the entire bag.

In considering the impediment of the bag to motion of the solid phase it should perhaps be noted that its impermeability is an important factor. The solid phase is expected to be dispersed not only by the action of forces transmitted from grain to grain, but also by the gas dynamic processes of pressure gradient and drag. Taking the bag to be impermeable eliminates the possible contribution of drag to the local expansion of the bed.

We may now summarize our representation of the influence of the bag as an impediment to normal motion of each of the phases. Again identifying side 1 of the internal boundary with the propelling charge we have:

$$p_1 + \frac{\epsilon_1 \rho_1}{g_o} u_{n_1}^2 - \frac{K \rho_1}{g_o} u_{n_1} |u_{n_1}| = p_2 + \frac{\epsilon_2 \rho_2}{g_o} u_{n_2}^2 \quad 2.3.3.11$$

For flexible sections of the bag we have the following boundary condition connecting values of intergranular stress on each side of the bag.

$$\sigma_1 - \sigma_2 = \begin{cases} -\frac{K \rho_1}{g_o} u_{n_1} |u_{n_1}| & \text{if } u_{n_1} < 0 \\ 0 & u_{n_1} \geq 0 \end{cases} \quad 2.3.3.12$$

But, on a section of the external circumferential boundary at which the bag is locally dilated to its initial radius, or, on a section of the rigid centercore tube, 2.3.3.12 is replaced by

$$\vec{u}_p \cdot \vec{n} = 0 \quad 2.3.3.13$$

Finally, we have the following expression for the stress supported by the bag.

$$F_{\text{bag}} = \begin{cases} \sigma_1 - \sigma_2 + \frac{K \rho_1}{g_o} u_{n_1} |u_{n_1}| & \text{if section rigid or} \\ & \text{if flexible and } u_{n_1} > 0 \\ 0 & \text{if flexible and } u_{n_1} < 0 \end{cases} \quad 2.3.3.14$$

Specific data have not presently been acquired in relation to bag charges to provide appropriate constitutive laws for the permeability and strength of the bag. For the present, we assume that each point on the surface of the bag is characterized initially by a value K_o of the friction factor and a value σ_{bag} of the normal stress that the bag can support. We assume $K = K_o$, locally, until such time as $F_{\text{bag}} \geq \sigma_{\text{bag}}$, locally, and that subsequently K decreases to zero linearly with time over a fixed interval t_{rupt} .

Effects of Reactivity of the Bag

We have not as yet said anything concerning the influence of the bag as a source of energetic gas. In the applications of interest to us an important element of the ignition train is the basepad whose thickness is very small by comparison with the typical dimensions of the chamber or the propelling charge. As it is initially attached to the rear endwall of the bag, a natural representation of its influence may be established within the framework of the internal boundary conditions. Combustion of the ignition charge introduces no momentum into a control volume which surrounds an element of the bounding surface of the bag. Hence 2.3.3.4 and 2.3.3.6 require no revision. However, the balances of the normal mass flux and the energy flux must be revised to become:

$$\varepsilon_1 \rho_1 u_{n_1} = \varepsilon_2 \rho_2 u_{n_2} - \dot{m}_{bp} \quad 2.3.3.15$$

and

$$(\varepsilon_1 \rho_1 u_{n_1}) (e_1 + \frac{p_1}{\rho_1} + \frac{u_{n_1}^2}{2g_o}) = (\varepsilon_2 \rho_2 u_{n_2}) (e_2 + \frac{p_2}{\rho_2} + \frac{u_{n_2}^2}{2g_o}) - e_{IG} \dot{m}_{bp} \quad 2.3.3.16$$

where \dot{m}_{bp} is the local rate of generation of mass per unit area and the enthalpy of the gas is resolved as the chemical energy e_{IG} , the influence of the condensed phase density being neglected. Care must also be taken with 2.3.3.4 since the tangential velocity component is no longer necessarily continuous in the event of mass transfer. This may be seen from 2.3.3.15 according to which $j_1 \neq j_2$ if $\dot{m}_{bp} \neq 0$.

As presently formulated, the computer code assumes that $K_o = 0$ at any point on the surface of the bag where $\dot{m}_{bp} \neq 0$. The values of \dot{m}_{bp} are assumed to be furnished as tabular data which describe the rate of discharge as a function of time.

The foregoing discussion has focused particular attention on the basepad. Naturally, other exothermic bag-related charge components, such as the nitrocellulose centercore tube, may be treated in the same manner. Moreover, by allowing the quantity e_{IG} , in equation 2.3.3.16 to be negative, we may incorporate the influence of not only exothermic but also endothermic reactive components of the bag.

3.0 METHOD OF SOLUTION

In chapter 1.0 we summarized our approach to the simulation of the interior ballistics of a bagged propelling charge as one in which several disjoint regions of flow are recognized. The regions are linked by explicitly represented internal boundary conditions. The nature of the flow in each region may be single- or two-phase and either lumped parameter, quasi-one-dimensional or fully two-dimensional with axisymmetry. In chapter 2.0 we presented a statement of the balance equations for each type of flow, together with the necessary constitutive laws, in cylindrical coordinates.

When we turn to the subject matter of the present chapter, namely the method of solution of these equations, we make the immediate assumption that a transformation of coordinates will always be desirable, the law of transformation being selected so that each internal boundary corresponds to a constant value of one or the other of the computational coordinates and so that each region of flow is transformed into a regular figure, a square or a unit line, in the computational plane.

In section 3.1 we proceed to tabulate the transformed balance equations, as well as those constitutive laws which are expressed as partial differential equations, without stating explicitly the laws of transformation. In fact, the laws of transformation may be problem-dependent and several procedures are in current use by the computational fluid dynamics community. We defer the discussion of our present choice to section 3.4 in which the programming strategy as a whole is addressed.

Section 3.2 provides additional restatements of the balance equations and the differential constitutive laws. Here we tabulate the characteristic forms of the equations which play an important role in our analysis of the solution at both the external and internal boundaries.

In section 3.3 we discuss the procedures according to which the partial differential equations are discretized so as to yield an integration scheme based on the method of finite differences. The discussion of section 3.3 distinguishes among mesh points located in the interior, on the boundaries, and at the corners of the computational regions. We conclude, in section 3.5, with some comments on special topics and numerical devices which have been incorporated into the present version of the code.

3.1 The Equations in Computational Coordinates

We explicitly tabulate the equations for four possible types of flow, namely: two-dimensional two-phase flow; quasi-one-dimensional two-phase flow; two-dimensional single-phase flow; and quasi-one-dimensional single-phase flow. The lumped parameter equations are, of course, indifferent to transformations of the spatial coordinates.

In general, we are concerned with a transformation which we may represent by:

$$\tau = t \quad 3.1.1$$

$$\zeta = \zeta(z, r, t) \quad 3.1.2$$

$$\eta = \eta(z, r, t) \quad 3.1.3$$

where t is the time and z and r are the usual axial and radial cylindrical coordinates. By introducing τ we facilitate the representation of partial derivatives. For ϕ_t will be understood to mean a derivative of ϕ with respect to time with z and r held constant while ϕ_τ will represent a derivative with respect to time in which ζ and η are held constant.

We assume that the transformation 3.1.1, 3.1.2, 3.1.3 is one-to-one, has continuous partial derivatives, and that the Jacobian determinant

$$\frac{\partial(\zeta, \eta)}{\partial(z, r)} = \zeta_z \eta_r - \eta_z \zeta_r \quad 3.1.4$$

never vanishes. Then the inverse transformation may be assumed to exist such that

$$t = \tau \quad 3.1.5$$

$$z = z(\zeta, \eta, \tau) \quad 3.1.6$$

$$r = r(\zeta, \eta, \tau) \quad 3.1.7$$

Let J be the Jacobian determinant corresponding to the inverse transformation

$$J = \frac{\partial(z, r)}{\partial(\zeta, \eta)} = 1 / \left(\frac{\partial(\zeta, \eta)}{\partial(z, r)} \right) \quad 3.1.8$$

Then we note the following useful relationships between the forward and inverse transformation derivatives:

$$\zeta_r = -z_\eta/J \quad 3.1.9$$

$$\zeta_z = r_\eta/J \quad 3.1.10$$

$$\eta_z = -r_\zeta/J \quad 3.1.11$$

$$\eta_r = z_\zeta/J \quad 3.1.12$$

We may also introduce the velocity components of a point which is fixed in the computational plane by writing

$$u_m = z_\tau \quad 3.1.13$$

$$v_m = r_\tau \quad 3.1.14$$

where z and r are understood to be defined functionally by 3.1.6 and 3.1.7.

Finally, we introduce contravariant components of velocity of each of the phases with respect to the time dependent frame of reference, namely:

$$w = (u - u_m)\zeta_z + (v - v_m)\zeta_r \quad 3.1.15$$

$$x = (u - u_m)\eta_z + (v - v_m)\eta_r \quad 3.1.16$$

$$w_p = (u_p - u_m)\zeta_z + (v_p - v_m)\zeta_r \quad 3.1.17$$

$$x_p = (u_p - u_m)\eta_z + (v_p - v_m)\eta_r \quad 3.1.18$$

3.1.1 Two-Dimensional Two-Phase Flow

The relevant balance equations have been stated in the physical plane as equations 2.1.1.1, 2.1.1.4, 2.1.1.5, 2.1.1.6, 2.1.1.7. In addition we must consider the differential constitutive laws 2.2.2.2, 2.2.6.2 and 2.2.7.1. In anticipation of certain formal simplifications of the characteristic equations discussed in section 3.2, we introduce a parameter λ into the solid phase momentum equation. When $\lambda = 1$, the pressure gradient is recognized explicitly as a differential term and when $\lambda = 0$, the pressure gradient is included with the nonhomogeneous terms. We emphasize that the distinction is purely formal at this stage since we proceed by simply adding $(\lambda - 1)$ times the pressure gradient to each side of 2.1.1.7. An additional modification to the equations is made by eliminating the internal energy from equation 2.1.1.5 in favor of the pressure and density.

The equations may now be stated in terms of the computational coordinates ζ and η , following the order in which we referenced them in the preceding paragraph and writing the momentum equations explicitly with respect to each of the velocity components.

$$\rho_\tau = - w\rho_\zeta - x\rho_\eta - \frac{\rho}{\epsilon} [\epsilon_\tau + w\epsilon_\zeta + x\epsilon_\eta] \quad 3.1.1.1$$

$$- \rho [\zeta_z u_\zeta + \eta_z u_\eta + \zeta_r v_\zeta + \eta_r v_\eta] + \frac{\xi_1}{\epsilon}$$

$$u_\tau = - wu_\zeta - xu_\eta - \frac{g_o}{\rho} [\zeta_z p_\zeta + \eta_z p_\eta] + \frac{\xi_2}{\epsilon \rho} \quad 3.1.1.2$$

$$v_\tau = - wv_\zeta - xv_\eta - \frac{g_o}{\rho} [\zeta_r p_\zeta + \eta_r p_\eta] + \frac{\xi_3}{\epsilon \rho} \quad 3.1.1.3$$

$$p_\tau = - wp_\zeta - xp_\eta + \frac{\epsilon^2}{g_o} [\rho_\tau + w\rho_\zeta + x\rho_\eta] + \xi_4 \quad 3.1.1.4$$

$$\epsilon_\tau = - w_p \epsilon_\zeta - x_p \epsilon_\eta + (1 - \epsilon) [\zeta_z u_{p_\zeta} + \eta_z u_{p_\eta} + \zeta_r v_{p_\zeta} + \eta_r v_{p_\eta}] + \xi_5 \quad 3.1.1.5$$

$$u_{p_\tau} = - w_p u_{p_\zeta} - x_p u_{p_\eta} - \frac{\lambda g_o}{\rho_p} [\zeta_z p_\zeta + \eta_z p_\eta] \quad 3.1.1.6$$

$$- \frac{g_o}{(1-\varepsilon)\rho_p} [\zeta_z \sigma_\zeta + \eta_z \sigma_\eta] + \frac{\xi_6}{(1-\varepsilon)\rho_p}$$

$$v_{p_\tau} = - w_p v_{p_\zeta} - x_p v_{p_\eta} - \frac{\lambda g_o}{\rho_p} [\zeta_r p_\zeta + \eta_r p_\eta] \quad 3.1.1.7$$

$$- \frac{g_o}{(1-\varepsilon)\rho_p} [\zeta_r \sigma_\zeta + \eta_r \sigma_\eta] + \frac{\xi_7}{(1-\varepsilon)\rho_p}$$

$$\sigma_\tau = - w_p \sigma_\zeta - x_p \sigma_\eta - \frac{\rho_p a^2}{g_o} [\varepsilon_\tau + w_p \varepsilon_\zeta + x_p \varepsilon_\eta] \quad 3.1.1.8$$

$$H_\tau = - w_p H_\zeta - x_p H_\eta + \alpha_p q \quad 3.1.1.9$$

$$d_\tau = - w_p d_\zeta - x_p d_\eta + B_1 + B_2 p^n \quad 3.1.1.10$$

In tabulating these equations we have represented the non-homogeneous terms by the quantities ξ_i , $i = 1, \dots, 7$. Specifically we have:

$$\xi_1 = \dot{m} + \psi - \frac{\varepsilon \rho v}{r} \quad 3.1.1.11$$

$$\xi_2 = - f_z + \dot{m}(u_p - u) - \psi u \quad 3.1.1.12$$

$$\xi_3 = - f_r + \dot{m}(v_p - v) - \psi v \quad 3.1.1.13$$

$$\begin{aligned} \xi_4 = & \frac{1}{\varepsilon \rho \left(\frac{\partial e}{\partial p}\right)_p} [\vec{f} \cdot (\vec{u} - \vec{u}_p) - s_p q + \dot{m}(e_p - e + p(\frac{1}{\rho_p} - \frac{1}{\rho})) \\ & + \frac{|\vec{u} - \vec{u}_p|^2}{2g_o} + \psi(e_{IG} - e - \frac{p}{\rho} + \frac{\vec{u} \cdot \vec{u}}{2g_o})] \end{aligned} \quad 3.1.1.14$$

$$\xi_5 = \frac{\dot{m}}{\rho_p} + (1 - \varepsilon) \frac{v_p}{r} \quad 3.1.1.15$$

$$\xi_6 = f_z + (\lambda - 1)(1 - \varepsilon)g_o [\zeta_z p_\zeta + \eta_z p_\eta] \quad 3.1.1.16$$

$$\xi_7 = f_r + (\lambda - 1)(1 - \varepsilon)g_o [\zeta_r p_\zeta + \eta_r p_\eta] \quad 3.1.1.17$$

3.1.2 Quasi-One-Dimensional Two-Phase Flow

As discussed in section 2.1.2, we are concerned, for the present, with flows of this type in which only the z-component of motion is non-trivial. We assume, moreover, that the flow can be described by reference to the computational coordinates τ and ζ so that terms involving η do not appear.

The computational forms of the equations for quasi-one-dimensional two-phase flow evidently follow from those of the preceding section by simply ignoring 3.1.1.3 and 3.1.1.7, setting $x = x_p = 0$ and deleting all the derivatives with respect to r or η . However, the non-homogeneous terms must be modified to reflect the varying cross-sectional area of the flow and the influence of mass addition or loss. The differential equations may be tabulated explicitly as follows:

$$\rho_\tau = - w\rho_\zeta - \frac{\rho}{\varepsilon} [\varepsilon_\tau + w\varepsilon_\zeta] - \rho\zeta_z u_\zeta + \frac{\xi_1}{\varepsilon} \quad 3.1.2.1$$

$$u_\tau = - wu_\zeta - \frac{g_o}{\rho} \zeta_z p_\zeta + \frac{\xi_2}{\varepsilon\rho} \quad 3.1.2.2$$

$$p_\tau = - wp_\zeta + \frac{c^2}{g_o} [\rho_\tau + w\rho_\zeta] + \xi_4 \quad 3.1.2.3$$

$$\varepsilon_\tau = - w_p \varepsilon_\zeta + (1 - \varepsilon) \zeta_z u_{p_\zeta} + \xi_5 \quad 3.1.2.4$$

$$u_{p_\tau} = - w_p u_{p_\zeta} - \frac{\lambda g_o}{\rho_p} \zeta_z p_\zeta - \frac{g_o}{(1 - \varepsilon)\rho_p} \zeta_z \sigma_\zeta + \frac{\xi_6}{(1 - \varepsilon)\rho_p} \quad 3.1.2.5$$

$$\sigma_{\tau} = - w_p \sigma_{\zeta} - \frac{\rho_p a^2}{g_o} [\varepsilon_{\tau} + w_p \varepsilon_{\zeta}] \quad 3.1.2.6$$

$$H_{\tau} = - w_p H_{\zeta} + \alpha_p q \quad 3.1.2.7$$

$$d_{\tau} = - w_p d_{\zeta} + B_1 + B_2 p^n \quad 3.1.2.8$$

It should be noted that the choice of subscripts of the ξ_i conforms with that of the previous section. The non-homogeneous terms are

$$\xi_1 = \dot{m} + \psi + \frac{2\pi}{A} [\Sigma R_1 \dot{m}_1 - \Sigma R_o \dot{m}_o] - \frac{\varepsilon o}{A} [A_{\tau} + w A_{\zeta}] \quad 3.1.2.9$$

$$\xi_2 = - f + \dot{m}(u_p - u) - \psi u + \frac{2\pi}{A} \Sigma R_1 \dot{m}_1 (u_1 - u) \quad 3.1.2.10$$

$$\begin{aligned} \xi_4 &= \frac{1}{\varepsilon o (\frac{\partial e}{\partial p})_p} [f(u - u_p) - s_p q + \dot{m}(e_p - e + p(\frac{1}{\rho_p} - \frac{1}{\rho})) \\ &\quad + \frac{(u - u_p)^2}{2g_o}) + \psi(e_{IG} - e - \frac{p}{\rho} + \frac{u^2}{2g_o}) \\ &\quad + \frac{2\pi}{A} \Sigma \dot{m}_1 R_1 (e_1 - e + \frac{p_1}{\rho_1} - \frac{p}{\rho} + \frac{(u - u_1)^2}{2g_o})] \end{aligned} \quad 3.1.2.11$$

$$\xi_5 = \frac{\dot{m}}{\rho_p} + \frac{(1 - \varepsilon)}{A} [A_{\tau} + w_p A_{\zeta}] \quad 3.1.2.12$$

$$\xi_6 = f + (\lambda - 1)(1 - \varepsilon) g_o \zeta_z p_{\zeta} \quad 3.1.2.13$$

3.1.3 Two-Dimensional Single-Phase Flow

Assuming a transformation of the type 3.1.1, 3.1.2, 3.1.3, the computational form of the equations for a flow of this type follow from those of section 3.1.1 by simply taking the limit $\varepsilon \rightarrow 1$ and ignoring attributes of the solid phase. Explicitly, we have:

$$\rho_{\tau} = - w\rho_{\zeta} - x\rho_{\eta} - \rho [\zeta_z u_{\zeta} + \eta_z u_{\eta} + \zeta_r v_{\zeta} + \eta_r v_{\eta}] + \xi_1 \quad 3.1.3.1$$

$$u_{\tau} = - wu_{\zeta} - xu_{\eta} - \frac{g_o}{\rho} [\zeta_z p_{\zeta} + \eta_z p_{\eta}] + \frac{\xi_2}{\rho} \quad 3.1.3.2$$

$$v_{\tau} = - wv_{\zeta} - xv_{\eta} - \frac{g_o}{\rho} [\zeta_r p_{\zeta} + \eta_r p_{\eta}] + \frac{\xi_3}{\rho} \quad 3.1.3.3$$

$$p_{\tau} = - wp_{\zeta} - xp_{\eta} + \frac{c^2}{g_o} [\rho_{\tau} + w\rho_{\zeta} + x\rho_{\eta}] + \xi_4 \quad 3.1.3.4$$

and the non-homogeneous terms are due only to divergence effects and the possible presence of an external ignition stimulus ψ :

$$\xi_1 = \psi - \frac{\epsilon \rho v}{r} \quad 3.1.3.5$$

$$\xi_2 = - \psi u \quad 3.1.3.6$$

$$\xi_3 = - \psi v \quad 3.1.3.7$$

$$\xi_4 = \frac{\psi}{\rho(\frac{\partial e}{\partial p})} [e_{IG} - e - \frac{p}{\rho} + \frac{\vec{u} \cdot \vec{u}}{2g_o}] \quad 3.1.3.8$$

3.1.4 Quasi-One-Dimensional Single-Phase Flow

Whereas the equations of section 3.1.3 follow by direct simplification of those of section 3.1.1, it does not follow that the equations of the present section may be deduced directly from those of section 3.1.2. The difference is due to the fact that we recognize the arbitrary orientation and curvature of the quasi-one-dimensional single-phase flow. Naturally, the equations require at most one spatial computational coordinate, but its dependence on both z and r must be considered. We assume that the flow can be described by the computational pair τ and ζ . Then the equations of motion may be written as:

$$\rho_{\tau} = - w\rho_{\zeta} - \rho \zeta_s u_{T_{\zeta}} + \xi_1 \quad 3.1.4.1$$

$$u_{T_{\tau}} = - wu_{T_{\zeta}} - \frac{g_o}{\rho} \zeta_s p_{\zeta} + \xi_2 \quad 3.1.4.2$$

$$p_T = -wp_\zeta + \frac{c^2}{g_o} [\rho_T + wp_\zeta] + \xi_4 \quad 3.1.4.3$$

Here, however, w is not given by 3.1.15 but is defined by

$$w = \zeta_s (u_T - u_m) \quad 3.1.4.4$$

where

$$u_m = \zeta_s (z_\tau z_\zeta + r_\tau r_\zeta) \quad 3.1.4.5$$

$$\zeta_s = (z_\zeta^2 + r_\zeta^2)^{-1/2} \quad 3.1.4.6$$

The non-homogeneous terms may be tabulated as:

$$\xi_1 = \psi + \frac{2\pi}{A} [\Sigma R_i \dot{m}_i - \Sigma R_o \dot{m}_o] - \frac{\rho}{A} [A_\tau + w A_\zeta] \quad 3.1.4.7$$

$$\xi_2 = -\frac{\psi u}{\rho} + \frac{2\pi}{A\rho} \Sigma R_i \dot{m}_i (u_i - u_T) \quad 3.1.4.8$$

$$\begin{aligned} \xi_4 = & \frac{1}{\rho \left(\frac{\partial e}{\partial p} \right)_o} \{ \psi (e_{IG} - e - \frac{p}{\rho} + \frac{u^2}{2g_o}) \\ & + \frac{2\pi}{A} \Sigma R_i \dot{m}_i (e_i + \frac{p_i}{\rho_i} + \frac{(u_T - u_i)^2}{2g_o} - e - \frac{p}{\rho}) \} \end{aligned} \quad 3.1.4.9$$

3.2 Characteristic Forms of the Balance Equations

A system of first order partial differential equations involving n independent variables is said to be hyperbolic if there exists a real hypersurface of dimension $n - 1$ on which the system may be expressed entirely in terms of derivatives internal to the hypersurface. If there are n distinct such surfaces at a given point, then the system is said to be totally hyperbolic.

In the present section we explicitly tabulate the characteristic forms for each of the four types of continuum flow discussed in the

preceding section and in the same order. However, we discuss only the acoustic characteristic forms associated with the propagation of infinitesimal pressure pulses. The equations of motion admit other characteristic forms which require no discussion here since the computational forms of the preceding section have already captured them. We refer to the energy equations for the gas phase, 3.1.1.4, 3.1.2.3, 3.1.3.4, and 3.1.4.3, which are clearly seen to involve total derivatives of p and ρ along the gas-phase streamline, and to equations 3.1.1.8 and 3.1.2.6, the constitutive law for the solid phase, which are clearly expressed in terms of total derivatives along the solid-phase streamline. Finally, the laws of surface heating and regression, 3.1.1.9, 3.1.1.10, 3.1.2.7, 3.1.2.8, also are expressed as total derivatives along the solid-phase streamline.

The derivation of the characteristic forms may be found elsewhere¹. Here we only summarize the necessary results.

3.2.1 Two-Dimensional Two-Phase Flow

In this, and in succeeding sections, we state the characteristic equations in a form suitable for the determination of numerical results for a boundary element defined by $\zeta = \text{constant}$. The corresponding results for a boundary on which $\eta = \text{constant}$ follow from considerations of symmetry.

A bicharacteristic ray lying in the $\tau - \zeta$ plane must satisfy the condition¹:

$$[(\frac{d\zeta}{d\tau} - w)^2 - c_*^2][(\frac{d\zeta}{d\tau} - w_p)^2 - a_*^2] = \lambda c_*^2 \frac{\rho}{\rho_p} \frac{1-\varepsilon}{\varepsilon} [\frac{d\zeta}{d\tau} - w]^2 \quad 3.2.1.1$$

where

$$c_*^2 = c^2(\zeta_z^2 + \zeta_r^2) \quad 3.2.1.2$$

and

$$a_*^2 = a^2(\zeta_z^2 + \zeta_r^2) \quad 3.2.1.3$$

Equation 3.2.1.1 reveals our motivation for the introduction of the parameter λ . When $\lambda = 0$, corresponding to the formal treatment

of the pressure gradient in the solid-phase momentum equation as a non-homogeneous term, equation 3.2.1.1 may be directly factored to yield the roots

$$\frac{d\xi}{d\tau} = w \pm c_* \text{ and } \frac{d\xi_p}{d\tau} = w_p \pm a_* \quad 3.2.1.4$$

We emphasize that 3.2.1.4 does not describe the actual characteristic roots of our system of equations and that these results may not be used to make deductions concerning the well-posedness of initial and boundary value problems. However, the analytical results predicated on the pseudo-characteristics corresponding to $\lambda = 0$ are useful in the formulation of the numerical algorithm for the determination of boundary values and it is in this capacity that we intend to use them.

We introduce

$$y = \frac{d\xi}{d\tau} - w \quad 3.2.1.5$$

$$y_p = \frac{d\xi_p}{d\tau} - w_p \quad 3.2.1.6$$

and we define

$$\xi_A = \xi_1^* + \frac{\varepsilon g_o}{c^2} \xi_4^* + \frac{\zeta_z}{y} \xi_2^* + \frac{\zeta_r}{y} \xi_3^* \quad 3.2.1.7$$

$$\xi_B = \xi_5^* - \frac{\zeta_r}{\rho_p y_p} (\xi_7^* + \frac{g_o \zeta_r}{y_p} \xi_8^*) - \frac{\zeta_z}{\rho_p y_p} (\xi_6^* + \frac{g_o \zeta_z}{y_p} \xi_8^*) \quad 3.2.1.8$$

where the ξ_i^* are related to the ξ_i of equations 3.1.1.11 through 3.1.1.17 according to

$$\xi_1^* = \xi_1 - [\varepsilon x \rho_\eta + \varepsilon \rho \eta_z u_\eta + \varepsilon \rho \eta_r v_\eta + \rho x \varepsilon_\eta] \quad 3.2.1.9$$

$$\xi_2^* = \xi_2 - [\varepsilon \rho x u_\eta + \varepsilon g_o \eta_z p_\eta] \quad 3.2.1.10$$

$$\xi_3^* = \xi_3 - [\epsilon \rho x v_\eta + \epsilon g_o n_r p_\eta] \quad 3.2.1.11$$

$$\xi_4^* = \xi_4 - x [p_\eta - \frac{c^2}{g_o} \rho_\eta] \quad 3.2.1.12$$

$$\xi_5^* = \xi_5 - [x_p \epsilon_\eta - (1 - \epsilon) n_z u_{p_\eta} - (1 - \epsilon) n_r v_{p_\eta}] \quad 3.2.1.13$$

$$\xi_6^* = \xi_6 - [\lambda(1 - \epsilon) g_o n_z p_\eta + (1 - \epsilon) \rho_p x_p u_{p_\eta} + g_o n_z \sigma_\eta] \quad 3.2.1.14$$

$$\xi_7^* = \xi_7 - [\lambda(1 - \epsilon) g_o n_r p_\eta + (1 - \epsilon) \rho_p x_p v_{p_\eta} + g_o n_r \sigma_\eta] \quad 3.2.1.15$$

and, in addition:

$$\xi_8^* = - x_p [\sigma_\eta + \frac{\rho_p a^2}{g_o} \epsilon_\eta] \quad 3.2.1.16$$

When $\lambda = 0$ and $y_p = \pm a_*$, corresponding to the solid-phase acoustic characteristics, we have the characteristic form:

$$\sigma_\alpha = - \frac{\rho_p y_p}{g_o (1 + \frac{w}{y_p})} \left\{ \frac{\xi_B + (1 - \epsilon)(1 + \frac{w}{y_p})(\zeta_z u_{p_\alpha} + \zeta_r v_{p_\alpha})}{\zeta_r^2 + \zeta_z^2} \right\} \quad 3.2.1.17$$

The derivative σ_α , taken along the bicharacteristic ray, may be related to ζ - and τ -derivatives according to:

$$\sigma_\alpha = \sigma_\zeta + \sigma_\tau / (\frac{d\zeta}{d\tau}) \quad 3.2.1.18$$

We also have the more general characteristic form, valid whether or not $\lambda = 0$:

$$-\frac{\varepsilon g_o}{c^2} y p_\alpha = -\frac{\xi_A}{1 + \frac{w}{y}} + \frac{\rho \xi_B y y_p}{(1 + \frac{w}{y})(y_p^2 - a_*^2)} \quad 3.2.1.19$$

$$+ \frac{\rho y y_p (1 - \varepsilon) (1 + \frac{w}{y}) (\xi_z u_{p_\alpha} + \xi_r v_{p_\alpha})}{(1 + \frac{w}{y})(y_p^2 - a_*^2)}$$

$$+ \varepsilon \rho (\xi_z u_\alpha + \xi_r v_\alpha) + \frac{\frac{g_o \rho}{\rho_p} y (1 + \frac{w}{y}) (\xi_r^2 + \xi_z^2)}{(1 + \frac{w}{y})(y_p^2 - a_*^2)} \sigma_\alpha$$

$$+ \rho y \frac{\frac{w}{y} - \frac{w}{y_p}}{1 + \frac{w}{y}} \varepsilon_\alpha$$

We may note that 3.2.1.19 reduces to 3.2.1.17 when $y_p = \pm a_*$. However, 3.2.1.19 will be used with $y = \pm c$, corresponding to the gas-phase pseudo-characteristic with $\lambda = 0$.

3.2.2 Quasi-One-Dimensional Two-Phase Flow

The characteristic forms in this case follow from those of the preceding section in a straightforward manner. Since the flow depends only on ζ and τ we have $v = v_p = x = x_p = 0$ and, moreover, all derivatives with respect to r and η vanish. Equation 3.2.1.1 defines the characteristic roots and 3.2.1.2, 3.2.1.3 simply state $c_* = \xi_z c$ and $a_* = \xi_z a$ respectively.

With regard to the non-homogeneous terms we note that the ξ_i^* are all equal to the ξ_i since the cross derivatives in equations 3.2.1.9 through 3.2.1.15 vanish. Moreover, $\xi_3 = \xi_7 = \xi_8^* = 0$. Finally, the ξ_i are, of course, defined by equations 3.1.2.9 through 3.1.2.13.

The condition of compatibility for the solid-phase is easily seen, from equation 3.2.1.17, to reduce to

$$\sigma_\alpha = - \frac{\rho_p y_p}{g_o (1 + \frac{w_p}{y_p})} \left\{ \frac{\xi_B}{\zeta_z^2} + \frac{1 - \varepsilon}{\zeta_z} \left(1 + \frac{w_p}{y_p} \right) u_{p_\alpha} \right\} \quad 3.2.2.1$$

Similarly, the more general result 3.2.1.19 reduces to:

$$\begin{aligned} - \frac{\varepsilon g_o}{c^2} y p_\alpha &= - \frac{\xi_A}{1 + \frac{w}{y}} + \frac{\rho \xi_B y y_p}{(1 + \frac{w}{y})(y_p^2 - a_*^2)} + \varepsilon \rho \zeta_z u_\alpha \\ &\quad + \frac{\rho y y_p (1 - \varepsilon) (1 + \frac{w}{y})}{(1 + \frac{w}{y})(y_p^2 - a_*^2)} \zeta_z u_{p_\alpha} \\ &\quad + \frac{g_o \rho y}{\rho_p} \frac{(1 + \frac{w}{y})}{(1 + \frac{w}{y})(y_p^2 - a_*^2)} \zeta_z^2 \sigma_\alpha \\ &\quad + \rho y \frac{\frac{w}{y} - \frac{w_p}{y}}{1 + \frac{w}{y}} \varepsilon_\alpha \end{aligned} \quad 3.2.2.2$$

3.2.3 Two-Dimensional Single-Phase Flow

As in the preceding section, these results follow as a reduction of those of 3.2.1. It is necessary to take the limit $\varepsilon \rightarrow 1$ and to neglect the references to the solid-phase. Thus the characteristics are simply

$$\frac{d\xi}{d\tau} = w \pm c_* \quad 3.2.3.1$$

Concerning the non-homogeneous terms we note that $\xi_5 = \xi_6 = \xi_7 = 0$

and, moreover, $\xi_5^* = \xi_6^* = \xi_7^* = \xi_8^* = 0$ so that $\xi_B = 0$ also. The remaining ξ_i are given by equations 3.1.3.5 through 3.1.3.8 and the ξ_i^* by 3.2.1.9 through 3.2.1.12 with the term involving ε_η deleted from 3.2.1.9.

The characteristic form is given by:

$$-\frac{g_o}{c^2} y p_\alpha = -\frac{\xi_A}{1 + \frac{w}{y}} + \rho(\zeta_z u_\alpha + \zeta_r v_\alpha) \quad 3.2.3.2$$

3.2.4 Quasi-One-Dimensional Single-Phase Flow

These results reduce from those of the preceding section by noting $\xi_3 = 0$, $v = x = 0$ so that the $\xi_i^* = \xi_i$, $i = 1, 2, 4$. Finally, $\zeta_r = 0$ and ζ_z is replaced by ζ_s as defined by 3.1.4.6 and the ξ_i are given by 3.1.4.7, 3.1.4.8, 3.1.4.9. The characteristic equation is simply

$$-\frac{g_o}{c^2} y p_\alpha = -\frac{\xi_A}{1 + \frac{w}{y}} + \rho \zeta_s u_{T_\alpha} \quad 3.2.4.1$$

3.3 Discretization and Integration Algorithms

In the two preceding sections we described the reformulation of the governing equations to accept a curvilinear coordinate system and we tabulated some characteristic forms with a view to the method of solution at the boundaries, both internal and external. The choice of curvilinear transformation is deferred to section 3.4.2. In the present section we consider the transformation from a continuum formulation to a finite difference formulation of the equations.

We describe the integration algorithms in four subsections. The basis of a finite difference formulation is, of course, the introduction of a finite mesh which covers the domain on which the solution is to be obtained. Values of the solution are determined only at the finitely many mesh points and the partial derivatives which appear in the continuum equations are replaced by finite difference counterparts. We distinguish points in the interior of a region, for which neighbors are present on all sides to form finite differences, and those on the boundaries, for which neighboring points are not available in certain directions. Finally, for two-dimensional regions, we further distinguish those boundary points which lie on the corners where the number of neighbors is minimized. We use quite different algorithms to integrate interior and boundary points. Moreover, further, special considerations are required at the corners. Sections 3.3.1, 3.3.2, 3.3.3 treat interior, boundary and corner

points, respectively. Finally, in section 3.3.4 we provide some discussion of the procedures appropriate in the case of a quasi-two-dimensional representation of the flow.

3.3.1 Integration at Interior Mesh Points

We first describe the algorithm for interior points of regions of two-dimensional flow, both two-phase and single-phase. Subsequently we comment on the reduction of the algorithm to quasi-one-dimensional and lumped parameter flows. The algorithm is basically that devised by MacCormack³¹, modified with respect to the convective terms in a manner suggested by Moretti³².

Consider the system of partial differential equations

$$\frac{\partial \psi}{\partial \tau} + B \frac{\partial \psi}{\partial \zeta} + C \frac{\partial \psi}{\partial \eta} = D \quad 3.3.1.1$$

Let $\psi_{i,j}^n$ be understood to mean a value of ψ at a mesh point enumerated by the finite ζ -coordinate i , the finite η -coordinate j and the finite τ -coordinate n . Similarly let $B_{i,j}^n$ mean $B(\psi_{i,j}^n)$ and likewise for C and D . Then the basic MacCormack scheme, with a consistent allowance for the non-homogeneous terms, may be expressed as follows.

$$\tilde{\psi}_{i,j} = \psi_{i,j}^n + [D_{i,j}^n - \frac{B_{i,j}^n}{\Delta \zeta} (\psi_{i+1,j}^n - \psi_{i,j}^n) \quad 3.3.1.2$$

$$- \frac{C_{i,j}^n}{\Delta \eta} (\psi_{i,j+1}^n - \psi_{i,j}^n)] \Delta \tau$$

$$\psi_{i,j}^{n+1} = 1/2 (\psi_{i,j}^n + \tilde{\psi}_{i,j}) + [\tilde{D}_{i,j} - \frac{\tilde{B}_{i,j}}{\Delta \zeta} (\tilde{\psi}_{i,j} - \tilde{\psi}_{i-1,j}) \quad 3.3.1.3$$

$$- \frac{\tilde{C}_{i,j}}{\Delta \eta} (\tilde{\psi}_{i,j} - \tilde{\psi}_{i,j-1})] \frac{\Delta \tau}{2}$$

³¹ MacCormack, R. W. "The Effect of Viscosity in Hypervelocity Impact Cratering" AIAA Paper No. 69-354 1969

³² Moretti, G. "Calculation of the Three-Dimensional, Supersonic, Inviscid, Steady Flow Past an Arrow-Winged Airframe" POLY-AE/AM Report No. 76-8 1976

The scheme is seen to involve a predictor level, yielding the trial update $\tilde{\psi}_{i,j}$, followed by a corrector level yielding the final update $\psi_{i,j}^{n+1}$. We also note that alternating forward and backward differences are used for the representation of the spacewise derivatives.

The modification suggested by Moretti relates to the discretization of the convective derivatives. These are always represented by upstream differences as follows, except where forbidden by proximity to a boundary:

Predictor

$$\frac{\partial \phi}{\partial \zeta} = \pm \frac{1}{\Delta \zeta} [\phi_{i\pm 1,j} - \phi_{i,j}] \quad 3.3.1.4$$

Corrector

$$\frac{\partial \phi}{\partial \zeta} = \pm \frac{1}{\Delta \zeta} [3\phi_{i\pm 1,j} - \phi_{i\pm 2,j} - 2\phi_{i,j}] \quad 3.3.1.5$$

The upper or lower sign is used according as the pre-multiplying velocity component is negative or positive, respectively. It should be noted that 3.3.1.5 is not a second order accurate form. It only yields formal second order accuracy in combination with 3.3.1.4. When the mesh point is adjacent to a boundary and the rule expressed by 3.3.1.4, 3.3.1.5 would require data outside the computational domain, we revert to the regular MacCormack prescription. At present, the second order corrector 3.3.1.5 is encoded but suppressed in regions of two-dimensional single-phase flow. The first order form 3.3.1.4 is used at both levels.

We also note that the matrices B and C involve terms like ζ_z . These are deduced by first expressing z_ζ , z_η , r_ζ , r_η by means of centered differences. Then ζ_z , ζ_r , η_z , η_r follow from equations 3.1.9 through 3.1.12.

The integration scheme is assumed to be stable when subjected to a usual Courant-Friedrichs-Lowy domain of dependence limitation³³. If C is the fastest local wavespeed we require:

³³ Richtmyer, R. D. and Morton, K. W. "Difference Methods for Initial Value Problems." Interscience

1967

$$C \frac{\Delta\tau}{\Delta\zeta} \leq \frac{r_\eta z_\zeta - z_\eta r_\zeta}{\sqrt{(r_\eta - kr_\zeta)^2 + (z_\eta - kz_\zeta)^2}} \quad 3.3.1.6$$

where $k = \pm\Delta\zeta/\Delta\eta$ according as $z_\eta z_\zeta + r_\eta r_\zeta \leq 0$. In practice, we further constrain this heuristic limit by dividing it by a safety factor which we have taken to be 1.1.

In 3.3.1.2 and 3.3.1.3 we have represented the non-homogeneous terms, embedded in the matrix D, as being integrated by a straightforward, explicit, predictor/corrector scheme. This is indeed the case for all terms except those associated with the interphase drag in the gas-phase balance equations. If we write $\vec{f} = (\vec{u} - \vec{u}_p) \phi (\vec{u} - \vec{u}_p)$, then, in the momentum equation, the vectorial prefactor is represented implicitly in the term \vec{u} . That is:

$$\vec{f} = \begin{cases} (\tilde{\vec{u}} - \vec{u}_p^n) \phi (\vec{u}^n - \vec{u}_p^n), & \text{predictor} \\ (\vec{u}^{n+1} - \tilde{\vec{u}}_p) \phi (\vec{u} - \tilde{\vec{u}}_p), & \text{corrector} \end{cases}$$

where the spacewise subscripts have been ignored. A similar procedure is adopted for the heating term in the energy equation, except that it is the density which is evaluated implicitly.

When we are concerned with a quasi-one-dimensional flow, 3.3.1.2 and 3.3.1.3 may be applied by simply deleting the η -terms or the subscripts involving j . At present, however, we have not encoded the second order corrector 3.3.1.5 for the convective terms. The convective derivatives are, at present, represented in the first order form 3.3.1.4 on both the predictor and the corrector steps. The implicit treatment of f is also employed in the quasi-one-dimensional two-phase regions.

When all the spacewise terms are deleted from 3.3.1.2 and 3.3.1.3, there results an algorithm for the integration of a lumped parameter region. However, in both the quasi-one-dimensional and the lumped parameter regions, additional elements of implicitness are introduced. All the non-homogeneous terms involving inter-region mass transfers are handled in a semi-implicit manner as we discuss further in the subsequent sections. Similarly, the inter-granular stress in a quasi-one-dimensional two-phase region may be

required to satisfy a transverse equilibrium condition at the future level and may also be thought of as subject to an implicit determination.

In contrast to the interphase drag, however, the additional elements of implicitness are introduced following a trial update by means of 3.3.1.2 and 3.3.1.3, and are associated with the enforcing of the physical boundary conditions at the future level.

3.3.2 Integration at Boundary Points

In the present section we consider only points on the boundaries of fully two-dimensional regions. Boundary points of quasi-one-dimensional regions arise only in connection with corners of fully two-dimensional regions or in the quasi-two-dimensional representation, in the present work, and we therefore discuss them in the next sections.

The method of solution at boundary points of the fully two-dimensional regions may be summarized as follows. A trial update of all state variables is made using the pseudo-characteristic forms. At the same time, we compute and save the partial derivatives of the state variables, with respect to the normal velocity components, as indicated by the pseudo-characteristic forms. Then the physical boundary conditions are enforced subject to the assumption that the state variables are related in a linear fashion to the normal flow components, the coefficients of proportionality being, of course, the partial derivatives indicated by the pseudo-characteristic forms.

With regard to nomenclature, it should be understood that on a predictor level the current storage level contains the state of the flow at time τ while the future storage level contains the predictor estimate of the state at time $\tau + \Delta\tau$; on a corrector level the current storage level contains the predictor estimate of the state at time $\tau + \Delta\tau$. On a corrector level, the past storage level contains the state of the flow at time τ .

There are three types of boundary conditions to consider. First we must consider the case when the boundary is impermeable to both phases as occurs at an external boundary or at a section of the mixture boundary when the bag is completely impermeable. The second case is that which arises when the mixture boundary is adjacent to a quasi-one-dimensional two-phase flow. The cases of mixture adjacent to a quasi-one-dimensional single-phase flow and of two-dimensional single-phase flow adjacent to quasi-one-dimensional single-phase flow follow as we take the limit $\epsilon \rightarrow 1$ in the one-dimensional and two-dimensional regions, respectively. The third and final case arises when the mixture is adjacent to a region of fully two-dimensional single-phase

flow. A relevant limiting subcase is that defined by a boundary between two two-dimensional single-phase regions of flow.

In TDNOVA, as presently structured, the actual computational sequence is as follows. Trial update values of the properties of the solid-phase are determined using the available pseudo-characteristic forms. Then values for the gas-phase are determined. Next, the physical boundary conditions are applied to the gas-phase to yield the final update values at the integration level--predictor or corrector--in question. Finally, the solid-phase properties are modified to satisfy the physical boundary conditions. This order of computation recognizes the dependence of the boundary values of intergranular stress on the values of the gas-phase pressure as indicated by equation 2.3.3.12.

In the subsequent discussion, however, we shall treat first the solid-phase in entirety and then the gas-phase in entirety, so that the reader should keep the actual computational sequence in mind.

3.3.2.1 The Solid-Phase

We consider, throughout this section, a boundary on which $\zeta = \text{constant}$. Results for a boundary on which $\eta = \text{constant}$ follow from considerations of symmetry. A vector normal to the boundary is given by (ζ_z, ζ_r) while a vector tangent to the boundary is $(-\zeta_r, \zeta_z)$. It should be noted that neither vector is normalized. In terms of these vectors we can define normal and tangential velocity components of the solid-phase

$$\hat{\mathbf{u}}_{p_n} = \zeta_z \mathbf{u}_p + \zeta_r \mathbf{v}_p \quad 3.3.2.1$$

$$\hat{\mathbf{u}}_{p_t} = -\zeta_r \mathbf{u}_p + \zeta_z \mathbf{v}_p \quad 3.3.2.2$$

neither of which is in physical units. The physical components are given by $\mathbf{u}_{p_n} = \hat{\mathbf{u}}_{p_n} (\zeta_z^2 + \zeta_r^2)^{-1/2}$ and similarly for \mathbf{u}_{p_t} .

We may likewise combine the components of the solid-phase momentum equation to get a normal equation of motion

$$\begin{aligned}
\zeta_z u_{p_\tau} + \zeta_r v_{p_\tau} &= \frac{\zeta_z \xi_6 + \zeta_r \xi_7}{(1 - \epsilon) \rho_p} - \frac{\lambda g_o}{\rho_p} [(\zeta_z^2 + \zeta_r^2) p_\zeta + (\zeta_z n_z + \zeta_r n_r) p_\eta] \\
&\quad - \frac{g_o}{(1 - \epsilon) \rho_p} [(\zeta_z^2 + \zeta_r^2) \sigma_\zeta + (\zeta_z n_z + \zeta_r n_r) \sigma_\eta] \\
&\quad - \zeta_z (w_p u_{p_\zeta} + x_p u_{p_\eta}) - \zeta_r (w_p v_{p_\zeta} + x_p v_{p_\eta}) \quad 3.3.2.3
\end{aligned}$$

In a similar way we may also deduce a tangential equation of motion for the solid-phase. As we have already discussed in the introduction to this report the present version of the code uses an evaluation of the tangential motion of the solid-phase based on an approximate statement of the requirement that the shear deformation vanish at the surface.

It should be noted that the current version of the code does compute a tangential velocity based on the integration of the tangential equation of motion. The value so obtained is, however, simply overlaid with a value based on the state at a point in the interior adjacent to the boundary.

Since it will be our hope, in future work, to refine our analysis we first document here the computational procedure based on the integration of the tangential equation of motion and then note the present overlay.

The tangential equation of motion may be expressed as

$$\begin{aligned}
\zeta_z v_{p_\tau} - \zeta_r u_{p_\tau} &= \frac{\zeta_z \xi_7 - \zeta_r \xi_6}{(1 - \epsilon) \rho_p} + \frac{g_o}{\rho_p} (\zeta_r n_z - \zeta_z n_r) p_\eta \quad 3.3.2.4 \\
&\quad + \frac{g_o}{(1 - \epsilon) \rho_p} (\zeta_r n_z - \zeta_z n_r) \sigma_\eta \\
&\quad - \zeta_z (w_p v_{p_\zeta} + x_p v_{p_\eta}) + \zeta_r (w_p u_{p_\zeta} + x_p u_{p_\eta})
\end{aligned}$$

The τ - and η -derivatives in 3.3.2.3 and 3.3.2.4 are discretized in the manner given in the preceding section, equations 3.3.1.2 and 3.3.1.3. The ζ -derivatives, normal to the boundary must, however, be resolved by one-sided finite difference forms. They are therefore resolved by the scheme 3.3.1.4, 3.3.1.5. The transformation derivatives ζ_z , ζ_r , η_z , η_r are deduced in the same manner as in the interior. However, a first order one-sided difference is used to evaluate the normal derivatives z_ζ , r_ζ .

It should be noted, in regard to accuracy, that the integration of 3.3.2.3 and 3.3.2.4 at the predictor level yields an estimate of \hat{u}_{p_n} , \hat{u}_{p_t} based on current storage level estimates of ζ_z and ζ_r and predictor level estimates of \tilde{u}_p , \tilde{v}_p . At the corrector level, the estimates of \hat{u}_{p_n} , \hat{u}_{p_t} are based on predictor level estimates of ζ_z and ζ_r and corrector level estimates of u_p^{n+1} , v_p^{n+1} . The higher order time dependence of the transformation derivatives is at present neglected.

At present, as already noted above, the value of \hat{u}_{p_t} obtained by integrating 3.3.2.4 is replaced by a value obtained by substituting into 3.3.2.2 values of u_p and v_p corresponding to the future storage level at the mesh point adjacent to the boundary in the computational domain.

Given estimates of the future values, predictor or corrector, of \hat{u}_{p_n} , \hat{u}_{p_t} , the components in cylindrical coordinates follow as:

$$u_p = \frac{\zeta_z \hat{u}_{p_n} - \zeta_r \hat{u}_{p_t}}{\zeta_z^2 + \zeta_r^2} \quad 3.3.2.5$$

$$v_p = \frac{\zeta_r \hat{u}_{p_n} + \zeta_z \hat{u}_{p_t}}{\zeta_z^2 + \zeta_r^2} \quad 3.3.2.6$$

Moreover, partial derivatives of u_p , v_p with respect to \hat{u}_{p_n} and \hat{v}_{p_n} follow by inspection of 3.3.2.5 and 3.3.2.6.

Next, estimates of the updated values of porosity and intergranular stress are determined as follows. The rate of propagation of intergranular disturbances is computed. If it is zero, the intergranular stress is taken to be zero and the porosity is updated

directly from the solid phase continuity equation using one-sided differences for the ζ -derivatives as prescribed by 3.3.1.4 and 3.3.1.5. If the rate of propagation is not zero, we use the pseudo-characteristic form 3.2.1.17 to integrate σ , whereupon ϵ follows from equation 3.1.1.8. In the former case the derivatives $\partial\sigma/\partial\hat{u}_{p_n}$ and $\partial\epsilon/\partial\sigma$ are set equal to zero. In the latter, the derivatives follow from 3.2.1.17 and 3.1.1.8, respectively. We note that, in the latter case, the storage level of resolution of the transformation derivatives and velocity components in \hat{u}_{p_n} is consistent with the results of integrating 3.3.2.3 and 3.3.2.4.

Now let us consider the influence of the physical boundary conditions on the updated values of u_p , v_p , ϵ and σ .

If the flow is adjacent to an external boundary the solid-phase is required to satisfy a constraint in the component of velocity normal to the external boundary. If the updated value of u_{p_n} is such as to indicate penetration of the boundary, it is replaced by the normal velocity of the boundary itself. Then, using the various partial derivatives which were computed during the trial update, the values of u_p , v_p , ϵ and σ are all adjusted in accordance with the change in u_{p_n} . A similar procedure is also followed at points on the external circumferential surface of the mixture when the bag is unruptured and fully dilated, and on the rigid sections of the centercore tube.

When the updated value of u_{p_n} does not indicate penetration of the external boundary, no revision is made to u_p , v_p , ϵ or σ . Accordingly, separation of the solid-phase from the boundary is accommodated automatically.

Now consider the case when the boundary is adjacent to a quasi-one-dimensional two-phase flow. In this case the relevant boundary condition--always assuming the motion of the solid-phase to be unconstrained by the bag--is expressed in terms of the intergranular stress as in equation 2.3.3.12. Then the trial value of σ is tested for consistency with the boundary condition. The necessary variation is computed and, by means of the various partial derivatives, u_p , v_p , ϵ and σ are all adjusted. If the quasi-one-dimensional flow is single-phase, 2.3.3.12 applies with $\sigma_2 = 0$. When the quasi-one-dimensional flow is two-phase, we also consider an implicit dependence of σ_2 on the normal velocity u_{p_n} through the term A_T in equation 3.1.2.12.

Then, if the flow in the two-dimensional region is dispersed, so that $\sigma_1 = 0$ necessarily, equation 2.3.3.12 acts to control the lateral expansion of the quasi-one-dimensional flow so as to ensure that $\sigma_2 = 0$ also.

The final possibility involves the case when the neighboring flow is two-dimensional, but single-phase. Then, of course, $\sigma_2 = 0$ in 2.3.3.12 and variations in u_p , v_p , ϵ follow from the necessary variation in σ_1 in order that 2.3.3.12 be satisfied.

3.3.2.2 The Gas-Phase

As in the preceding discussion of the solid-phase we consider a boundary on which $\zeta = \text{constant}$. Normal and tangential velocity components may be defined for the gas-phase by analogy with 3.3.2.1 and 3.3.2.2 as

$$\hat{u}_n = \zeta_z u + \zeta_r v \quad 3.3.2.7$$

$$\hat{u}_t = -\zeta_r u + \zeta_z v \quad 3.3.2.8$$

A normal equation of motion is not used. At each integration level a trial estimate of \hat{u}_n is deduced using the current storage level values of u and v . A tangential equation of motion is required, however, and we have

$$\begin{aligned} \zeta_z v_t - \zeta_r u_t &= \frac{\zeta_z \xi_3 - \zeta_r \xi_2}{\epsilon \rho} - \frac{g_o}{\rho} [\zeta_z n_r - \zeta_r n_z] p_n \\ &\quad - \zeta_z [wv_\zeta + xv_n] + \zeta_r [wu_\zeta + xu_n] \end{aligned} \quad 3.3.2.9$$

In making use of 3.3.2.9 the rules of discretization are the same as those which we have discussed in connection with the solid-phase. Equation 3.3.2.9 leads to an estimate of \hat{u}_t at the future level which may be combined with \hat{u}_n to yield trial values of u and v analogously with 3.3.2.5 and 3.3.2.6. Of course, the use of boundary values based on 3.3.2.9 is admissible only if the gas is not entering the mixture from an external region. However, the updated values of u and v corresponding to 3.3.2.9 are retained until the physical boundary conditions have been imposed and the direction of the flow has been determined.

The trial values of u and v are used in equation 3.2.1.19 to establish a trial update value for the pressure p which, in turn, is used in equation 3.1.1.4 to establish a trial update value of the density ρ .

As with the tangential velocity, the use of a value of ρ from the characteristic form 3.1.1.4 is admissible only if the direction of flow corresponds to efflux from the mixture, the determination of which is postponed until the physical boundary conditions have been imposed.

During the trial update of the gas-phase boundary conditions the partial derivatives $\partial u / \partial \hat{u}_n$, $\partial v / \partial \hat{u}_n$, $\partial p / \partial \hat{u}_n$ and $\partial \rho / \partial p$ are deduced from the relations 3.3.2.5, 3.3.2.6, 3.2.1.19 and 3.1.1.4 on the basis of the current storage values used to compute the various coefficients. These derivatives are used to correct the boundary values when we impose the physical boundary conditions which we now discuss.

If the flow is adjacent to an impermeable boundary we have the condition $\hat{u}_n = 0$ unless a reactive substrate is present. When a reactive substrate is present the boundary condition on \hat{u}_n may be regarded as posed for the exterior flow whereupon \hat{u}_n on the boundary of the mixture follows from the continuity equation. The trial value of \hat{u}_n may be corrected and then corrected values of u , v , p and ρ follow by means of the partial derivatives. An impermeable boundary may occur when the mixture is contiguous with an external boundary or when the bag has a sufficiently high value of the flow resistance factor K in 2.3.3.11. As presently formulated the code takes a value of $K > 100$ to mean that the bag is completely impermeable.

If the mixture is contiguous with a quasi-one-dimensional flow, the momentum equation 2.3.3.11 is solved simultaneously with the condition of continuity, making due allowance for the presence of a reactive sublayer, and the conditions of compatibility between \hat{u}_n and p expressed by the pseudo-characteristic condition 3.2.1.19 and the coefficient of the mass flux term embedded in ξ_4 of the quasi-one-dimensional equation 3.1.2.3 or 3.1.4.3 according as the external flow is two-phase or single-phase. The combination of these equations leads to a quadratic equation for \hat{u}_n which may then be used to correct the trial values by means of the differential coefficients. Corrections are also applied to the quasi-one-dimensional flow so that the mass flux is expressed implicitly in terms of the updated value of \hat{u}_n .

This implicit application of the normal momentum equation is particularly important when the transverse dimensions of the quasi-one-dimensional region become small and the dependence on the mass flux becomes stiff. The failure to express the momentum equation implicitly will result either in very small time steps or in oscillations of the boundary values.

If the direction of flow corresponds to efflux from the mixture, the update is complete. Otherwise, it is necessary to replace the boundary values of tangential velocity and density in the mixture by values deduced from the tangential momentum jump and the finite energy balance respectively.

As we have discussed in the introduction, special measures have been taken with respect to the treatment of the tangential component of velocity. This topic is discussed in section 3.5. The solution of the energy equation, with due allowance for a reactive sublayer, is straightforward and requires no discussion here.

The third situation which may occur at the boundary involves a two-dimensional single-phase exterior flow. The steps are similar to those of the preceding section except that characteristic forms are used to update the exterior as well as the interior flow. The momentum equation 2.3.3.11 is solved simultaneously with the equation of continuity, with allowance for a reactive sublayer, and with the internal and external conditions of compatibility between pressure and normal velocity. Finally, the direction of flow is established and the tangential velocity and density on the receiver side of the boundary are established from the finite jump conditions. As in the case of a one-dimensional exterior flow, transfer to the mixture involves the assumption of a tangential momentum loss as described in section 3.5.

It has been tacitly assumed in the foregoing that all transfers of gas across internal boundaries are such that the Mach number does not exceed unity on either side. At present TDNOVA does not support supersonic transfers. If the Mach number is found to exceed unity when the momentum balance is satisfied, the value of \hat{u}_n is replaced by a value which yields sonic flow. In view of the uncertainties in the balance equations themselves as well as in the constitutive laws for two-phase flow at near sonic conditions, this approach is believed to be adequate for all cases involving the mixture. However, in the event that the boundary in question separates two single-phase regions, an allowance for fully supersonic flow, when admissible by the equations of motion, would be a useful extension to the present capability of TDNOVA. The need for such an extension will, however, have to be determined following the accumulation of computational experience with the fully-two-dimensional treatment of the ullage.

3.3.3 Integration at Corner Points

The discussion of this topic is given from the perspective of a point located on a corner of the mixture. The corners of two-dimensional regions of ullage may be regarded as subcases of the present discussion for which the appropriate simplifications are readily perceived.

With regard to the corners of the mixture we will distinguish three cases of increasing physical and analytical complexity. The first case may be described as a fully attached corner in which both sides of the mixture are bounded by an impermeable wall. The second case may be described as a partially separated corner in which one side of the mixture is bounded by an impermeable wall and the other is bounded by a quasi-one-dimensional single- or two-phase flow or by a two-dimensional single-phase flow. The third case may be described as a fully separated corner in which each side of the mixture is bounded by a quasi-one-dimensional or two-dimensional single-phase flow or by a quasi-one-dimensional two-phase flow. We discuss these three cases in three successive subsections.

3.3.3.1 Fully Attached Corner

In this case the relevant boundary conditions are given in terms of the normal velocity components of both phases with respect to each of the sides which define the corner. The intergranular stress and the pressure may be deduced from the pseudo-characteristic forms. In our previous study¹ we selected the characteristic direction in accordance with the structure of the flow near the corner. In the present work we have selected the $\tau - \eta$ direction for the resolution of the pseudo-characteristic forms, independently of the structure of the flow, and for both phases.

3.3.3.2 Partially Separated Corner

In this case we have a boundary condition for each phase in the form of the normal velocity component for the side which is attached to the external boundary. This condition replaces the use of \hat{u}_t and \hat{u}_{pt} as described in section 3.3.2. Otherwise the analysis of 3.3.2 may be used with the characteristic direction chosen normal to the separated boundary of the mixture, for both phases.

It is also necessary in this case to impose boundary conditions on the external flow contiguous with the separated side. These are furnished in the form of a condition on the normal velocity component with respect to the attached side. If the exterior flow is two-phase, as in the case of the centercore igniter, it should be noted that the influence of a basepad, represented as a source term, may require the consideration of a flux condition on the gas-phase in a fashion directly analogous to the case which occurs when the mixture, bounded by a reactive bag, is adjacent to an impermeable wall.

The characteristic forms of the quasi-one-dimensional equations are used to deduce thermodynamic state variables which are consistent with the kinematic boundary conditions.

3.3.3.3 Fully Separated Corner

In this case the flow is overdetermined. As a simple example, consider a fully separated corner bounded on each side by a quasi-one-dimensional single-phase flow. The boundary values in the quasi-one-dimensional regions are connected through conditions which involve a flow loss due to dissipation as the flow turns the corner. Hence, the external pressure approaches different limiting values as one approaches the corner on each of the two sides. On the exterior, if it is two-dimensional, one has all the usual problems associated with a backstep in inviscid flow³⁴ compounded by the possibility that the surface of the mixture may be permeable.

In view of these complications we adopt the simplest possible approach. The normal component of velocity of each of the phases is assumed to be equal to that of its neighbor on each side of the mixture. The pressure is taken to be the average of the neighboring values. The density is taken to be an average also unless the flow corresponds to an efflux at one neighboring point. In the latter case the corner value is taken to be the same as that at the neighbor where influx occurs. Exactly the same procedure is used for two-dimensional regions of ullage exterior to the mixture.

When the exterior flow is quasi-one-dimensional on both sides of the corner, trial values are deduced for the exterior boundary values and for the state of the lumped parameter corner region, all based on normal mass fluxes across the mixture boundaries as deduced from the neighboring values. Then the physical conditions of compatibility of the exterior one-dimensional flows with the lumped parameter corner region are imposed simultaneously with the acoustic characteristic forms. The updated values are, of course, tested to ensure that the sonic limit is not exceeded. The boundary values of density in the exterior quasi-one-dimensional regions follow from either the characteristic forms or from the energy balance according as the flows are directed into or out of the corner region respectively.

If the quasi-one-dimensional region is two-phase, allowance must be made in the continuity and energy balances with the inner region, for the presence of a reactive layer corresponding to the part of the basepad which overlaps the centercore tube.

A further possibility arises when one external region is two-dimensional while the other is quasi-one-dimensional. In this case the corner region is quasi-one-dimensional and the boundary conditions at the interface between the two quasi-one-dimensional regions contiguous with the corner are determined using the characteristic forms and the finite mass, momentum and energy balances with due allowance for a surface source term.

³⁴ Roache, P. J. "Computational Fluid Dynamics"
Hermosa Publishers

1972

3.3.4 Integration of the Quasi-Two-Dimensional Flow

When the flow is treated according to a quasi-two-dimensional formulation we have three coaxial flows, two of which may be two-phase, bounded at each end by a single-phase lumped parameter region.

At each step trial values at the interior points are deduced for each region using values of the transverse fluxes which were established at the preceding level. A suitable allowance is made for the presence of reactive substrates of the bag, even though rupture is complete, for the sake of maintaining the global balances as closely as possible.

The gas-phase pressure is assumed to equilibrate across each cross-section of the tube. The values of the transverse fluxes are therefore adjusted so as to yield identical values of pressure in each of the three regions using the differential coefficients indicated by the term ξ_4 of equations 3.1.2.3 and 3.1.4.3. The quadratic dependence of pressure jump on mass flux, illustrated by equation 2.3.3.11, is neglected.

The transverse fluxes deduced in this way are used, in combination with the law governing the interphase drag and the radial component of the equation of motion of the solid-phase, neglecting pressure gradient and granular stress, to yield the influence of radial gas flow on radial motion of the propelling charge boundaries. The radial motion of the boundaries is also influenced by considerations of the requirement of transverse equilibrium of the intergranular stress which is hypothesized to have an isotropic character.

Intergranular stresses can exist only at a cross-section in which no radial ullage is present. In such a cross-section the intergranular stresses in the propelling charge and the centercore, if present, must be equal. These considerations lead to the determination of an equilibrium value for the intergranular stress in much the same fashion as that used to determine the pressure. The boundary motion is evaluated implicitly for this purpose and the differential coefficient connecting intergranular stress and radial boundary motion is identified from the term involving $\partial A / \partial \tau$ in the solid-phase equation of continuity and from the rate of propagation of intergranular disturbances. Some care is required in deducing the equilibrium value since the rate of propagation of intergranular disturbances is zero when the solid-phase is dispersed.

By analogy with the fully separated corner in the two-dimensional case, an independent analysis of the radial motion of the ends of the propelling charge is not conducted. The radial motion of the end points is assumed to be the same as that of the neighbors in the interior.

If the end of the propelling charge is in contact with an external boundary, the physical boundary conditions specify the axial velocity of each phase in each of the three coaxial regions. The thermodynamic state variables follow from the characteristic equations. The porosity follows from the equation of continuity for the solid-phase, when dispersed, and from the pseudo-characteristic form, when packed.

When the propelling charge is bounded by a lumped parameter region the velocity of the solid-phase is updated by reference to the momentum equation using one-sided differences to deduce all derivatives. The intergranular stress is required to vanish in this case and suitable adjustment of the porosity and velocity is made through the differential coefficients connecting these quantities. As with the transverse flow, the quadratic dependence of pressure on axial flow rate across the boundaries is neglected and the pressure in the lumped parameter region and each of the three coaxial regions is assumed to be the same. This physical boundary condition is imposed simultaneously with the characteristic relations between pressure and axial velocity for each of the three regions of continuum flow and the differential relationships between pressure in the lumped parameter region and rates of mass addition from each of the continua. Following the determination of the pressure, the three values of gas velocity are suitably corrected by reference to the characteristic forms. Values of density are deduced either from the characteristic forms, when the flow is directed into the lumped parameter region, or from an energy balance, with allowance for a reactive layer, when the flow is directed into the continuum region in question.

Details of the analysis when either of the radial ullage regions collapses locally due to expansion of the mixture and of the treatment at burnout are given in section 3.5.

3.4 Specification of Computational Mesh

We turn now to a discussion of the computational coordinates used in each of the subregions of the combustion chamber. In section 3.4.1 we discuss the programming strategy according to which the level of modeling of regions of ullage is established. In section 3.4.2 we discuss the procedure according to which we presently establish boundary fitted meshes for two-dimensional regions.

3.4.1 Programming Strategy

We discuss the programming strategy by reference to the relevant TDNOVA input variables to which we refer by their Fortran names.

Initially, a fully two-dimensional representation is always made of the propelling charge. It is assumed to be described by four boundary elements each of which has a continuously turning tangent. In most cases of practical interest the boundary elements are straight and consist of the rear and forward endwalls and the inner and outer circumferential boundaries. The rear endwall is taken to be a computational boundary defined by $\zeta = 0$ while the forward endwall is characterized by $\zeta = 1$. Similarly, the inner and outer circumferential boundaries correspond to $\eta = 0$ and $\eta = 1$, respectively.

The two-dimensional mesh in the propelling charge always involves a total of INDIMZ ζ -points and INDIMR η -points. The distribution of these points along each of the boundary elements is at the discretion of the user. If freedom of allocation is given to the code, the minimum mesh spacing will be maximized on each boundary element subject to the constraints imposed by the user.

The external boundaries are defined similarly to the boundaries of the propelling charge and are assumed to consist of four elements each of which has a continuously turning tangent. The elements are, in order of correspondence to their counterparts on the propelling charge boundary, the breechface, the projectile base, the tube centerline and the tube wall.

It is important to note that, in its present configuration, TDNOVA requires that the values of r increase monotonically on the breechface and projectile base and that the values of z increase monotonically on the tube centerline and the tube wall.

During the part of the solution in which the propelling charge is treated as fully-two-dimensional, the representation of the ullage depends on the input quantities NMSH, NMPT, ZFRAC and RFRAC, as we now discuss.

3.4.1.1 Static Mesh Allocation Mode

If NMSH = 0, the static mesh allocation option is employed. Each region of ullage contiguous with a mixture boundary element, see figure 1.3, is represented as quasi-one-dimensional, and each corner region of ullage is represented as lumped parameter. The distribution of mesh points in each quasi-one-dimensional region is controlled by the distribution of points on the boundary element of the propelling charge with which it is contiguous. For example, all mesh points in the region of ullage bounded by the breechface and rear endwall of the bag are defined by r -coordinates identical with their counterparts

on the rear endwall of the bag. But, for convenience in the tabulation of the solutions, the preparation of plots, and the determination of flow cross-sections, the z-coordinates are selected so as to place the mesh points on the breechface. Similarly, the mesh points corresponding to the ullage in front of the propelling charge are formally located on the projectile base, those corresponding either to ullage interior to the propelling charge, or to a centercore igniter, are placed on the tube centerline, and those corresponding to ullage exterior to the propelling charge are placed on the tube wall.

The single point corresponding to each of the lumped parameter corner regions is located formally on the appropriate corner of the external boundary in the static mesh allocation mode.

An important point to abstract from the foregoing discussion is the following. The flow through the end regions of ullage is assumed to be essentially radial so that the normal section of the flow is adequately captured by a surface on which $r = \text{constant}$. Similarly, the flow through the inner and outer ullage regions is assumed to be sufficiently close to axial that the flow sections can be described as surfaces of constant z .

We also note that in the static mesh allocation mode a total of $(\text{INDIMZ} + 2)(\text{INDIMR} + 2)$ mesh points are used to describe the flow. At present TDNOVA admits a maximum of 333 mesh points.

3.4.1.2 Dynamic Mesh Allocation Mode

If $\text{NMSH} = 1$, the dynamic mesh allocation mode is employed and in this case the input quantities NMPT, ZFRAC and RFRAC become active.

NMPT represents a maximum value for the number of mesh points which may be utilized at any time and is taken to include a minimum contribution of $\text{INDIMZ} * \text{INDIMR}$ points which are necessarily allocated to the propelling charge.

Consider now the region of ullage contiguous with the rear endwall of the bag. As in the static mesh allocation mode, INDIMR points are allocated to this region for the purpose of resolving the radial structure of the flow. The input quantity ZFRAC is used to establish the necessity of treating this region as two-dimensional rather than quasi-one-dimensional. The region will be treated as two-dimensional if each point on the rear endwall of the bag is located a distance from the breechface which is at least equal to two times ZFRAC times the length of the combustion chamber as a whole, as measured along a line of constant radius. The length of the combustion chamber as a whole is taken to be a measurement along the tube centerline.

Not only the region of ullage contiguous with the rear endwall but also the corner regions of ullage which terminate it are tested in respect to minimum axial extent since the representation of the corner regions is determined by that of the regions with which they are contiguous.

A similar procedure is conducted with respect to the ullage contiguous with the forward endwall of the propelling charge and also with the inner and outer regions of ullage, except that in the latter case, the quantity RFRAC is used and the length of the chamber is replaced by the radius of the tube.

However, a centercore igniter, if present, is always treated as a quasi-one-dimensional flow, independently of NMSH and independently of its lateral dimensions.

When the eligibility of the regions of ullage for treatment in a fully-two-dimensional fashion has been established, mesh points are allocated in such a fashion that the total does not exceed NMPT, that no two-dimensional region of ullage has a mesh spacing normal to the mixture which violates the ZFRAC or RFRAC criterion as the case may be, and so that the minimum mesh spacing is maximized. With regard to the ZFRAC and RFRAC criteria it should be noted that each two-dimensional region always has a minimum of three mesh points in each direction. It is for this reason that the factor of two is incorporated into the test for minimum extension normal to the propelling charge.

If a region of ullage contiguous with the mixture is determined to be quasi-one-dimensional, its mesh points are distributed in exactly the same fashion as in the static mesh allocation mode. If the region is determined to be two-dimensional and is contiguous, let us say, with the rear endwall the mesh is allocated as follows.

The boundary of the region of ullage contiguous with the rear endwall of the bag, for which $\zeta = 0$ in the mixture, is taken to be a line of $\zeta = 1$ for the ullage and mesh points are located with the same z- and r-coordinates as their counterparts on the bag endwall. The points on the breechface become points of $\zeta = 0$ for the mesh in the ullage and are given r-coordinates identical with their counterparts on the ullage boundary $\zeta = 1$. Thus the lines on which $\eta = \text{constant}$ in the ullage are lines of constant radius. On $\eta = 0$ and on $\eta = 1$ the mesh is specified so as to yield a uniform spacing. The distribution in the interior is determined according to the algorithm described in section 3.4.2.

If the corner region contiguous with the $\eta = 0$ boundary of the ullage region in question is quasi-one-dimensional, its axial distribution of mesh points is governed by those on the $\eta = 0$ coordinate line but the radial coordinates are chosen so as to place the points formally on the centerline.

If the corner region is two-dimensional the mesh on its boundary is defined as follows. The distribution on the line $\eta = 1$ of the corner region is identical with that of the line $\eta = 0$ in the region of ullage contiguous with the rear endwall of the bag. The distribution on the line $\zeta = 1$ of the corner region is identical with that on the line $\zeta = 0$ of the region of ullage contiguous with the inner boundary of the bag. To define the distribution on the line $\zeta = 0$ in the corner region, a chord is drawn from the point ($\zeta = 0, \eta = 1$) to the corner of the external boundary. A series of equispaced points is defined on this line and these in turn are projected along lines of constant radius so as to be located on the curved breechface. A similar procedure is conducted at the centerline.

The procedure we have outlined is conducted in a similar fashion for all the two-dimensional regions of ullage until the mesh has been defined on the boundaries of all two-dimensional regions and completely for all quasi-one-dimensional and lumped parameter regions. The distribution of mesh points in the interior of the two-dimensional regions is the subject of the next section.

When the number of mesh points assigned to a given region changes, the state variables at the new complement of mesh points are defined by a linear interpolation of the old values. If the old mesh was one-dimensional, the old values are applied uniformly along the freshly introduced coordinate line. Conversely, if the new mesh is one-dimensional, the values are taken to be those corresponding to the coordinate lines adjacent to the mixture or adjacent to the regions of ullage contiguous with the mixture if we are dealing with a corner region.

3.4.1.3 Transformation to Quasi-Two-Dimensional Representation

We conclude the present discussion with some comments on the transformation from the fully-two-dimensional representation to the quasi-two-dimensional representation.

When the propelling charge has been ignited at all points and the bag has completely ruptured, the input datum PTOL is used to determine the suitability of a quasi-two-dimensional analysis. At each axial location in the chamber, the difference between the values of pressure at the tube wall and the centerline is divided by the value at the tube wall. If this quantity is less than PTOL at all axial stations, an irrevocable transformation to a quasi-two-dimensional representation is made.

The axial distribution of the propellant is assumed to be defined

by the current storage for the line $\eta = 0$. Values of the porosity are defined by integrating with respect to η at each ζ -mesh point and normalizing by the local cross-sectional area of the propelling charge. This approach provides values of porosity which satisfy a global mass balance as estimated by a trapezoidal rule. The solid-phase axial velocity field is also defined as an average with respect to η . At each ζ -location the radial coordinates and velocities of the inner and outer boundaries of the propelling charge are taken to be the values in current storage at $\eta = 0$ and $\eta = 1$ respectively. The intergranular stress and surface regression are taken to be the values corresponding to $\eta = 0$.

The rear and forward external boundaries are defined respectively by the intersections of the breechface and projectile base with the centerline of the tube. The gas-phase properties are not averaged with respect to η in the present version of the code. The values used to initialize the quasi-two-dimensional region are taken to be those in current storage for the line $\eta = 0$. Values of the radial component of the gas velocity are, however, saved at both the internal and external circumferential boundaries since these are used in the quasi-two-dimensional representation to define the transverse mass fluxes between the coaxial quasi-one-dimensional flows.

As a final comment we note that following the transformation to a quasi-two-dimensional representation, the mesh is taken to move so as to preserve its shape at the instant of transformation.

3.4.2 Mapping Algorithm

The distribution of mesh points in the interior of the two-dimensional regions is presently established by means of an algorithm due to Thompson et al³⁵. The computational coordinates ζ and η may be embedded into a pair of elliptic equations as follows.

$$\zeta_{zz} + \zeta_{rr} = 0 \quad 3.4.2.1$$

$$\eta_{zz} + \eta_{rr} = 0 \quad 3.4.2.2$$

³⁵Thompson, J. F., Thames, F. C. and Mastin, C. W. "Automatic Numerical Generation of Body-Fitted Curvilinear Coordinate System for Field Containing Any Number of Arbitrary Two-Dimensional Bodies." *J. Comp. Phys.* 15, pp. 299-319. 1974

We do not solve 3.4.2.1 and 3.4.2.2 directly. Rather, we solve the inverted system.

$$\alpha z_{\zeta\zeta} - 2\beta z_{\zeta n} + \gamma z_{nn} = 0 \quad 3.4.2.3$$

$$\alpha r_{\zeta\zeta} - 2\beta r_{\zeta n} + \gamma r_{nn} = 0 \quad 3.4.2.4$$

where

$$\alpha = z_n^2 + r_n^2$$

$$\beta = z_\zeta z_n + r_\zeta r_n$$

$$\gamma = z_\zeta^2 + r_\zeta^2$$

As we have described in the preceding section, Dirichlet data are prescribed for these equations on the boundaries of all two-dimensional regions. Then equations 3.4.2.3 and 3.4.2.4 are discretized by replacing all derivatives by second order accurate finite differences and the resulting system is solved by the method of successive over-relaxation³⁴.

This procedure is used to define the initial distribution of mesh points in the propelling charge. Subsequently, however, the mesh within the propelling charge is assumed to follow the motion of the solid-phase so that the coordinate scheme may be described as solid-phase Lagrangian.

In the two-dimensional regions of ullage, however, the equi-potential mesh algorithm is employed at each level of each integration step. The velocity of the mesh, as required by the balance equations, is determined from a first order finite difference of the coordinate field with respect to time.

3.5 Special Topics

In this concluding section we document details of certain special topics. We address, in successive subsections, the treatment of the tangential velocity component of the gas phase; the treatment of the flow as burnout occurs; the treatment when a region of ullage, or the centercore igniter, collapses locally; the ignition of propellant located on the boundaries; and, finally, the treatment of the boundary values of the solid-phase in the igniter charge in the quasi-two-dimensional representation.

3.5.1 Treatment of Tangential Velocity of Gas Entering Mixture

We have already noted in several places in the present report that, in order to render the numerical analysis more tractable, we consider a loss of tangential momentum when gas enters the mixture. The purpose of the present note is to document the details of the method whereby this loss is calculated.

Considering only the influence of pressure gradient and interphase drag, and treating the solid-phase as stationary, the unsteady motion of the gas-phase may be described by the equation

$$\frac{Du}{Dt} = - \frac{1}{\rho} \nabla p - a k u^2 \quad 3.5.1.1$$

where $k = \text{sgn}(u)$ and the coefficient a may be identified from the law 2.2.4.3.

Now let u_∞ be a steady state solution subject to the assumption that ∇p is constant so that

$$a k_\infty u_\infty^2 = - \frac{1}{\rho} \nabla p \quad 3.5.1.2$$

Evidently, 3.5.1.2 permits us to recast 3.5.1.1 as

$$\frac{Du}{Dt} = a(k_\infty u_\infty^2 - k u^2) \quad 3.5.1.3$$

Then treating a , k_∞ , u_∞ , k as constants, we may integrate 3.5.1.3

along the gas streamline with the following result. Let u_0 be an initial value of u . Then, if $u_0 u_\infty > 0$, we have

$$\frac{u}{u_\infty} = \frac{u_\infty(e^{2aku_\infty t} - 1) + u_0(e^{2aku_\infty t} + 1)}{u_\infty(e^{2aku_\infty t} + 1) + u_0(e^{2aku_\infty t} - 1)} \quad 3.5.1.4$$

But, if $u_0 u_\infty < 0$, then we introduce

$$t_* = \frac{\tan^{-1}(-u_0/u_\infty)}{ak_\infty u_\infty} \quad 3.5.1.5$$

whereupon u is governed by

$$\frac{u}{u_\infty} = \begin{cases} \frac{u_\infty \tan(ak_\infty u_\infty t) + u_0}{u_\infty - u_0 \tan(ak_\infty u_\infty t)} & \text{if } t < t_* \\ \frac{e^{2ak_\infty u_\infty(t - t_*)} - 1}{e^{2ak_\infty u_\infty(t - t_*)} + 1} & \text{if } t \geq t_* \end{cases} \quad 3.5.1.6$$

In order to make use of these results we proceed as follows. The initial quantity u_0 is identified with the tangential velocity of the gas in the ullage prior to transport into the mixture. The quantity u_∞ is identified with the tangential component of velocity of the gas-phase within the mixture at a mesh point adjacent to the boundary. The quantities a and k_∞ are determined from the current storage on the boundary. Finally, the relaxation time t is evaluated as the result of dividing the initial diameter of a propellant grain by the normal velocity of the gas entering the mixture.

This procedure should be understood to represent nothing more than an evaluation of the boundary value as an average of the values external and internal to the interface using weighting coefficients

which are sensitive to the mechanical relaxation time in the mixture.

3.5.2 Treatment at Burnout

Burnout is assumed to occur in either the propelling charge or the centercore igniter when the porosity exceeds the value 0.999. At this point the value of porosity is replaced by the value 1.0 and the velocity of the solid-phase, possibly required for the formation of finite differences at neighboring points for which burnout has not yet occurred, is assumed to be equal to that of the gas-phase. In fact this limit is approached asymptotically in all cases involving burnout in the NOVA code¹⁴ because of the influence of the interphase drag.

When the solution is being determined according to a quasi-two-dimensional representation the local cross section of the mixture is taken to fill completely the tube so that the outer and inner regions of radial ullage are formally represented as collapsed at a section where burnout occurs.

3.5.3 Treatment When Region Collapses

Physically reasonable values of the state variables are retained in all computational regions at all times even when they are locally collapsed due to proximity of the propelling charge to an external boundary. When a region is collapsed the values of the state variables are taken to be equal to those in the mixture at the appropriate boundary point. At present, a region is taken to be collapsed whenever its transverse dimension is less than 1 mm.

3.5.4 Ignition of Boundary Points

As in our preceding study¹ the surface temperature of grains on the boundary of the propelling charge is replaced by the value at its neighbor in the interior whenever the neighbor has a higher value. This device is introduced to ensure ignition at the boundaries in cases when the local gas convection is very weak due to the presence of an impermeable boundary.

3.5.5 Boundary Values of Solid-Phase in Centercore Igniter

As presently formulated, TDNOVA does not allow flux of the solid-phase ignition charge through the ends of the centercore tube. Towards the end of the interior ballistic cycle it may be found that the grains of black powder tend to move at significantly different velocities than the grains of propellant which envelope the centercore region. Accordingly, the condition of impermeability at the ends of the centercore tube may result in considerable condensation of the solid-phase in cases where the tendency toward efflux is pronounced. Indeed, the boundary values of porosity in the centercore may decrease to values much less than the settling condition whereas the values everywhere else are close to unity. This numerical difficulty is exacerbated by the fact that the radial motion of the ends of the bag is not determined on an independent basis, but is, rather, tied to the motion of the neighboring interior point.

In subsequent work this problem will be eliminated in a physically correct fashion, namely by incorporating a flux boundary condition for the solid-phase and accounting for the presence of the black powder in the axially distributed ullage which receives it. For the present we have simply incorporated a continuative boundary condition for the porosity and intergranular stress of the solid-phase in the centercore igniter, at both ends, during the quasi-two-dimensional part of the solution.

4.0 A COMPUTATIONAL EXAMPLE

The purpose of the present chapter is to illustrate the operability of the code TDNOVA. To this end we select a problem based as closely as possible on an existing bag charge, namely the 155 mm M203. Certain compromises are made, however, partly for reasons of economy and partly because of the uncertainties attached to the process of flamespreading through black powder. The data base used for the computational example is discussed in section 4.1. In order to acquaint the reader with the nature of the code input files, the discussion of the data is given in some detail. The solution itself is discussed in section 4.2.

4.1 Discussion of Input Data

The problem to be studied involves the complete interior ballistic cycle of a single bag top zone 155 mm howitzer propelling charge. The propellant is represented as contained within a bag which is permeable over the rear end wall and over the first third of the external circumferential boundary. The bag is impermeable, initially, over the forward two-thirds of the external circumferential boundary and the outer part of the forward end closure. The bag surrounds a centercore igniter which is represented as being uniformly distributed over the length of the charge. The boundary between the centercore igniter and the propelling charge is taken to be fully permeable.

Figure 4.1.1 provides an illustration of the representation of the charge in its initial configuration. The calculation reflects such details of the geometry of the confining boundaries as the shape of the breechblock and the boattail of the projectile. The geometrical data are based on the configuration of the M199 cannon and the M438A1 projectile.

Continuing with the description of the initial configuration of the charge, we note that the boundary is taken to be an exterior envelope of the bag, including all additives. The thickness of the bag is neglected and the propellant is assumed to be uniformly distributed within the exterior envelope. Accordingly, the initial porosity of the charge will be represented as slightly greater than the settling porosity which would be observed in practice. The representation of the forward two-thirds of the external circumferential boundary as impermeable is intended to reflect the presence of a lead foil liner which is incorporated into the bag in order to reduce the buildup of copper deposits on the rifling of the tube by the rotating band of the projectile. The representation of the outer part of the forward end closure as initially impermeable is intended to reflect the presence of the salt bag.

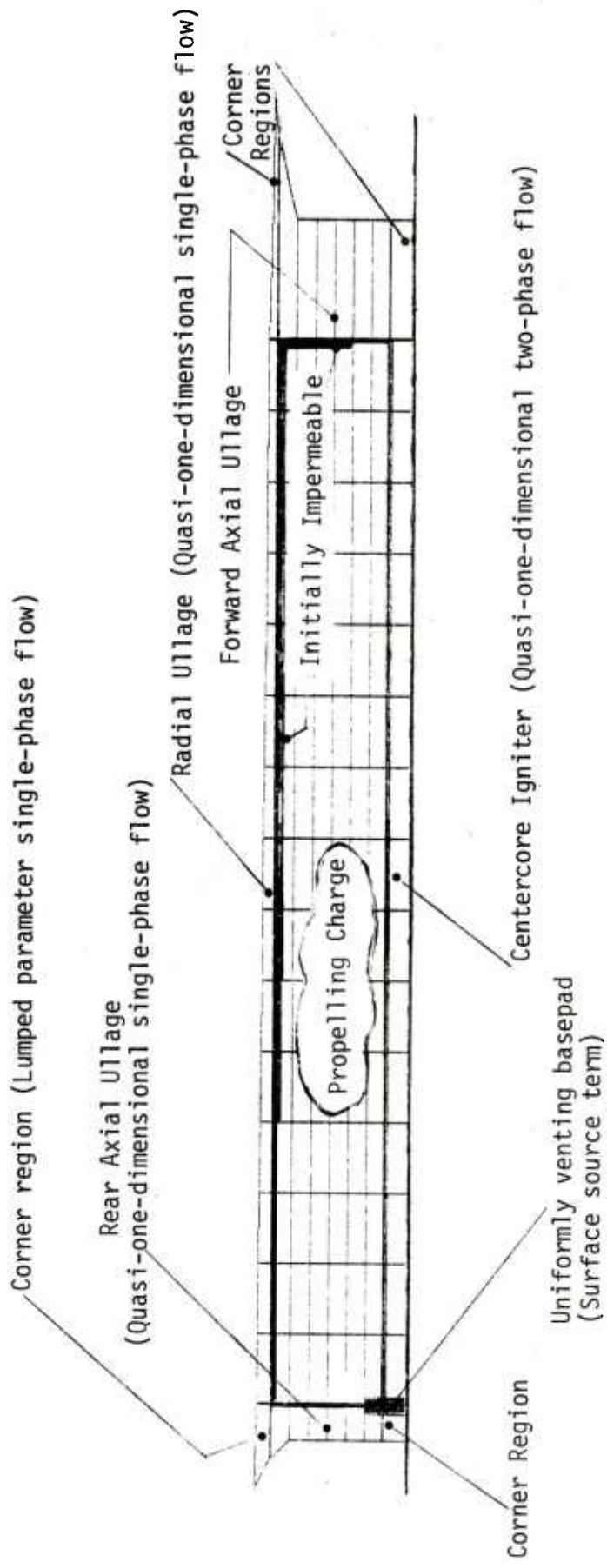


Figure 4.1.1 Representation of Computational Example (155mm M203)

In describing the boundary of the charge as an exterior envelope of the bag, it should be understood that the word external is used in a topological sense. Accordingly, the internal circumferential boundary of the charge is located so as to include the centercore tube within the region occupied by the propellant rather than the region occupied by the igniter. In the present calculation neither the reactivity of the centercore tube nor the resistance to flow of the gas phase through the tube wall is considered. It is probable that the permeability of the centercore tube is strongly influenced by its reactivity and susceptibility to thermal attack, processes for which our current model can make only ad hoc allowance through the specification of predetermined tabular data. The neglect of these processes in the present calculation is intended as a simplification in the face of an absence of data the determination of which we emphatically encourage.

Reactivity of the bag is considered, however, over that part of the rear endwall which is covered by the basepad. The basepad also covers the centercore igniter tube in the present axisymmetric representation so that the calculation will reflect an initial thermal stimulus, by the basepad, both to the centercore charge and to the main propelling charge. The rate of discharge of products of combustion by the basepad is specified by a table of predetermined values. The thickness of the basepad, as with all components of the bag, is ignored and the mass generation is viewed as a surface phenomenon.

The real initial thermal stimulus created by the discharge of the products of combustion of a primer located in the breechblock is not represented. The initial stimulus in the present calculation is taken to be due to the reaction of the basepad in accordance with the prespecified discharge data.

Subsequently, the spreading of a convective flame through both the centercore igniter and the main charge is modeled as part of the macroscopic two-phase flow.

At the beginning of this chapter we observed that while the computational example was selected with a view to relevance to an existing charge, certain compromises in the data are made for the sake of simplification. We have already mentioned such details as the neglect of the thickness of the bag and the reactivity and impermeability of the centercore tube. Additional compromises are made in respect to the representation of the black powder igniter charge. First, the igniter charge is represented as uniformly distributed over the length of the charge. It is, in fact, confined to about two-thirds of the length. This simplification is intended to circumvent

the computational burden of representing a discontinuous distribution of porosity over the length of the centercore igniter. Second, the heat of combustion of the black powder, both in the basepad and the centercore, is given a substantially higher value than is obtained in reality. This compromise is made in order to permit the calculated gas-phase temperature to be correct when the specific heat is taken to be that of the main propelling charge. In later work we will, of course, include a composition dependence of the thermodynamic properties of the gas-phase so that this second compromise will no longer be necessary. The decision to give fidelity of representation of the temperature priority over the internal energy is based on the desire to assure a strong thermal stimulus to the propellant so that the calculation need not be continued for too extended a period of time prior to the onset of flamespreading.

The third compromise is based on the same consideration. The ignition temperature of the black powder is specified as being just a few degrees over ambient. In fact, the ignition temperature of black powder is known to be rather high, namely 469°C ³⁶. However, the process of flamespreading through black powder is believed to be outside the scope of the present formulation since we neglect altogether the stimulus associated with the discharge of hot molten salts. Our treatment of the igniter charge according to a two-phase representation is based solely on our desire to reflect the impediment to axial flow of the gas-phase by the black powder grains. The use of an extremely low ignition temperature for the black powder may possibly be interpreted as an ad hoc compensation for the thermal stimulus induced by molten salts which are transported in mechanical equilibrium with the macroscopic flow of the gas. However, we emphasize that the present goal is simply to ensure that flamespreading does indeed occur within the context of a model which embeds only a convective stimulus.

We turn now to a discussion of the data given in Table 4.1 which lists the complete TDNOVA input for the computational example.

Control parameters are set by the user to determine the type of output to be obtained. Several forms of graphical output are available, including isometric carpet plots of the state variables, contour plots, flowfield plots and a flamespreading map. It should be noted that the figures presented in section 4.2 were not produced by the control data of Table 4.1, but were produced by a separate run of a post-processing routine using the solutions as saved on the disc. All TDNOVA solutions may be restarted from disc storage.

³⁶ Lenchitz, C. and Hayes, E. "An Analysis of Black Powder Ignition and Performance. Ignition Properties of Black Powder, Phase I." Proc. 16th JANNAF Combustion Meeting

1979

Table 4.1 Input Data for Computational Example

	155mm	M203	Charge	M199 Cannon	M483A1 Projectile
CONTROL PARAMETERS					
NPRINT	(0 = no print, 1 = print)				1
NSUMRY	(0 = no summary tables, 1 = yes)				1
NPLOT	(0 = no isometric carpet plots, 1 = plot)				1
NVHL	(0 = hidden lines deleted, 1 = retained)				0
NPLCON	(0 = no contour plots, 1 = plot)				0
NPLFLO	(0 = no flow plots, 1 = plot)				0
NPLFLM	(0 = no flamespread plot, 1 = plot)				0
NDSKW	(0 = no disc save, 1 = disc save)				1
NDSKR	(0 = no disc start, >0 = disc start at step NDSKR)				0
ISOMETRICALLY PLOTTED QUANTITIES (1 = YES, 0 = NO)					
Mesh 1 Porosity	0	Granular stress	0	Pressure	0
Density	0	Gas axial velocity	0	Solid axial velocity	0
Gas radial velocity	0	Solid radial velocity	0	Gas temperature	0
Particle surface temperature	0				
CONTOUR PLOTTED QUANTITIES (1 = YES, 0 = NO)					
Mesh 0 Porosity	0	Granular stress	0	Pressure	0
Density	0	Gas axial velocity	0	Solid axial velocity	0
Gas radial velocity	0	Solid radial velocity	0	Gas temperature	0
Particle surface temperature	0				
Scale factor for plotting (-)					0.65
Length of z-axis in CALCOMP plots (in)					25.01
Length of r-axis (in)					4.01
Length of ordinate axis (in)					5.00
LOGOUT PARAMETERS					
Number of steps before logout					1000
Time increment before logout (msec)					0.200
Number of pressure summary stations					2
Time increment for pressure summary storage (msec)					0.200
			100		

Table 4.1 (continued)

TERMINATION PARAMETERS	
Maximum number of steps before termination	1200
Maximum integration time (msec)	25.0
Maximum projectile travel (cm)	520.7
MESH PARAMETERS	
Mesh allocation mode (0 = static, 1 = dynamic)	0
Maximum number of storage points for dynamic mesh allocation	0
Number of mesh points in axial direction	16
Number of mesh points in radial direction	7
Number of iterations to determine initial mesh	200
Safety factor for C-F-L criterion	1.1000
Maximum fractional displacement for convergence of initial mesh distribution	0.100D-04
Over-relaxation factor for determination of initial mesh distribution	1.600
Pressure tolerance factor for reduction to quasi-two-dimensional representation (-)	0.1
Axial spatial resolution factor (-)	0.100
Radial spatial resolution factor (-)	0.100
AMBIENT CONDITIONS	
Initial temperature (deg.K)	294.4
Initial pressure (MPa)	0.1014
Charge Standoff (cm)	0.0
SOLID-PHASE CONSTITUTIVE DATA	
Initial mass of granular bed (kg)	11.8620
Initial porosity of granular bed (-)	0.0
Settling porosity of granular bed (-)	0.0
Speed of compression wave (m/sec)	152.4
Speed of expansion wave (m/sec)	1270.0

Table 4.1 (continued)

SOLID-PHASE CONSTITUTIVE DATA (cont.)

Density of solid-phase (gm/cc)	1.5830
Thermal conductivity (J/cm-sec-deg.K)	0.0016
Thermal diffusivity (cm**2/sec)	0.0006

GAS-PHASE CONSTITUTIVE DATA

Ratio of specific heats (-)	1.24300
Molecular weight (gm/gm-mol)	23.360
Covolume (cc/gm)	1.030

SOLID-PHASE COMBUSTION CHARACTERISTICS

Max Pressure (MPa)	Burn Rate Constant (cm/sec)	Pre-Exponent (cm/sec-MPa ⁿ)	Exponent (-)
69.	0.	0.4117	0.6337
690.	0.	0.2218	0.7864

GRAIN GEOMETRY

External Diameter (cm)	1.060
Length (cm)	2.408
Diameter of perforations (cm)	0.086
Number of perforations (-)	7.

CONFIGURATION OF REAR OF BAG

Axial Position(cm)	Radial Position(cm)	Flow Res. Data	Reactivity Data	No. Pts Pre-assigned	Data (0=D,1=N)
2.540	1.270	0	1	0	0
2.540	3.387	0	0	0	0
2.540	7.620	0	0	0	0

Table 4.1 (continued)

CONFIGURATION OF FRONT OF BAG

Axial Position(cm)	Radial Position(cm)	Flow Res. Data	Reactivity Data	No. Pts Pre-assigned	Data (0=D,1=N)
78.740	1.270	0	0	0	0
78.740	3.387	1	0	0	0
78.740	7.620	0	0	0	0

CONFIGURATION OF INSIDE OF BAG

Axial Position(cm)	Radial Position(cm)	Flow Res. Data	Reactivity Data	No. Pts Pre-assigned	Data (0=D,1=N)
2.540	1.270	0	0	0	0
78.740	1.270	0	0	0	0

CONFIGURATION OF OUTSIDE OF BAG

Axial Position(cm)	Radial Position(cm)	Flow Res. Data	Reactivity Data	No. Pts Pre-assigned	Data (0=D,1=N)
2.540	7.620	0	0	0	0
27.940	7.620	1	0	0	0
78.740	7.620	0	0	0	0

CONFIGURATION OF BREECH

Axial Position(cm)	Radial Position(cm)
0.0	0.0
0.0	7.061
-3.454	8.484

CONFIGURATION OF PROJECTILE BASE

Axial Position(cm)	Radial Position(cm)
87.380	0.0
87.380	7.137
96.420	7.849

Table 4.1 (continued)

CONFIGURATION OF INSIDE BOUNDARY

Axial Position(cm)	Radial Position(cm)
0.0	0.0
87.380	0.0

CONFIGURATION OF OUTSIDE BOUNDARY

Axial Position(cm)	Radial Position(cm)
-3.454	8.484
92.460	8.052
96.420	7.849

REPRESENTATION OF IGNITION TRAIN

NCCORE	(0 = no centercore, 1 = yes)	1
BASEPAD REACTIVITY DATA		1
NTABIG	(0 = no external stimulus, 1 = yes)	0

PROPERTIES OF SOLID-PHASE IN CENTERCORE

SOLID-PHASE CONSTITUTIVE DATA

Initial mass of granular bed (kg)	0.1134
Initial porosity of granular bed (-)	0.0
Settling porosity of granular bed (-)	0.40000
Speed of compression wave (m/sec)	442.0
Speed of expansion wave (m/sec)	1270.0
Density of solid-phase (gm/cc)	1.7990
Thermal conductivity (J/cm-sec-deg.K)	0.0016
Thermal diffusivity (cm**2/sec)	0.0006

SOLID-PHASE COMBUSTION CHARACTERISTICS

Ignition temperature (deg.K)	300.0
Chemical energy (J/gm)	2489.

Max Pressure (MPa)	Burn Rate Constant (cm/sec)	Additive Pre-Exponent (cm/sec-MPa ⁿ)	Exponent (-)
0.5167	0.0	2.508	0.462
690.	0.0	2.007	0.133

Table 4.1 (continued)

GRAIN GEOMETRY			
External diameter (cm)			0.300
Length (cm)			0.0
Diameter of perforations (cm)			0.0
Number of perforations (-)			0.
PROPERTIES OF PROJECTILE			
Projectile mass (kg)			46.720
BORE RESISTANCE DATA			
Projectile Travel(cm)		Resistive Pressure(MPa)	
0.0		1.720	
1.016		23.100	
2.540		34.100	
3.937		25.000	
5.207		22.400	
11.430		17.200	
520.700		10.300	
BAG FLOW RESISTANCE DATA			
Type	Initial Friction Factor(-)	Rupture Stress(MPa)	Rupture Interval(msec)
1	1000.000	0.101	0.0
DATA TO DESCRIBE REACTIVITY OF BAG SUBSTRATE 1			
Energy released during decomposition (J/gm)			2489.
BAG SUBSTRATE DISCHARGE CHARACTERISTICS			
Time(msec)	Rate of Discharge(gm/cm**2-sec)		
0.0			2.620
0.100			26.200
30.000			26.200

Table 4.1 (Concluded)

LOCATION OF POINTS FOR PRESSURE SUMMARY TABLE

Axial Location(cm)	Wall(0) or Axis(1)
0.010	0
87.370	0

The choice of isometrically and contour plotted variables is further defined by the blocks of data listed under the heading "isometrically plotted quantities" and "contour plotted quantities".

Logout of the solution, in the form of printed tables of the solution, disc storage of the same and any of the optional forms of plotting may be had at multiples of a fixed number of integration steps and a fixed increment of time. If summary tables are to be constructed, the user also specifies a fixed time increment for storage. Termination of the solution occurs whenever any of a maximum number of steps, a maximum integration time or a maximum projectile displacement is satisfied.

The present computational example is based on the static mesh allocation mode. Thus a fixed complement of 16 axial mesh points and 7 radial mesh points is assigned to the fully two-dimensional representation of the propelling charge. The centercore igniter and the ullage on each side of the propelling charge are each treated as quasi-one-dimensional and the four corner regions are therefore treated as lumped parameter. A total of 162 mesh points are therefore in use during the fully two-dimensional part of the solution.

The initial distribution of the mesh within the propelling charge is established by successive overrelaxation of a pair of coupled elliptic equations subject to boundary conditions which describe the distribution of points on the bag surface. A maximum of 200 iterations is permitted to establish convergence to within a fractional displacement of 10^{-5} using an overrelaxation factor of 1.6. Because of the small number of points and the regularity of the boundary geometry only 36 iterations were actually required to produce convergence to within 0.8×10^{-5} .

The pressure tolerance factor is specified as 0.1 with the significance that a transformation of the problem to a quasi-two-dimensional representation will occur following the completion of flamespreading and total rupture of the bag when the difference between the values of pressure at the centerline and the tube wall does not exceed 10% of the value at the tube wall at any axial station in the chamber. The axial and radial spatial resolution factors have been set equal to 0.1, but as the static mesh allocation mode has been elected these values do not influence the calculation.

The fully two-dimensional part of the calculation required 448 steps, the transition to a quasi-two-dimensional representation occurring at 3.08 msec. A total of 120 CPU seconds were required on

the ITEL AS-6 processor. The conclusion of the calculation as a quasi-two-dimensional flow required an additional 309 steps, muzzle exit occurring after 757 steps in total and at 16.5 msec. An additional 31 CPU seconds were required for this part of the calculation. Computation times on the CDC 7600 should be approximately 30% faster. It should be noted, however, that the ITEL machine uses a 32-bit word whereas the CDC machine uses a 60-bit word. Hence, the present calculations which are performed in double precision on the ITEL machine could, in principle, be performed on the CDC machine in single precision, with only a slight increase in round-off error. Such a measure could introduce a further reduction in CPU time by a factor of two to four. Thus it is expected that the present example can be completed in approximately 110 CPU seconds as a double precision calculation on the CYBER 7600 and in approximately 28-55 CPU seconds if a single precision copy of the code were developed.

Returning to Table 4.1 we note the ambient conditions for the problem. Both phases are at room temperature and atmospheric pressure. The charge standoff has been entered as 0 cms. However, it should be understood that this datum is added to all the axial coordinates used to define the initial bag configuration. These data represent the charge as having a standoff of 2.54 cm with respect to the breech face. Hence, a subsequent run with the bag moved back to contact the breech face would require that the standoff parameter be set equal to -2.54 cm, provided that the present tabular description of the bag boundary were retained.

A total of 11.8 kg of propellant is used, type M30A1. The thermochemical data are as used in a previous study by Horst²⁰.

The bag is described by four tables of points which respectively define the rear endwall, the forward endwall, the internal circumferential boundary and the external circumferential boundary. Each entry in each table consists of six data. The first two are the axial and radial coordinates of a point on the boundary element in question. The third datum is a pointer to a data set which describes the flow resistance of the boundary element defined by the point in question and its successor in the table. The fourth datum is a pointer to a reactivity data set for the same segment. The physical attributes defined by the resistance and reactivity data sets are applied to the mesh point allocated to the boundary point in question and to all mesh points in the segment defined by its successor in the table, but not to the successor itself. The fifth datum defines a number of points to be pre-allocated to the boundary segment. Since zero values are used, the allocation is performed automatically by the code in such a fashion as to maximize the minimum mesh spacing along each side of the bag. The sixth and final datum describes the nature of

the boundary condition to be used in establishing the mesh. The zero entry implies that Dirichlet data will be used.

The geometry of the external boundaries is established by four additional tables. However, these consist only of values of the coordinates.

With regard to the definition of the rear of the bag it will be noted that a reactivity data set is referenced for the inner part of the endwall. This is intended to describe the basepad. We see, in Table 4.1, that the data define the existence of a centercore igniter and that the same reactivity data set is referenced in this context. This simply means that the rate of discharge of that part of the basepad which covers the end of the centercore tube will be the same as that which covers the inner segment of the bag endwall. No external stimulus, as used in the NOVA code¹⁴, is considered.

The subsequent body of data describes the properties of the centercore igniter and is intended to describe black powder, the notable exceptions being the chemical energy and the ignition temperature, as discussed previously. The burning rate is taken from Rose et al³⁷.

It should be noted that for both the main charge and the igniter charge the initial porosity has been entered as zero. The code action in such a case is to establish the value from the entered value of mass and the computed value of the volume available to the charge. The settling porosity of the main charge is also entered as zero with the consequence that the initial value will be used as a default. However, the settling porosity of the igniter is specifically entered as 0.4 and it will be this value which is used, rather than the computed initial value.

The projectile mass corresponds to the M438A1 projectile and the bore resistance data are as used previously by Horst²⁰.

Only one bag flow resistance data set is used. The friction factor is set equal to 1000. In the present version of the code a value equal to or greater than 100 is understood to mean that the section in question is totally impermeable to the gas-phase. The rupture pressure is set equal to one atmosphere and the rupture interval is entered as zero so that the local transition from fully impermeable to fully permeable behavior occurs at the instant when the internal pressure exceeds the external pressure by one atmosphere.

³⁷Rose, J. E. and Hardt, A. P. "Black Powder--A Modern Commentary--1979." Proc. 10th Symposium on Explosives and Pyrotechnics, Franklin Research Center, Phila., PA Feb. 14-16 1979

Only one reactivity data set is entered. Its entries consist of a value of chemical energy and a table of the rate of discharge per unit area as a function of time.

The final entry to the code consists of the axial locations of two points at which pressure histories are to be established. The locations refer to the breech and mouth of the chamber and are assumed to be located on the tube wall.

4.2 Discussion of the Solution

We turn now to the details of the solution. The use of an extremely low ignition temperature for the black powder in the centercore has the result that flamespreading occurs quite rapidly through the igniter. The combustion of the centercore establishes a strong radial convection which quickly heats the propellant in the vicinity of the centercore to the point of ignition. This burning propellant yields additional hot gas which flows both radially and axially to promote the process of convective flamespreading through the propellant.

The path of flamespreading is illustrated in figure 4.2.1 which is a Lagrangian map of the process in the sense that the locus of the ignition front is referred to the original configuration of the propelling charge. The convective flame is seen to have a conoid shape whose apex travels through the centercore.

Motion of the propellant during flamespreading is not substantial. Figures 4.2.2 and 4.2.3 respectively display the complete computational mesh at the initial instant and just prior to the completion of flame-spreading. The forward endwall of the propelling charge has hardly moved at the conclusion of flamespreading. However, significant deformation of the bag has occurred at the rear endwall as a consequence of the vigorous venting of the basepad. The centercore is seen to have introduced a perceptible radial expansion of the charge near the rear. Not so obvious is the compression of the front of the bag due to excess gas pressure applied to the outside of the still impermeable external boundary.

Figures 4.2.4 and 4.2.5 display distributions of porosity at 0 and 3 msec. In these figures the porosity has been plotted as zero rather than unity in the ullage for the sake of clarity. It should be noted that the initial porosity in the centercore is approximately 0.8. This high value is a consequence of representing the igniter charge as uniformly distributed over the length of the centercore. At the conclusion of flamespreading the distribution of porosity has not changed

greatly, as may be seen in figure 4.2.5.

Figures 4.2.6 through 4.2.18 present the structure of the pressure field at various times throughout the entire interior ballistic cycle.

At the earliest time shown, figure 4.2.6, there is a significant excursion near the rear of the bag due to the venting of the basepad. We observe, by reference to Table 4.1, that the basepad is represented as initially producing a surface mass flux of $2.62 \text{ gm/cm}^2\text{-sec}$ and that this value rises to $26.2 \text{ gm/cm}^2\text{-sec}$ over a period of 0.1 msec. Since the products of the basepad will initially have internal energy approximately equal to $e_{IG}/\gamma \approx 2000 \text{ J/gm}$ and pressure of the order of 1 atmosphere or 0.1 MPa, it follows that the initial density of the reactants will be approximately $2 \times 10^{-4} \text{ gm/cm}^3$. Accordingly, the gas velocity associated with the predetermined flux will initially have the approximate value 1.27×10^4 which corresponds to a Mach number of 0.16. As the flux rises by a factor of ten over 0.1 msec, the pressure is seen, from the solution, only to increase between two- and three-fold. Thus the Mach number associated with the predetermined flux increases to the range 0.5-0.8. Accordingly, the momentum flux becomes a significant component of the total thrust. As the propelling charge is relatively impermeable, the reactants of the basepad flow predominantly into the rear ullage. The contribution of the momentum flux is therefore to produce a significantly higher pressure in the propelling charge than in the ullage and this condition may be expected to persist until the ambient pressure reaches a value of approximately ten atmospheres so that the momentum flux associated with the predetermined surface flux no longer makes a significant contribution to the thrust.

Because the propellant is relatively impermeable by comparison with the centercore the pressure is somewhat depressed at the centerline. By 0.4 msec the pressure has nearly equilibrated over the tube cross section at the rear except in the immediate vicinity of the basepad. Some numerical distortion is to be expected during this phase of the calculation due to the coarseness of the mesh and both the localization and discontinuous nature of the model of the basepad venting characteristics.

At 0.6 msec, figure 4.2.8, the pressure front is seen to be advancing axially through both the centercore and the main charge although the rate of advance through the latter is somewhat retarded. By 1.0 msec, figure 4.2.9, the pressure front has penetrated almost halfway through the charge. Because the forward part of the outside of the bag is impermeable, a discontinuity in pressure is seen to develop as the ignition and combustion gases flow around the outside. The excursion due to the basepad is still visible.

By 1.6 msec, figure 4.2.10, the pressure field is nearly one-dimensional over the rear part of the charge. The discontinuity in pressure supported by the impermeable section of the bag is clearly visible. The excess pressure is, of course, supported by the inter-granular stress and is responsible for some compression of the forward part of the charge.

At 2.0 msec, figure 4.2.11, it may be inferred that part of the outside of the bag has ruptured since the pressure has become continuous. By 2.8 msec, figure 4.2.12, the pressure field is very nearly one-dimensional. Only the discontinuity at the extreme forward end of the outside of the bag contributes to the radial structure.

At 3.078 msec, figure 4.2.13, flamespreading is complete and so is bag rupture. The pressure tolerance criterion is satisfied and figure 4.2.14 depicts the quasi-two-dimensional representation of the pressure at the same instant.

Figure 4.2.13 also makes it clear that some refinement of the calculation of the pressure at the fully separated corners of the bag is desirable. The use of a simple average of the neighbors on each side of the corner clearly results in an aphysical excursion.

The excursion does quickly disappear, however, as is seen in figure 4.2.15 which displays the pressure at 3.4 msec. A similar smoothing out of the excursions at the corners is also seen if the fully two-dimensional solution is continued, although we do not present such results in this report.

Figures 4.2.16 and 4.2.17 present the distributions of pressure at 10 msec and 12.5 msec. Because the centercore igniter has functioned so well in the present calculation, virtually no waves of ignition are seen, the pressure field being very smooth indeed. What is remarkable, however, is the distribution of the propellant which may be inferred from the positions of the internal boundaries. The charge is seen to have expanded to the wall of the tube as a consequence of the ignition blast. Moreover, the center of the charge is hollow. The ullage induced by the expansion of the centercore is extremely persistent, a result anticipated by an earlier, more restricted study¹⁹.

Figure 4.2.18 completes the history of the pressure field by presenting the distribution at muzzle exit.

Figures 4.2.19, 4.2.20 and 4.2.21 provide a description of the velocity field of the solid-phase at 1.0, 2.0 and 3.0 msec respectively.

In these figures the velocity is represented by a directed line segment rooted at the center of each mesh element and with magnitude scaled so that no line segment passes through its respective mesh element boundary. Accordingly, the scale factors change from figure to figure. One may observe the gradual development of the velocity field as the convective flame traverses the charge. At 3.0 msec, moreover, the compression of the forward part of the charge by the excess external gas pressure is clearly visible.

Figures 4.2.22, 4.2.23 and 4.2.24 illustrate the velocity field of the gas-phase at the same three times. At 1.0 msec the flow is strongly radial, especially in the ullage to the rear of the bag. At 2.0 msec, the maximum velocity is associated with convection from the centercore into the forward part of the charge. The axial velocity in the ullage which surrounds the external circumference of the bag is seen to be developing. By 3.0 msec this flow has become predominant and is driving a strong inward convection in the forward region of ullage.

Figures 4.2.25 through 4.2.28 present distributions of gas-phase density at 1.0, 2.0, 3.0 and 4.0 msec, the latter figure corresponding to the quasi-two-dimensional flow. While the pressure tends to be nearly continuous, at least across the permeable internal boundaries, the density is strongly structured. Very high densities are seen in regions which have been compressed by the advancing pressure wave and in which heating by local combustion has not yet occurred to any great degree. By 4.0 msec, the density is relatively uniform although a significant elevation is seen at the front part of the centercore in which expansion is still underway.

An alternative representation of the density field at 1.0, 2.0 and 3.0 msec is provided by figures 4.2.29 through 4.2.31 in which contour levels are plotted.

Figures 4.2.32, 4.2.33 and 4.2.34 illustrate the distribution of gas-phase temperature at 1.0, 2.0 and 3.0 msec. As with the density, discontinuities of temperature may persist at the internal boundaries. These figures also provide a feeling for the path of the convective flame.

We have commented on the deformation of the propelling charge by the igniter blast. Figures 4.2.35, 4.2.36 and 4.2.37 illustrate the distributions of intergranular stress at 1.0, 2.0 and 3.0 msec respectively. Stresses in excess of 1 MPa are induced at the front of the charge by the combined influences of the excess external gas pressure, the axial thrust of the advancing flame, and the outward thrust of the burning centercore.

We conclude with figures 4.2.38, 4.2.39 and 4.2.40 which illustrate the surface temperature of the solid phase at 1.0, 2.0 and 3.0 msec. Since the present simple combustion model takes the solid-phase to ignite when a threshold value is reached, the path of the convective flame may be inferred from the extent of the upper plateau in each of the figures. At 3.0 msec only the forward outside corner of the charge, still confined by the impermeable bag, has yet to ignite.

STEP 483

TIME (MSEC) 4.000

CONTOURS OF IGNITION DELAY (MSEC)

○	0.38541
▲	1.05173
+	1.71806
X	2.38438
◊	3.05071

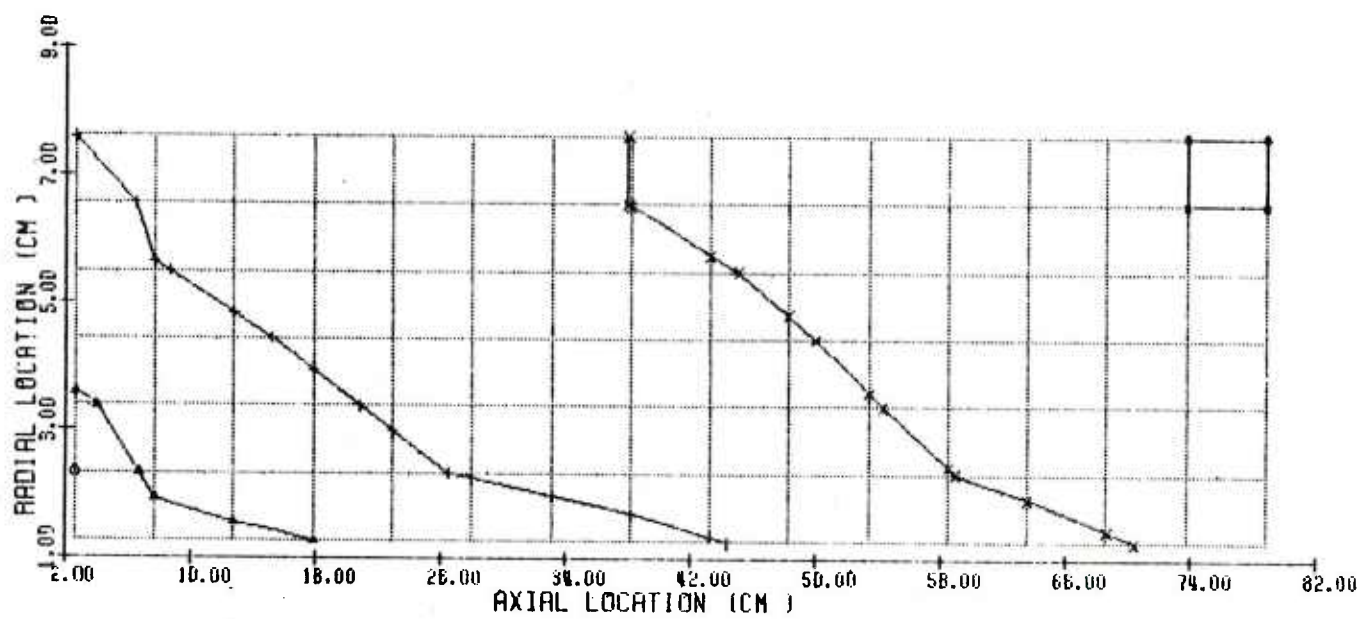


Figure 4.2.1 Contours of Ignition Delay

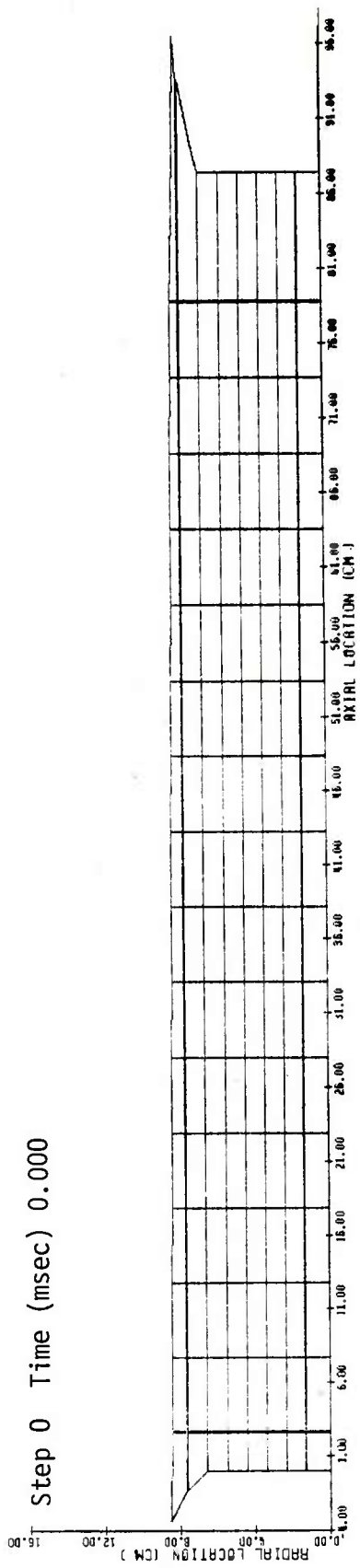


Figure 4.2.2 Mesh at 0.0 msec

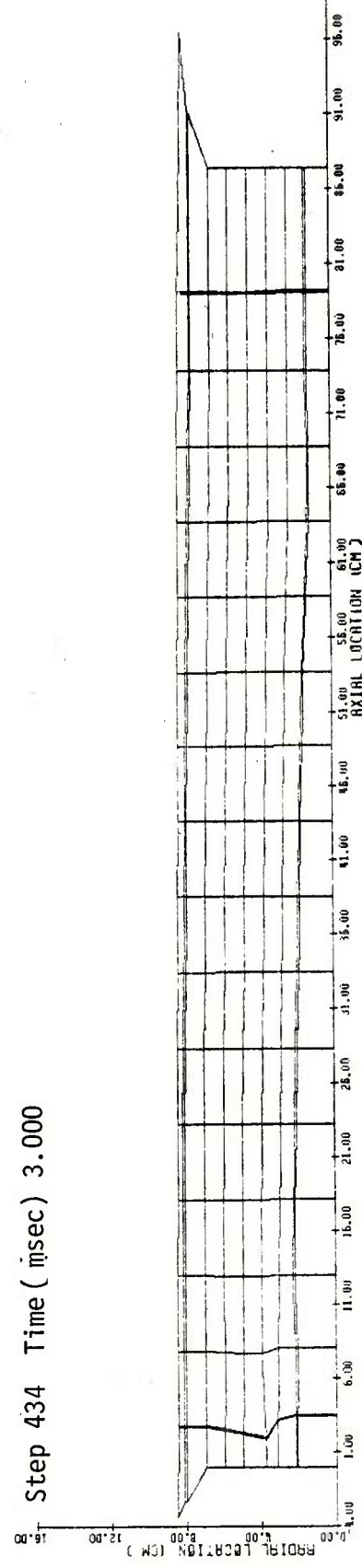


Figure 4.2.3 Mesh at 3.0 msec

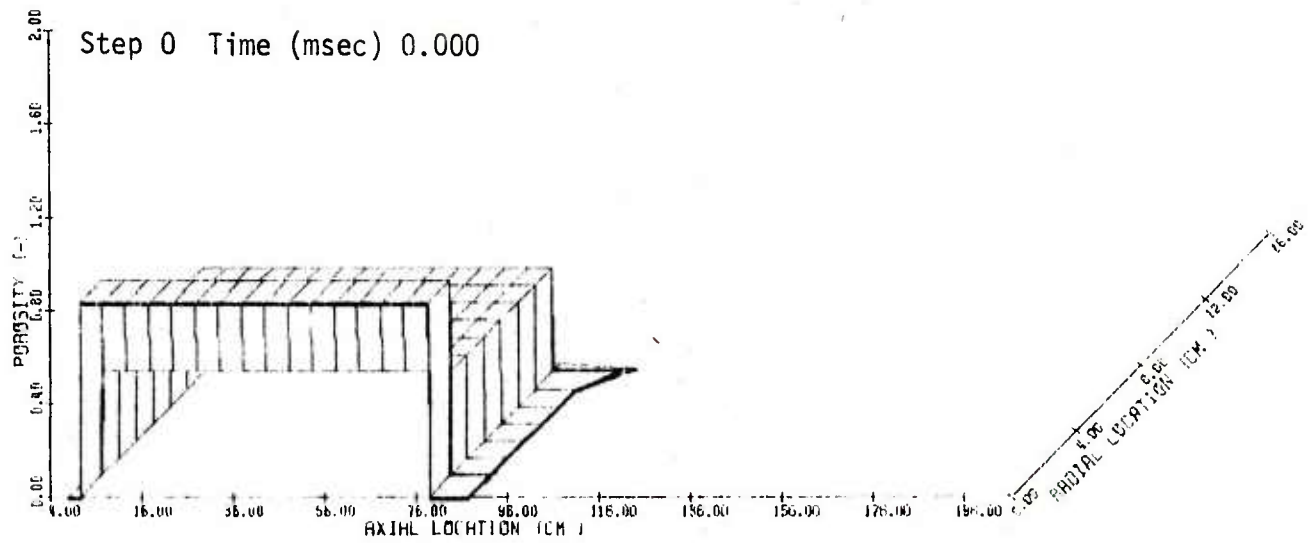


Figure 4.2.4 Porosity at 0.0 msec

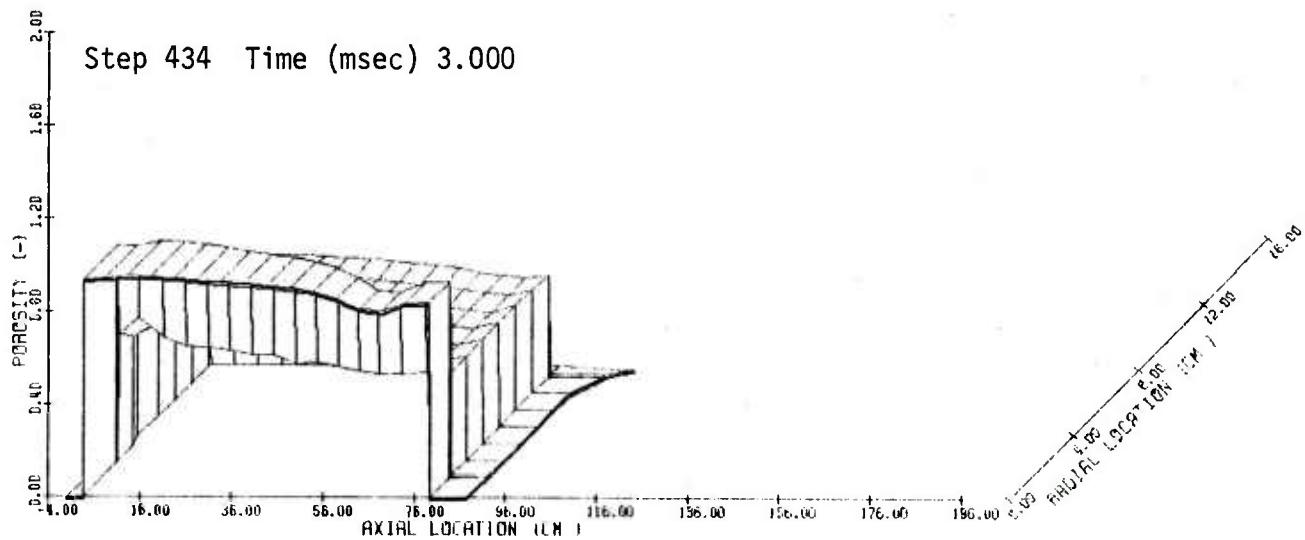


Figure 4.2.5 Porosity at 3.0 msec

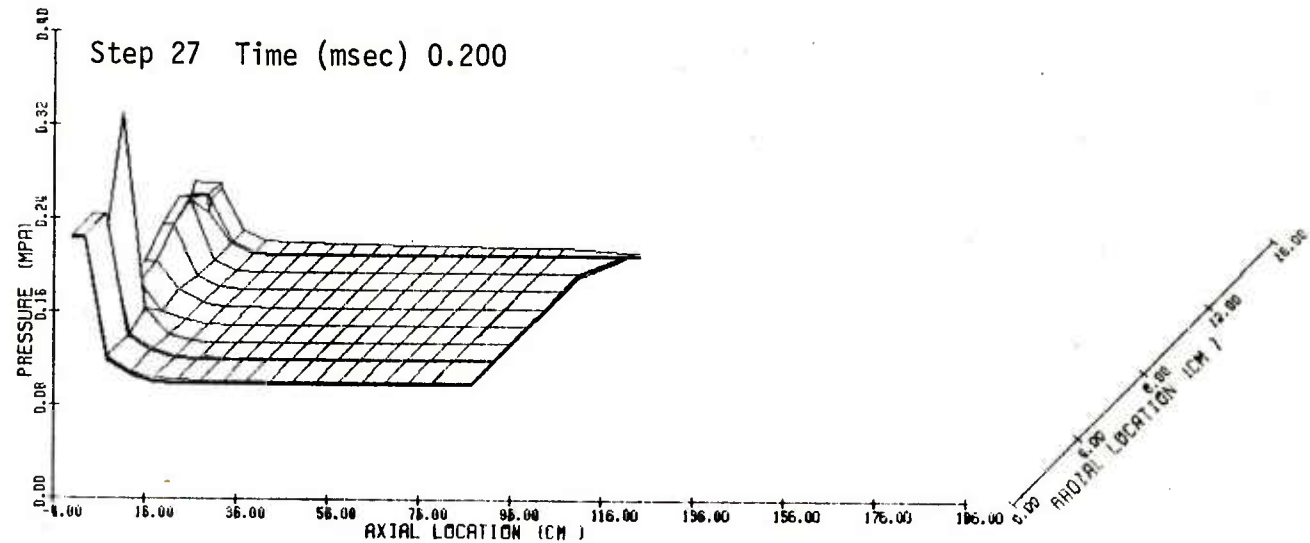


Figure 4.2.6 Pressure at 0.2 msec

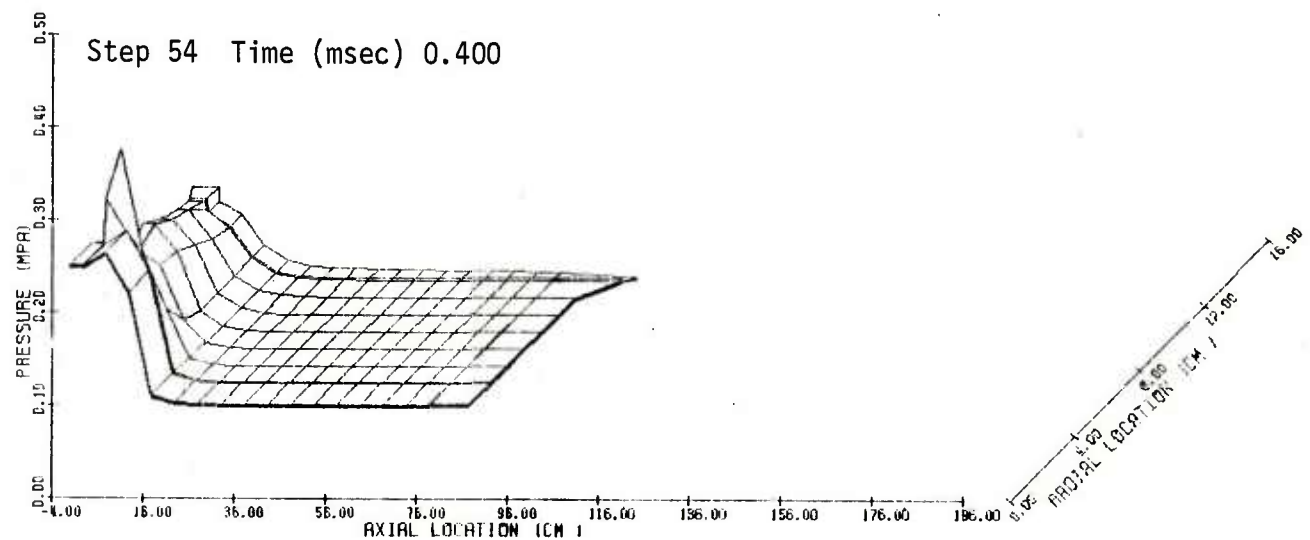


Figure 4.2.7 Pressure at 0.4 msec

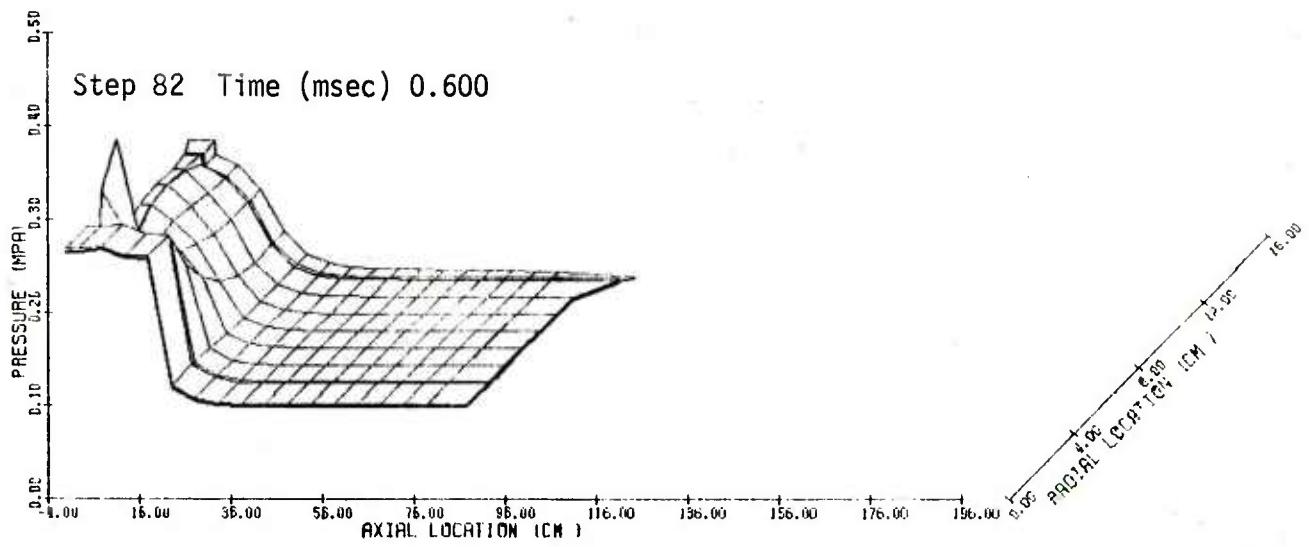


Figure 4.2.8 Pressure at 0.6 msec

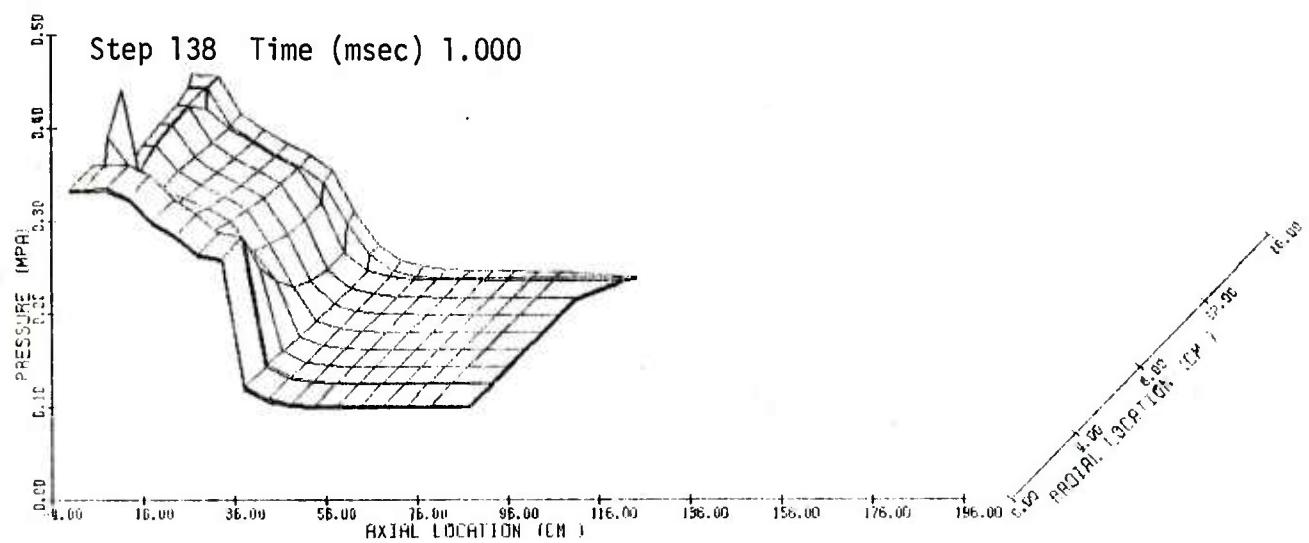


Figure 4.2.9 Pressure at 1.0 msec

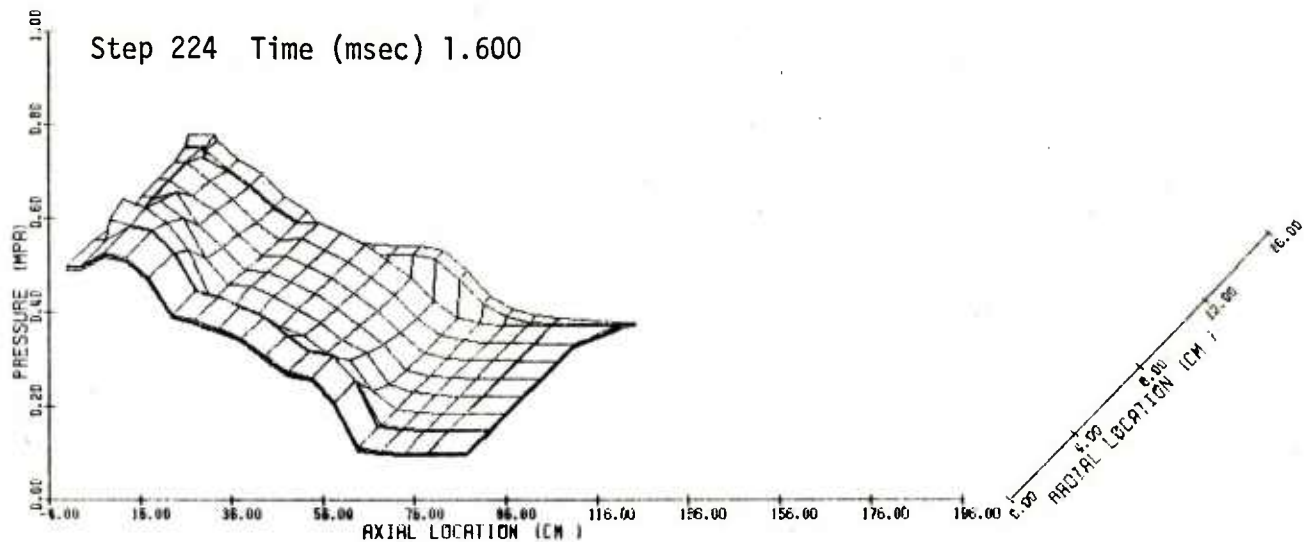


Figure 4.2.10 Pressure at 1.6 msec

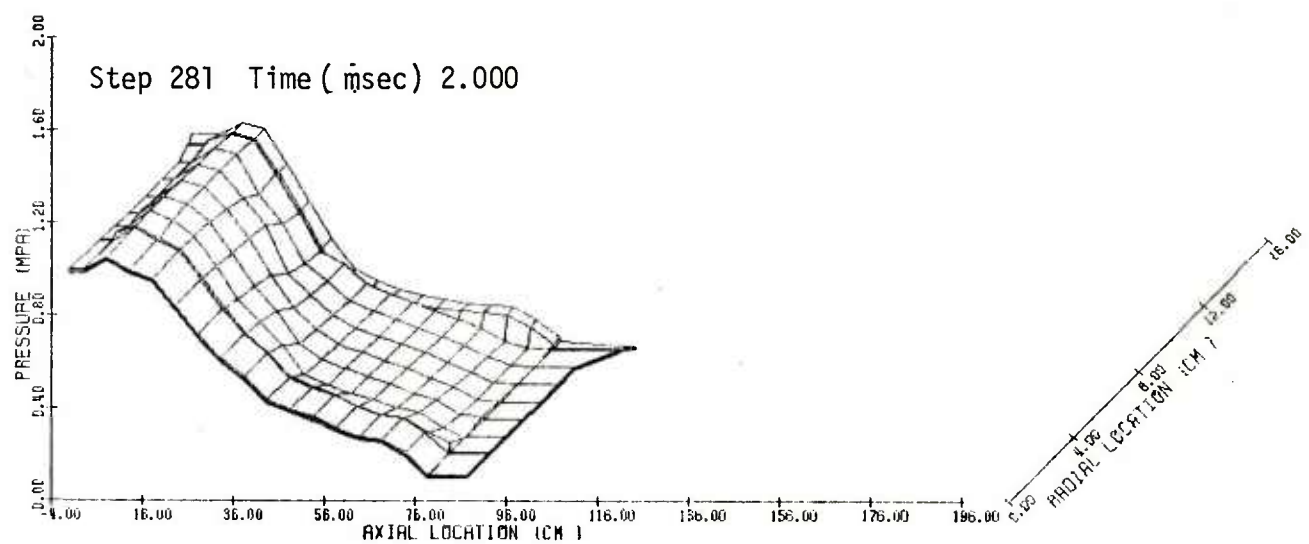


Figure 4.2.11 Pressure at 2.0 msec

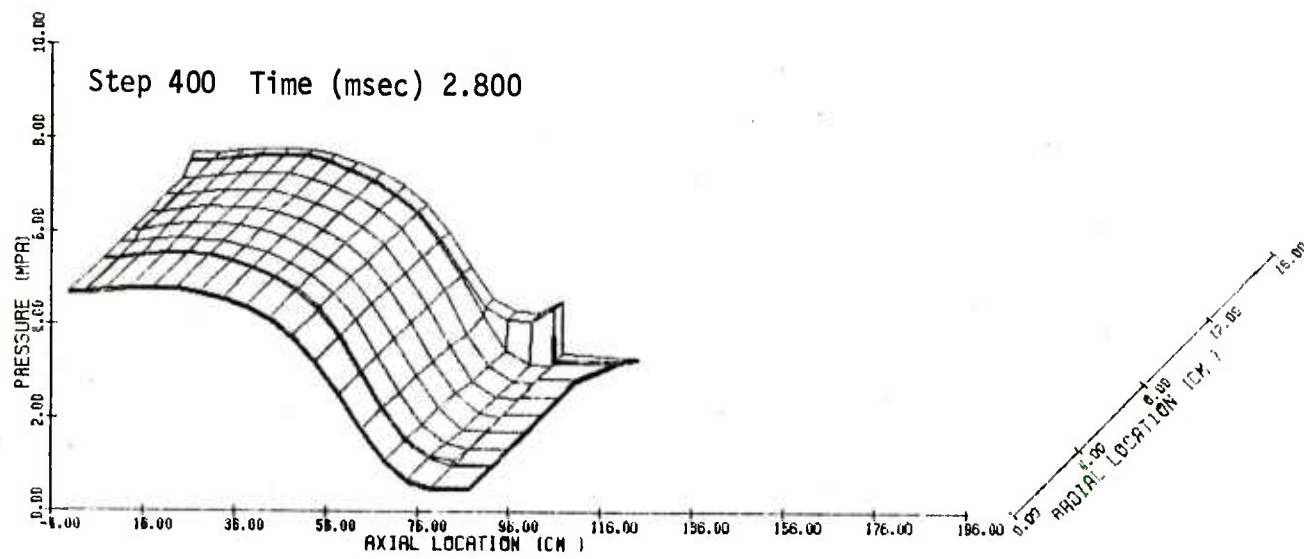


Figure 4.2.12 Pressure at 2.8 msec

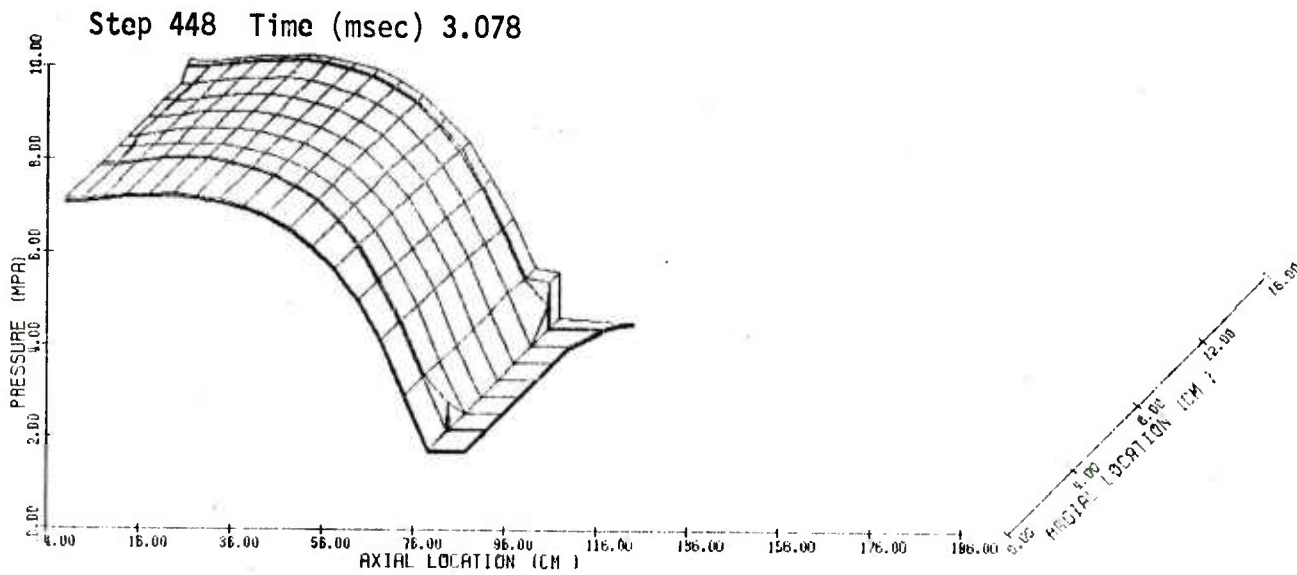


Figure 4.2.13 Pressure at 3.078 msec (Fully-Two-Dimensional)

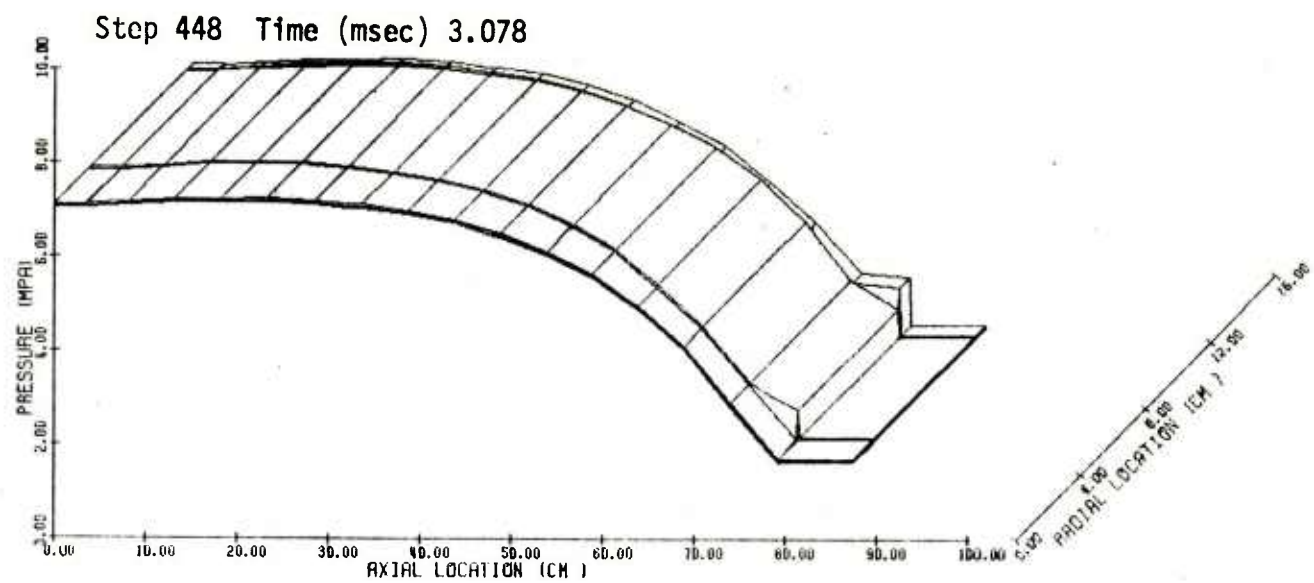


Figure 4.2.14 Pressure at 3.078 msec (Quasi-Two-Dimensional)

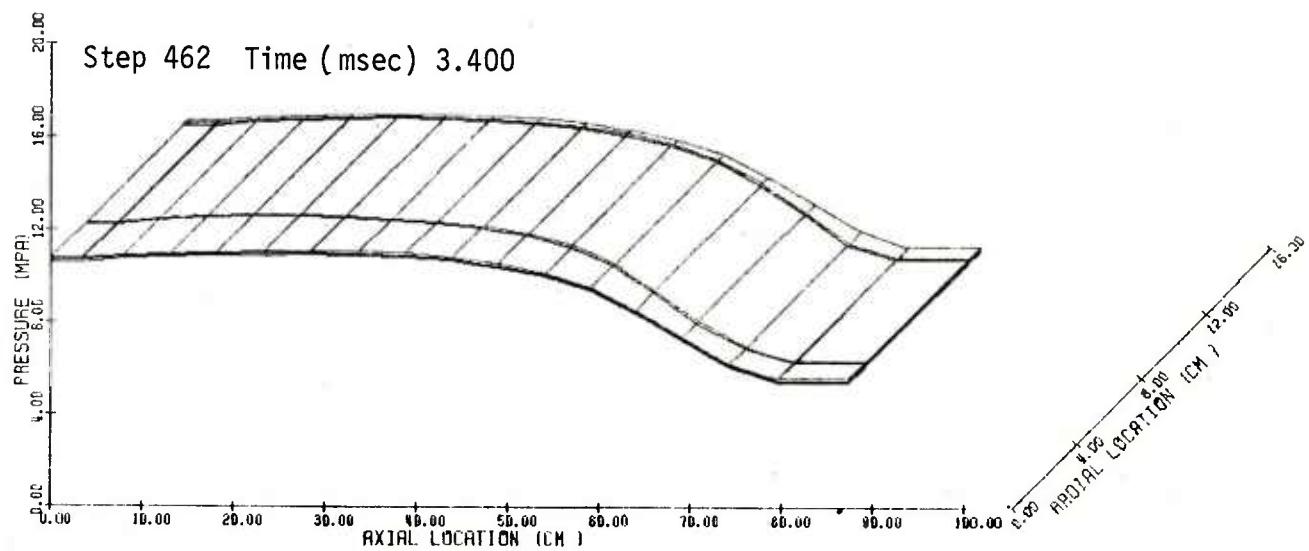


Figure 4.2.15 Pressure at 3.4 msec

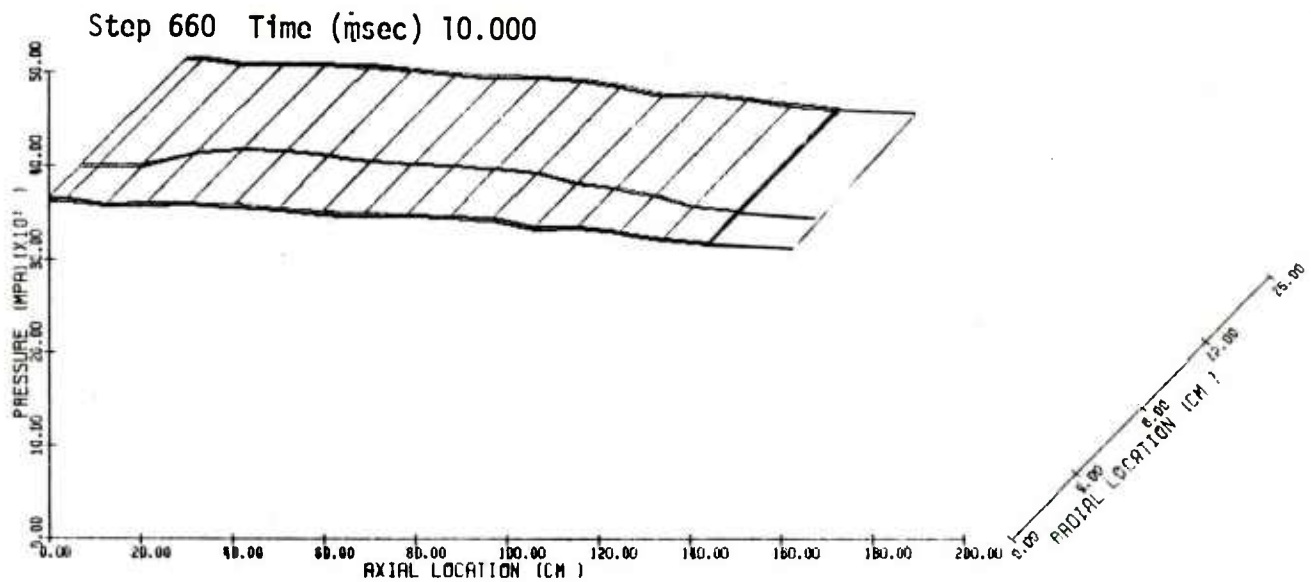


Figure 4.2.16 Pressure at 10.0 msec

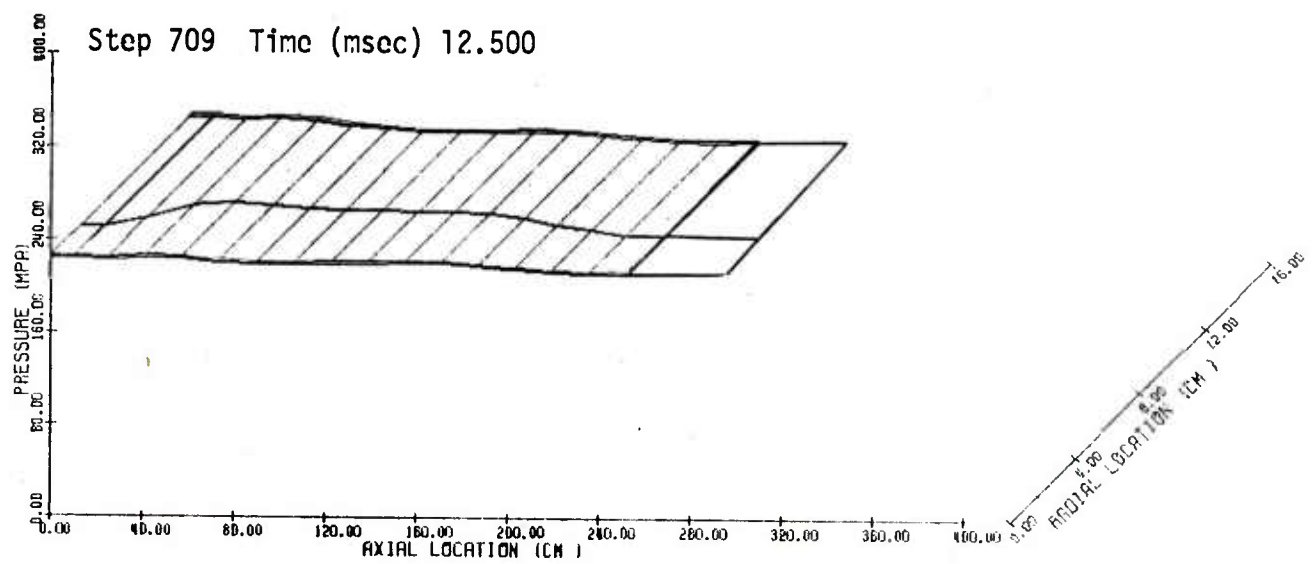


Figure 4.2.17 Pressure at 12.5 msec

Step 757 Time (msec) 16.519

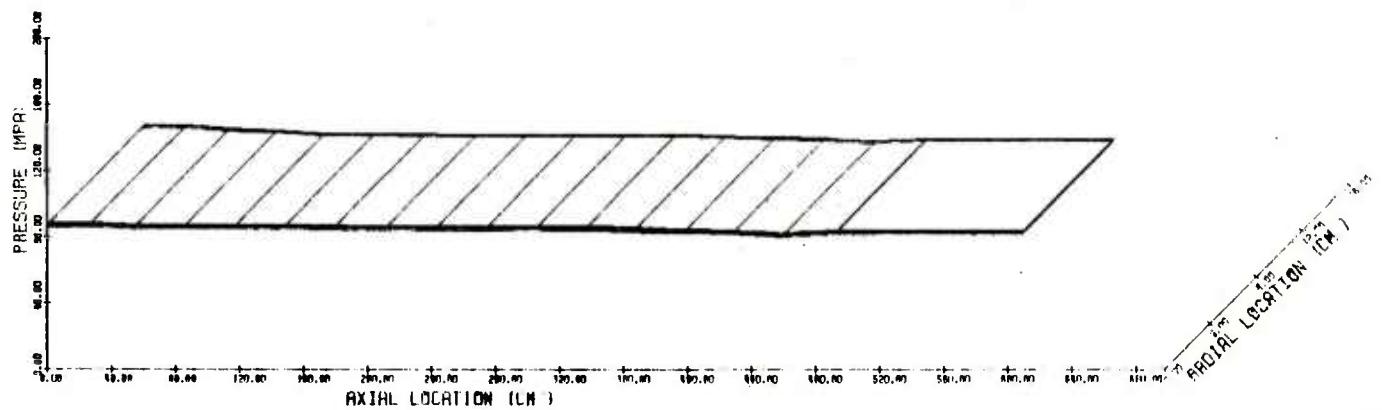


Figure 4.2.18 Pressure at 16.519 msec (Muzzle Exit)

Step 138 Time (msec) 1.000

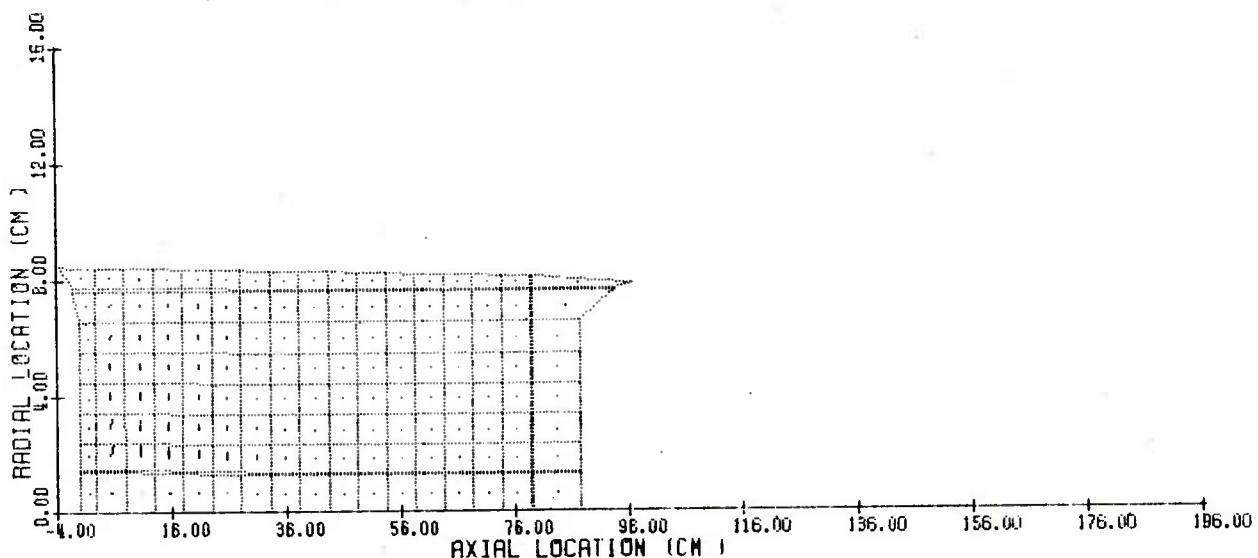


Figure 4.2.19 Velocity Field of Solid Phase at 1.0 msec

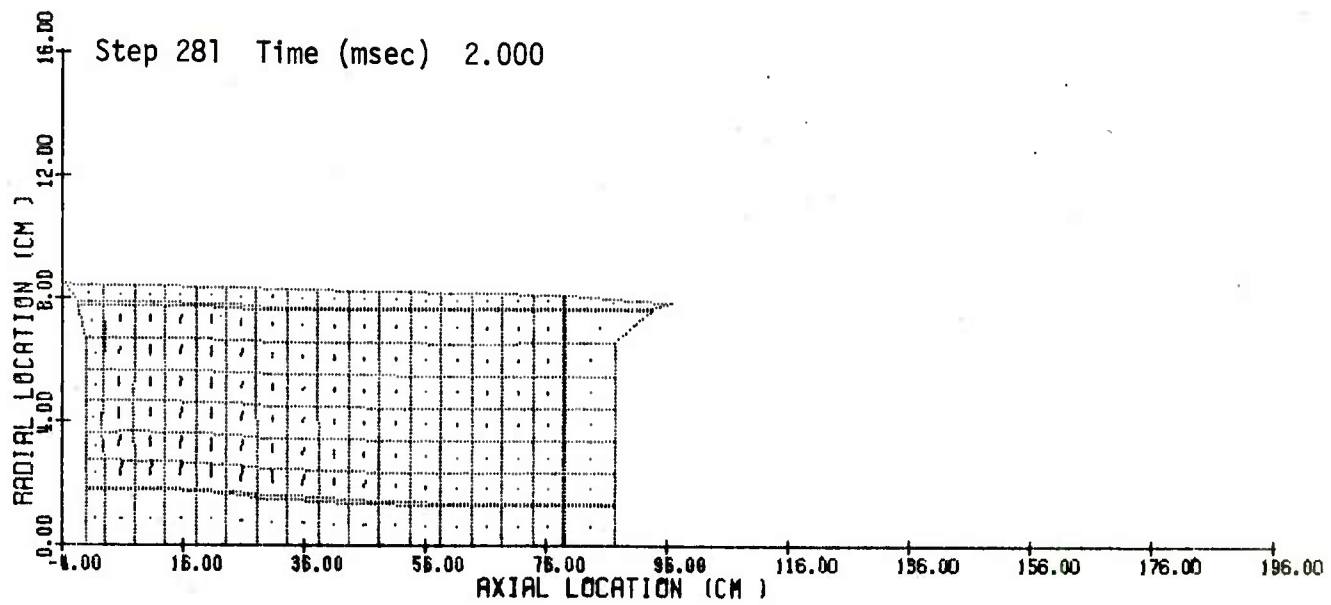


Figure 4.2.20 Velocity Field of Solid Phase at 2.0 msec

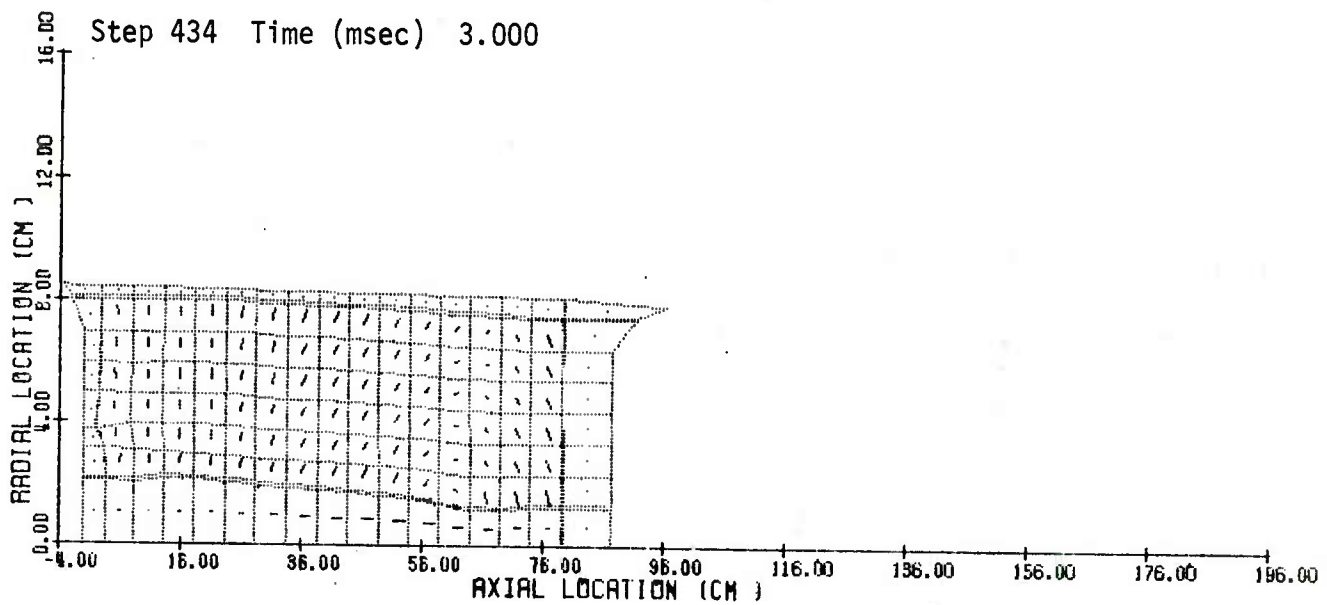


Figure 4.2.21 Velocity Field of Solid Phase at 3.0 msec

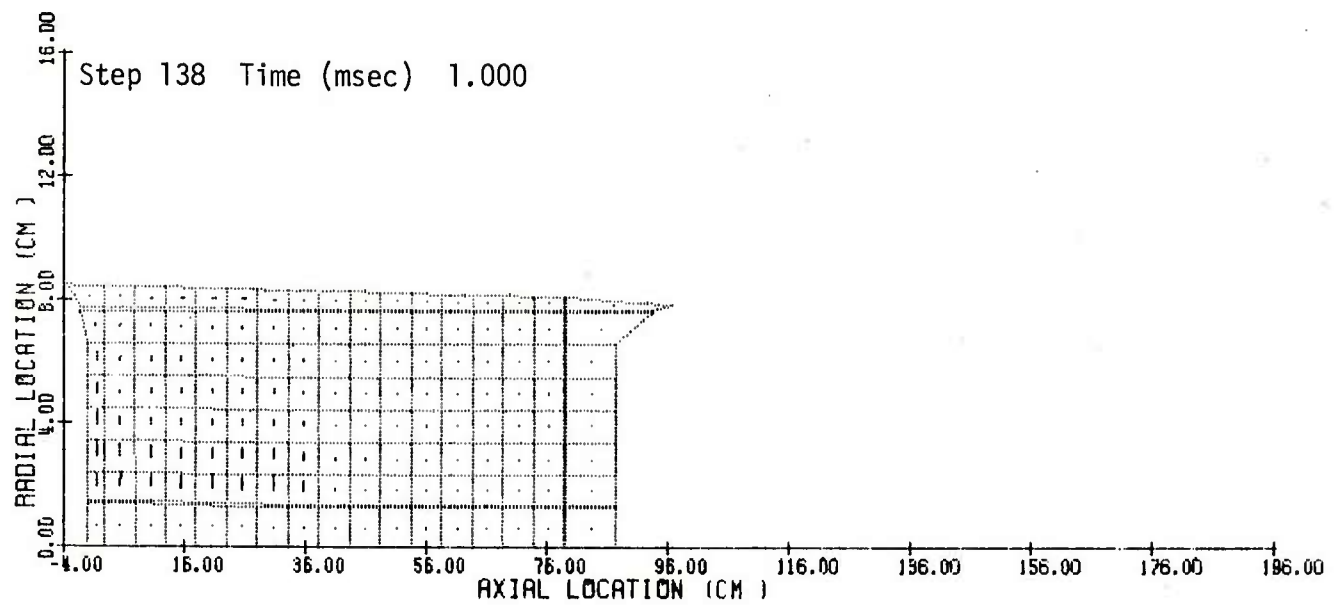


Figure 4.2.22 Velocity Field of Gas Phase at 1.0 msec

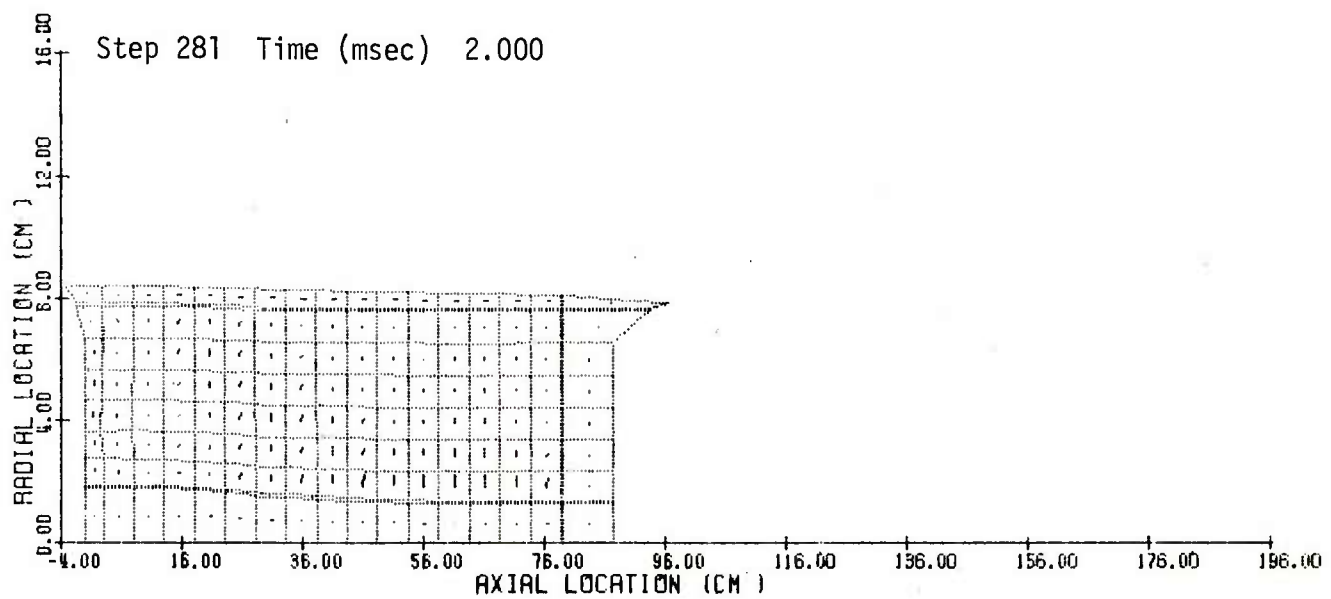


Figure 4.2.23 Velocity Field of Gas Phase at 2.0 msec

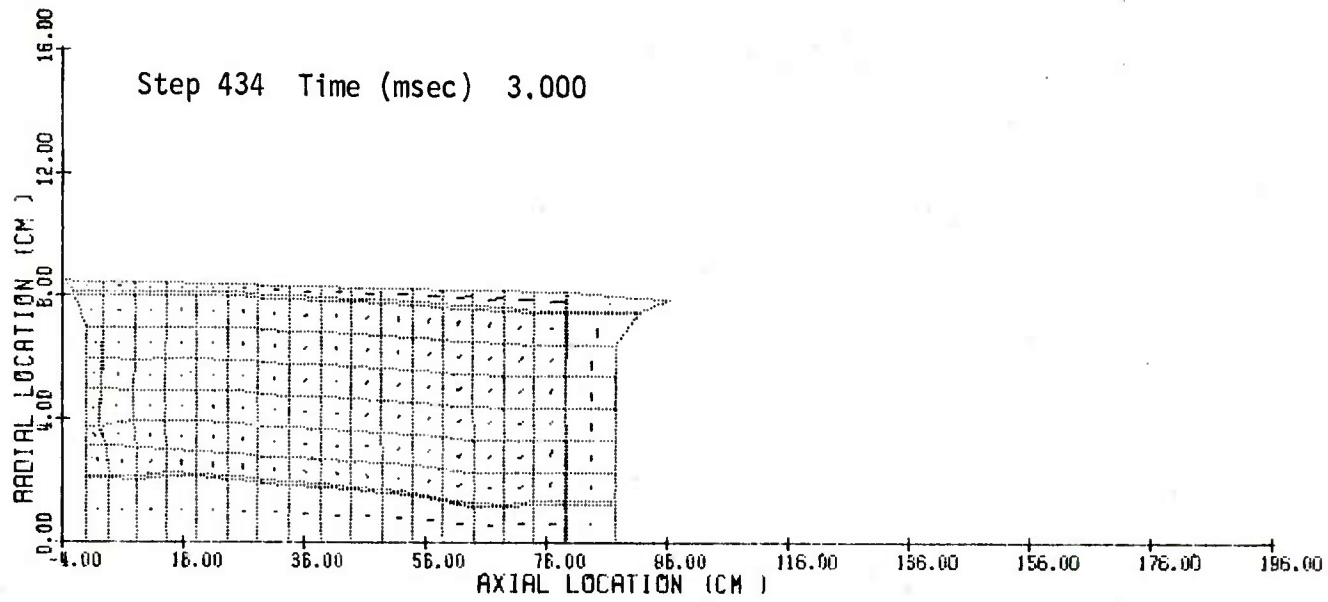


Figure 4.2.24 Velocity Field of Gas Phase at 3.0 msec

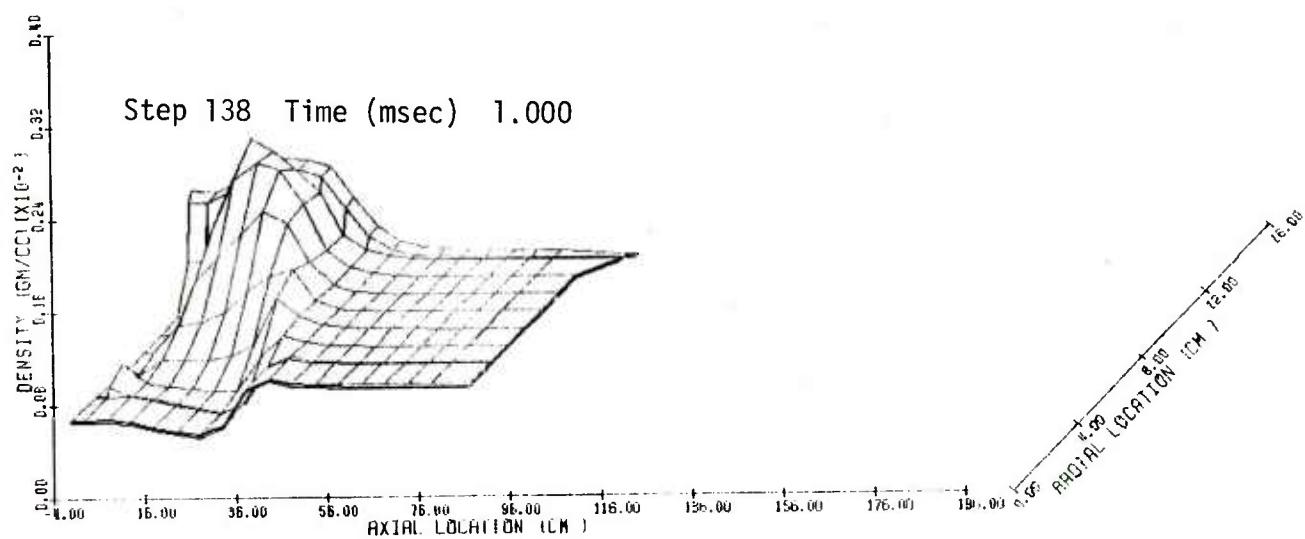


Figure 4.2.25 Density of Gas at 1.0 msec

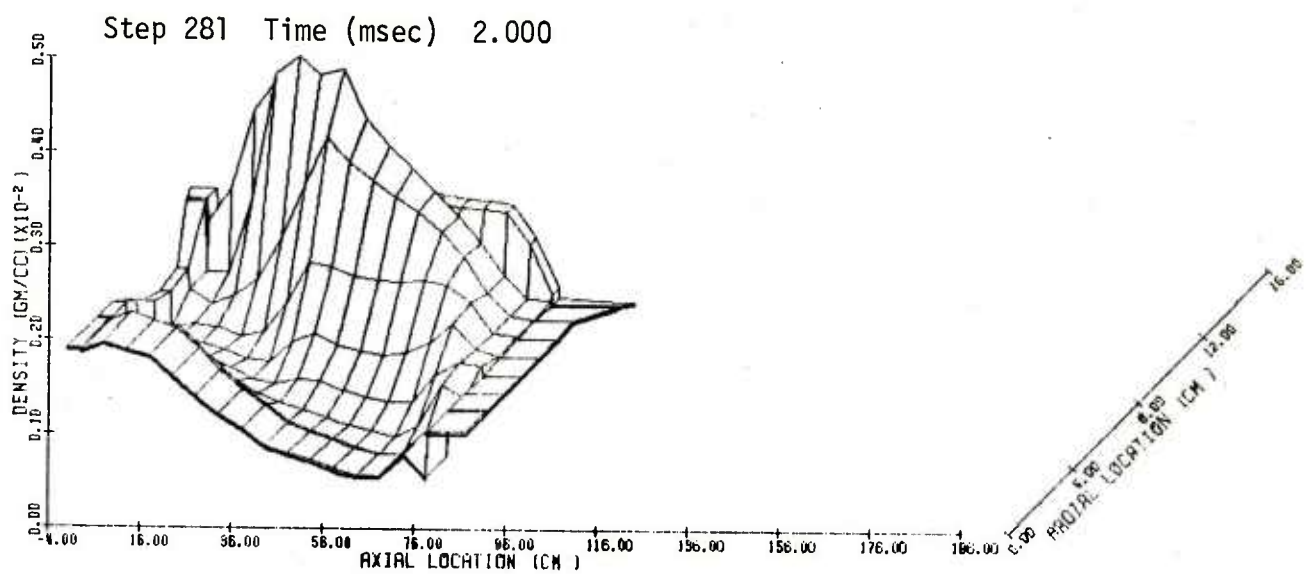


Figure 4.2.26 Density of Gas at 2.0 msec

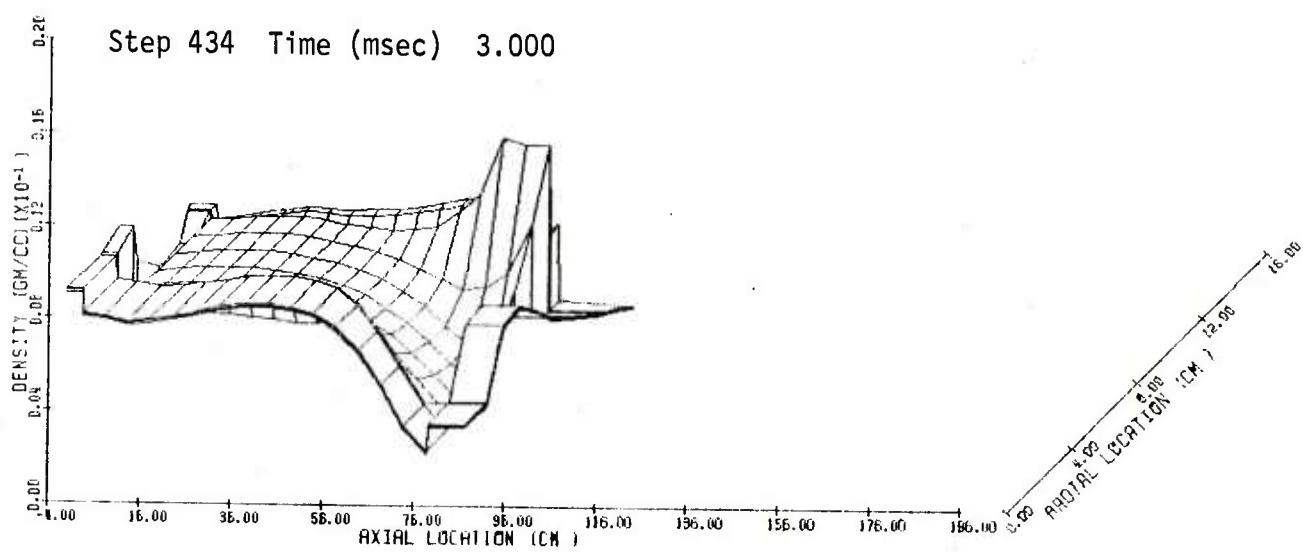


Figure 4.2.27 Density of Gas at 3.0 msec

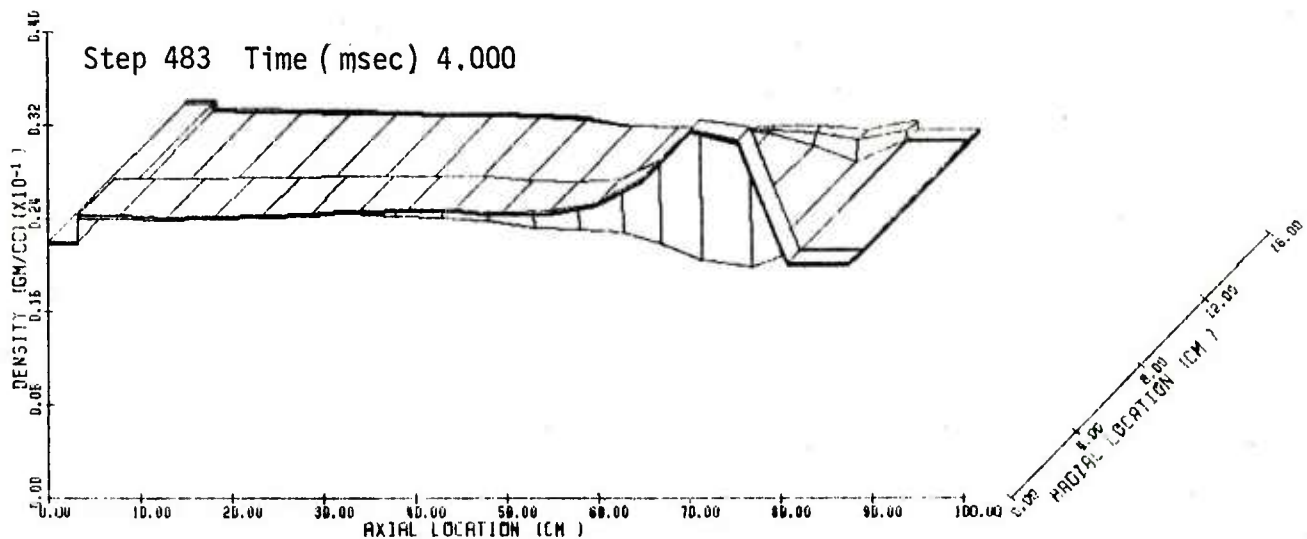


Figure 4.2.28 Density of Gas at 4.0 msec

STEP 138

TIME (MSEC) 1.000

CONTOURS OF DENSITY (GM/CC)

○	0.00054
△	0.00091
+	0.00128
×	0.00165
◊	0.00202

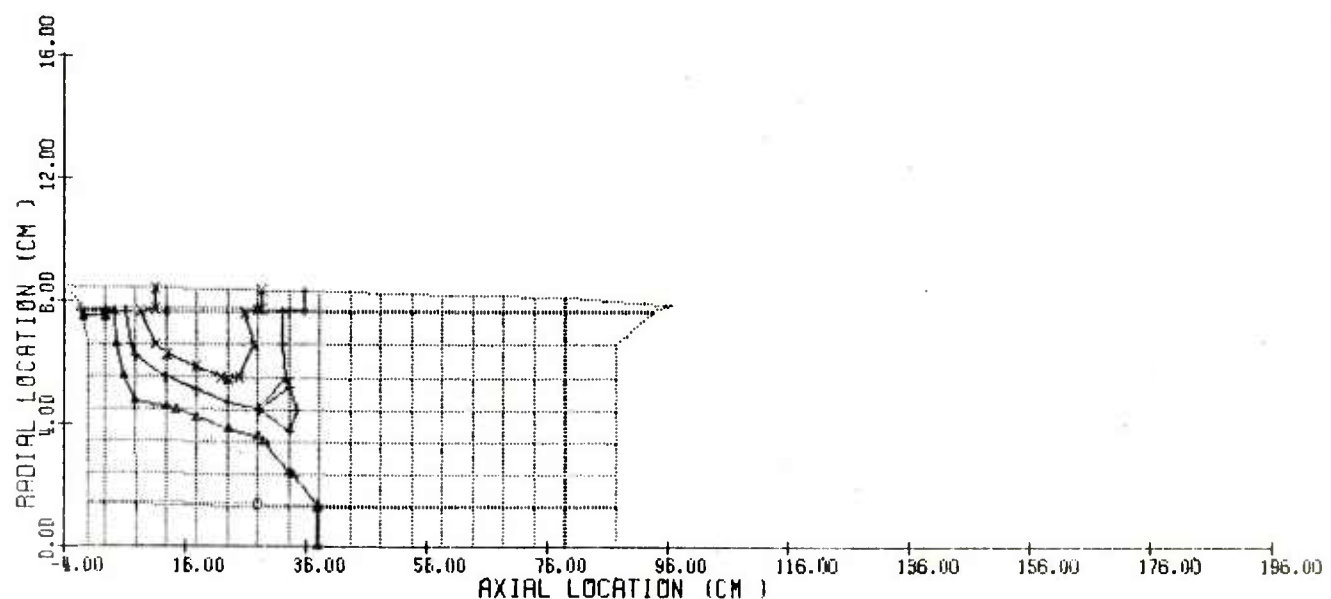


Figure 4.2.29 Contours of Gas-Phase Density at 1.0 msec

STEP 281

TIME (MSEC) 2.000

CONTOURS OF DENSITY (GM/CC)

O	0.00056
A	0.00134
+	0.00211
X	0.00289
◆	0.00367

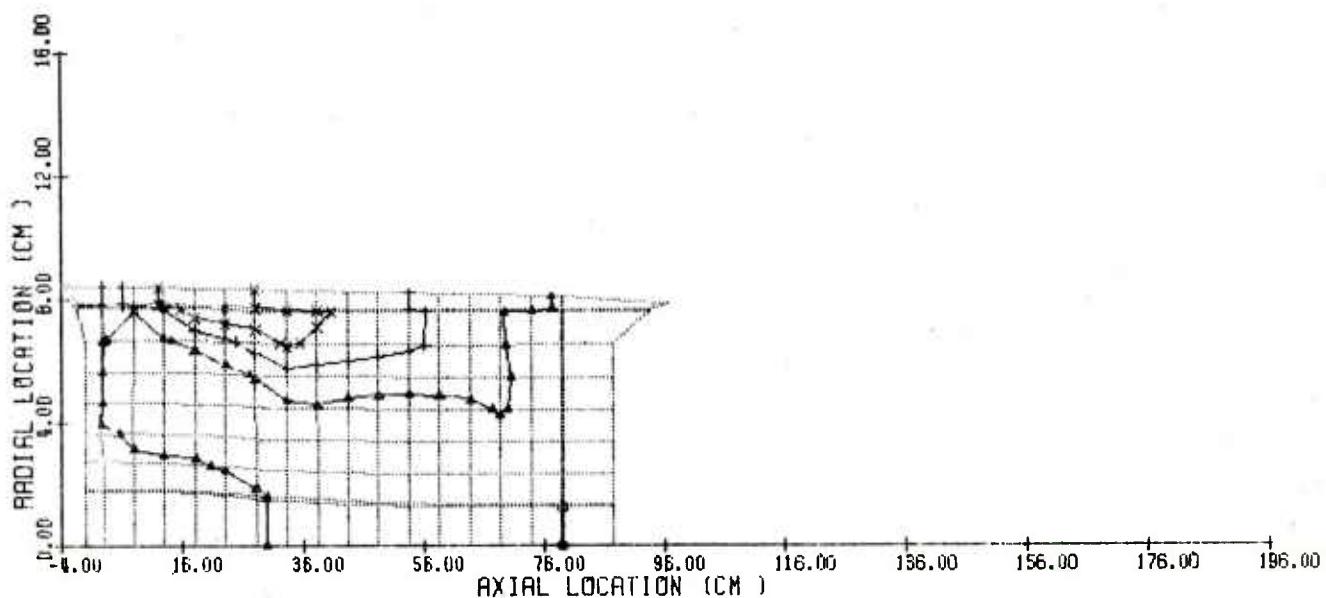


Figure 4.2.30 Contours of Gas-Phase Density at 2.0 msec

STEP 434

TIME (MSEC) 3.000

CONTOURS OF DENSITY (GM/CC)

○	0.00218
△	0.00429
+	0.00640
×	0.00852
▽	0.01063

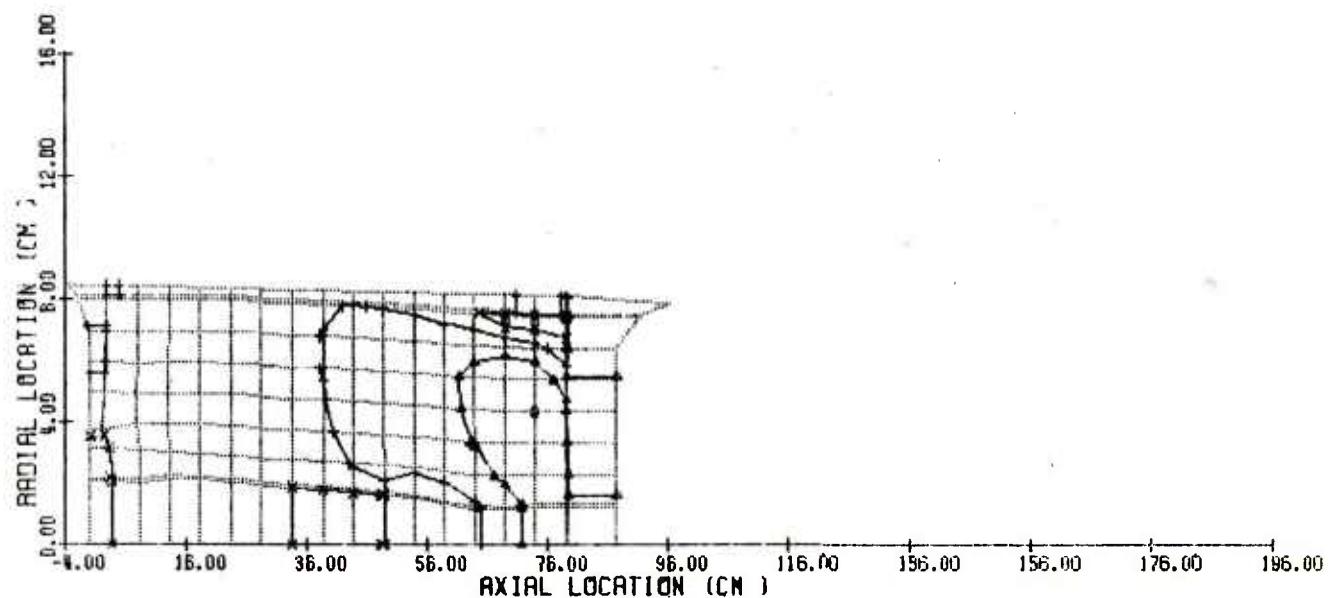


Figure 4.2.31 Contours of Gas-Phase Density at 3.0 msec

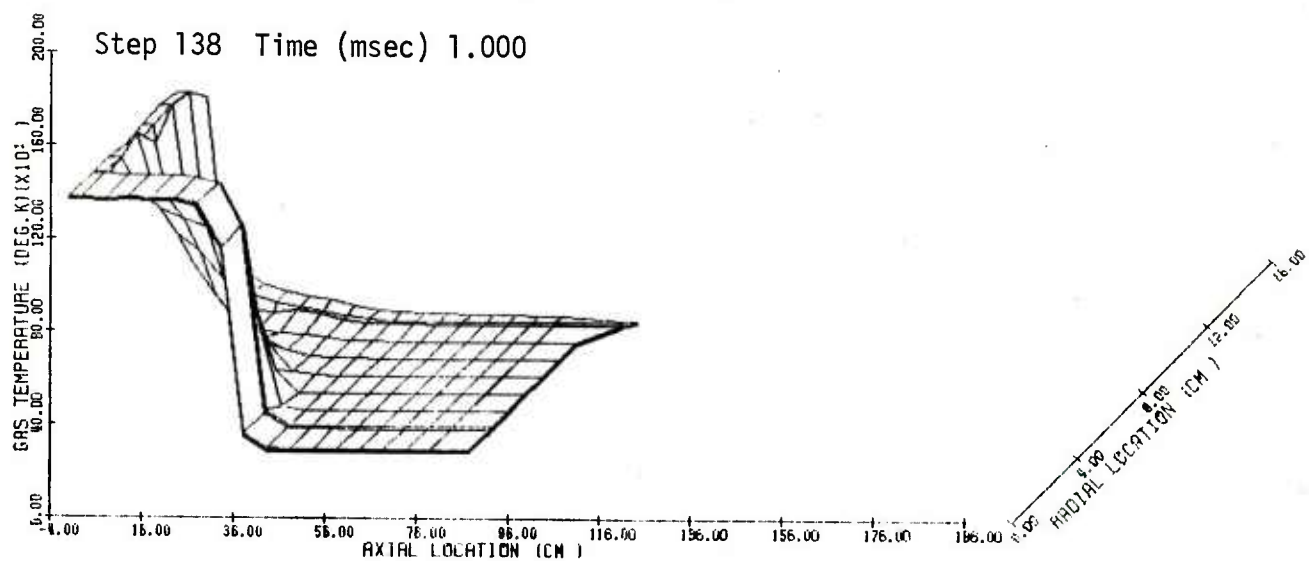


Figure 4.2.32 Temperature of Gas at 1.0 msec

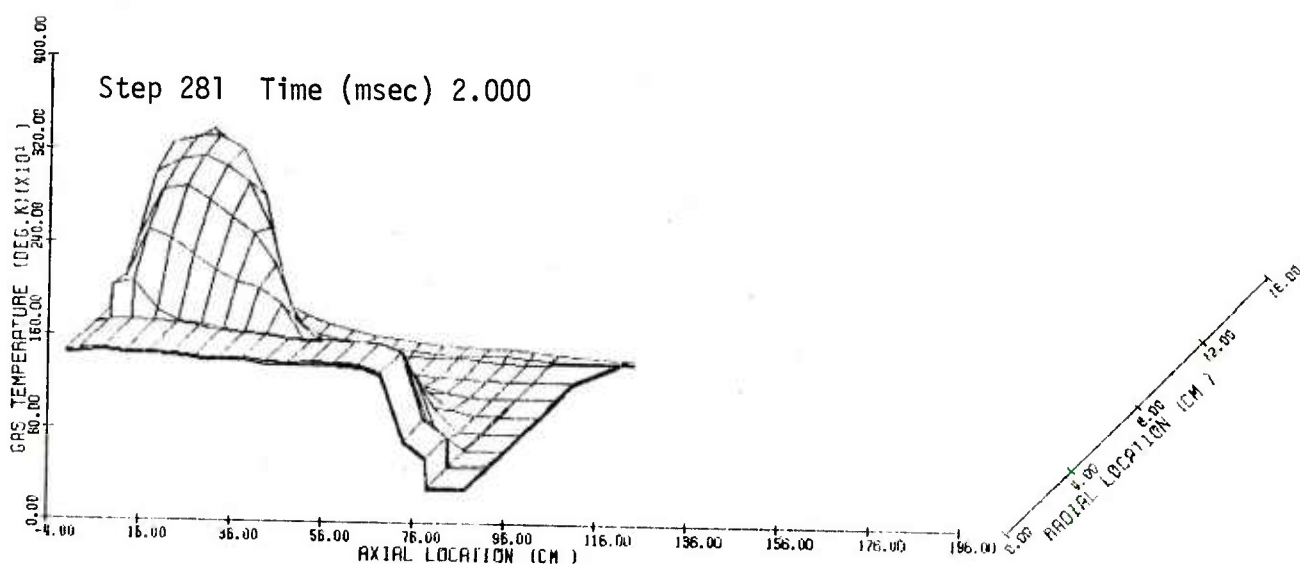


Figure 4.2.33 Temperature of Gas at 2.0 msec

Step 434 Time (msec) 3.000

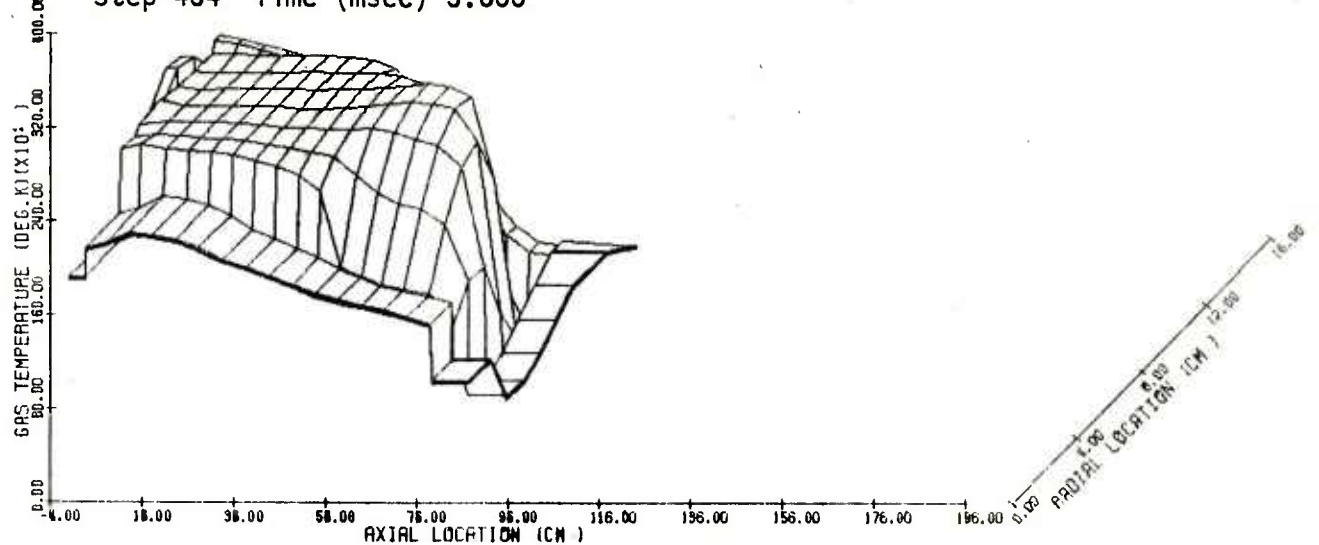


Figure 4.2.34 Temperature of Gas at 3.0 msec

Step 138 Time (msec) 1.000

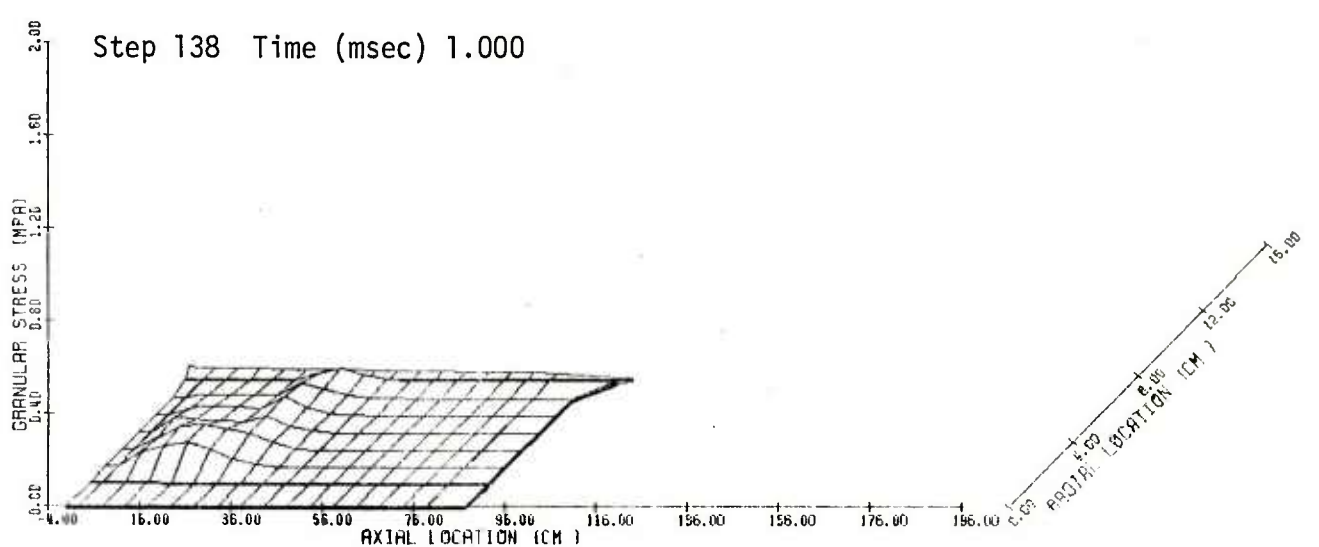


Figure 4.2.35 Granular Stress at 1.0 msec

Step 281 Time (msec) 2.000

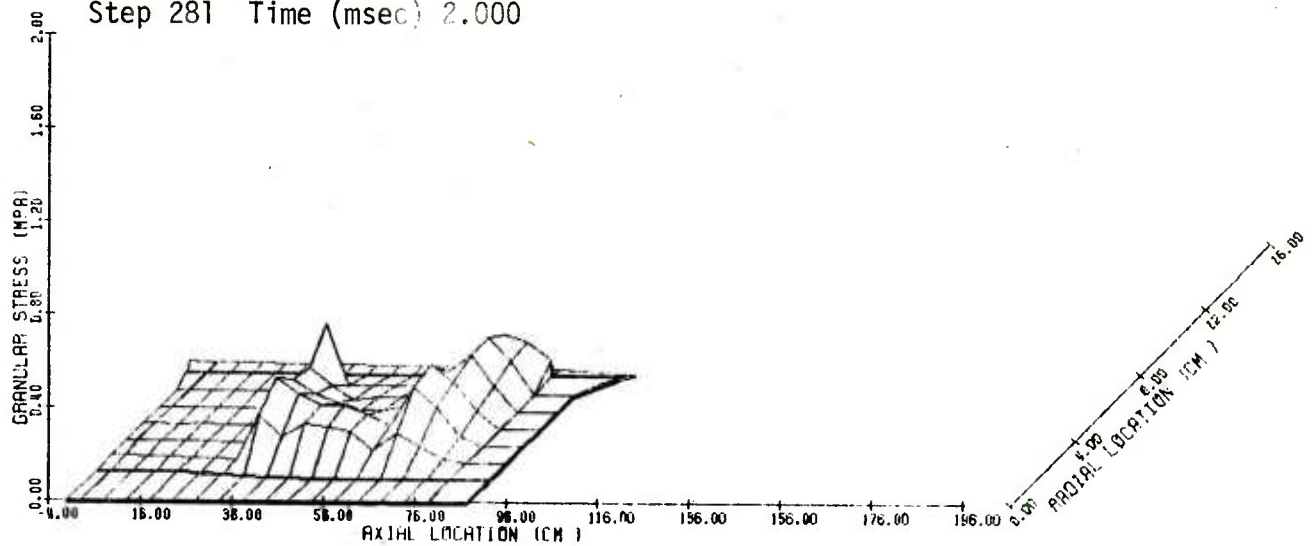


Figure 4.2.36 Granular Stress at 2.0 msec

Step 434 Time (msec) 3.000

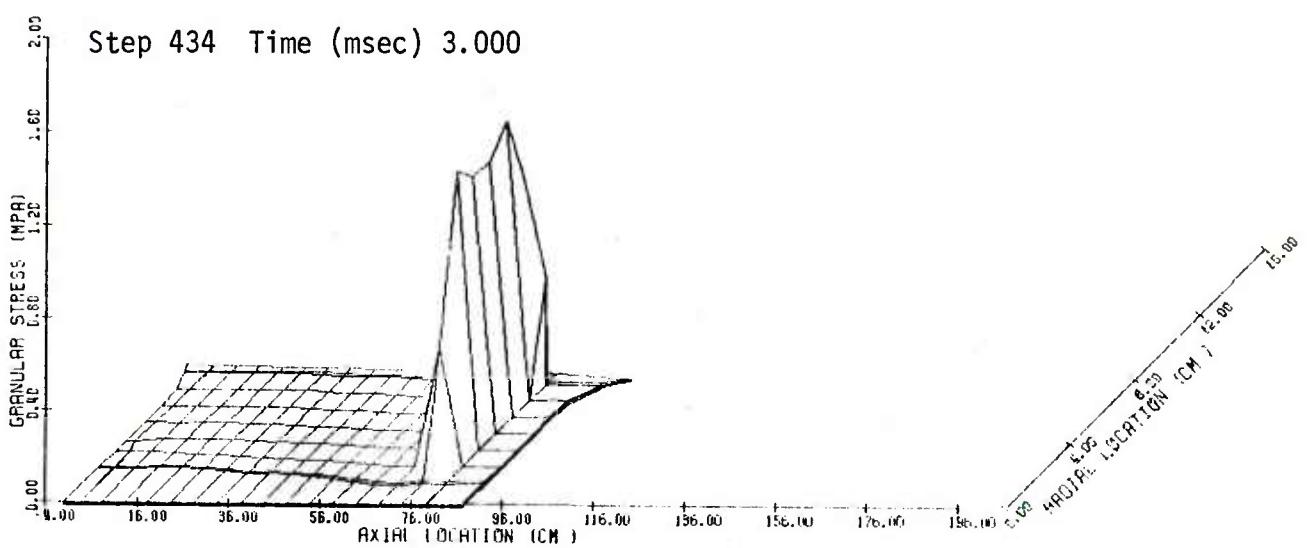


Figure 4.2.37 Granular Stress at 3.0 msec

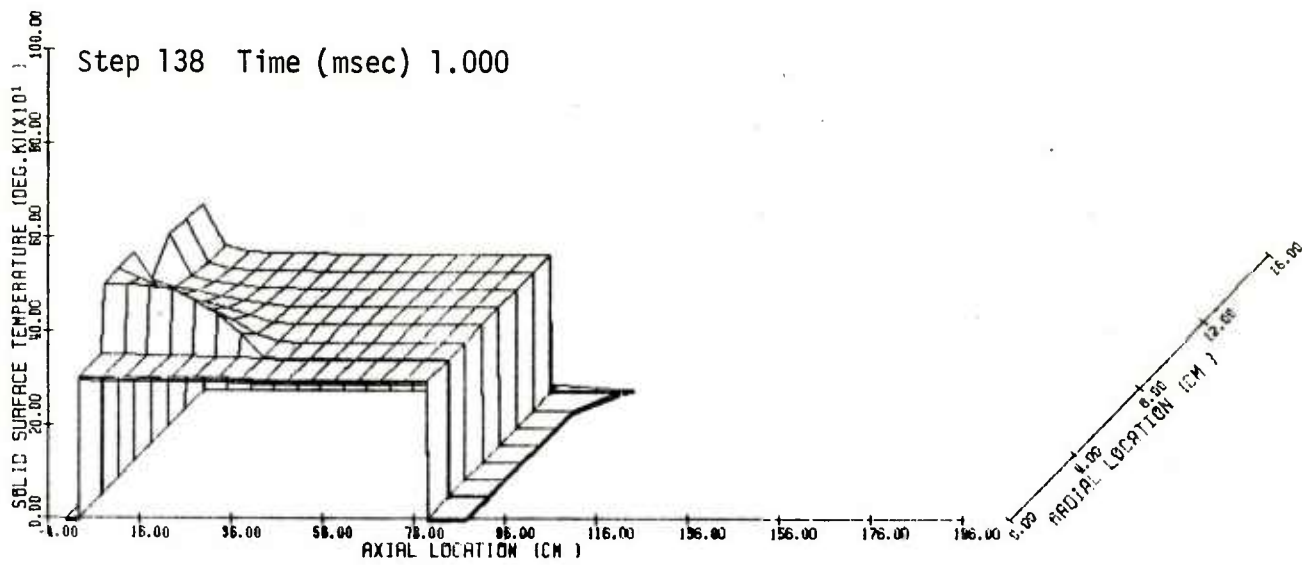


Figure 4.2.38 Surface Temperature of Solid-Phase at 1.0 msec

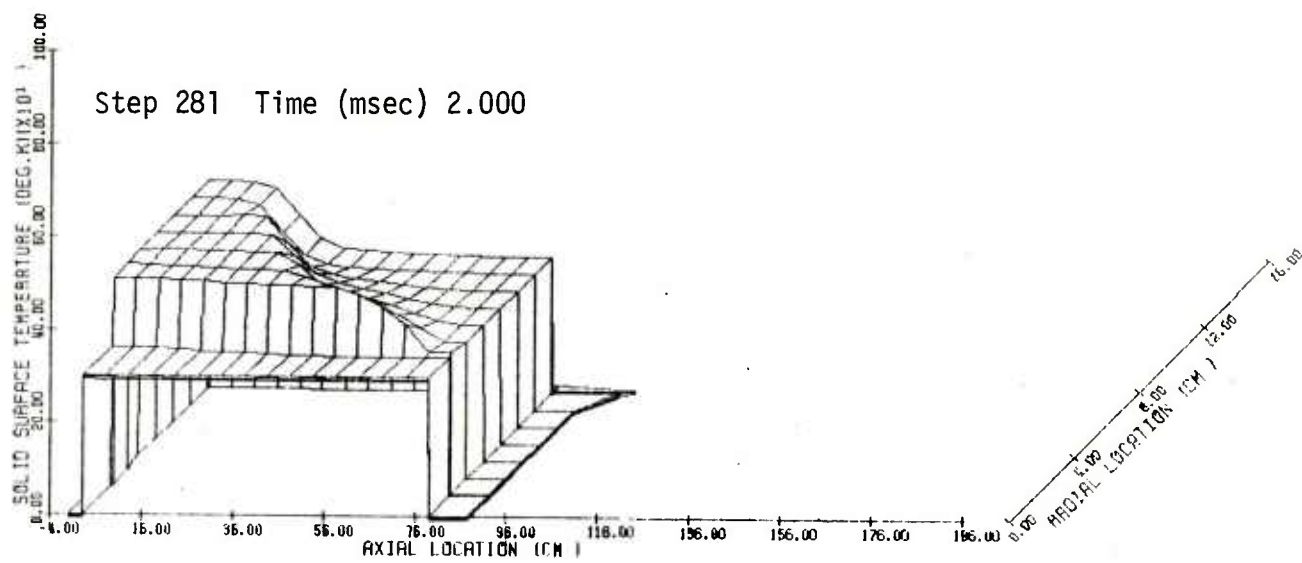


Figure 4.2.39 Surface Temperature of Solid-Phase at 2.0 msec

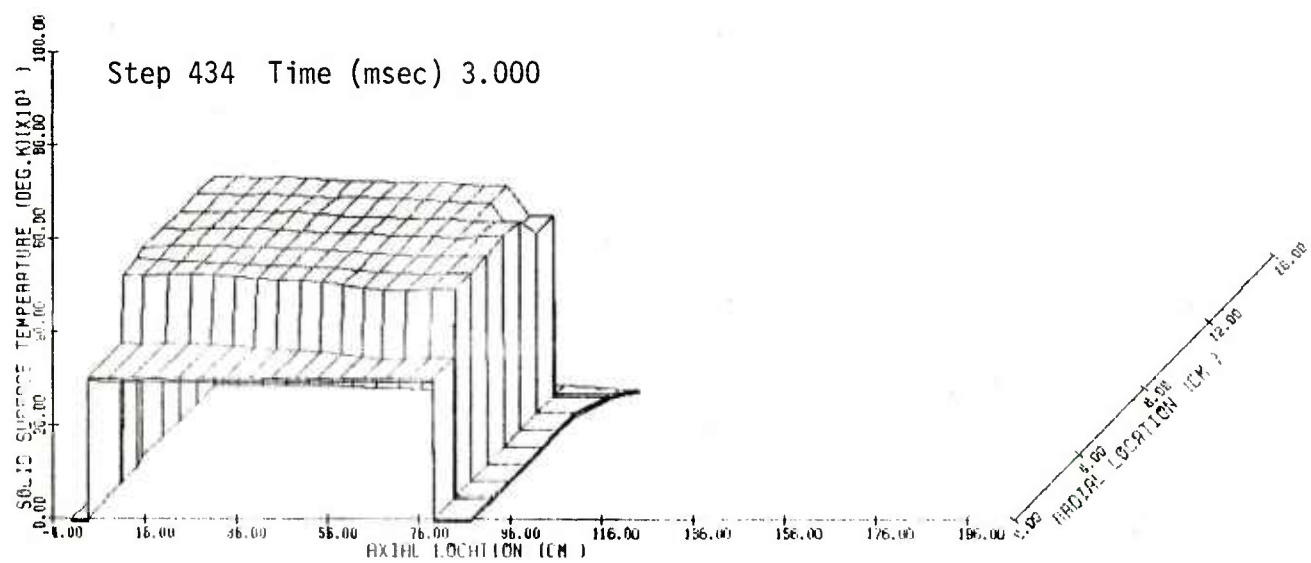


Figure 4.2.40 Surface Temperature of Solid-Phase at 3.0 msec

REFERENCES

1. Gough, P. S.
 "Two Dimensional Convective Flamespreading in Packed
 Beds of Granular Propellant"
 Ballistic Research Laboratory Report ARBRL-CR-00404 July 1979
 (AD #A075326)
2. Budka, A. J. and Knapton, J. D.
 "Pressure Wave Generation in Gun Systems--A Survey"
 Ballistic Research Laboratory Memorandum Report 2567 1975
 (AD #B008893L)
3. Kent, R. H.
 "Study of Ignition of 155-mm Gun"
 Ballistic Research Laboratory Report 22. 1935
 (AD #494703)
4. Heddon, S. E. and Nance, G. A.
 "An Experimental Study of Pressure Waves in Gun
 Chambers"
 NPG Report 1534. 1957
5. Horst, A. W., Jr. and Smith, T. C.
 "The Influence of Propelling Charge Configuration
 in Gun Environment Pressure-Time Anomalies"
 Proc. 12th JANNAF Combustion Meeting. 1975
6. May, I. W., Clarke, E. V., and Hassmann, H.
 "A Case History: Gun Ignition Related Problems and
 Solutions for the XM-198 Howitzer"
 Ballistic Research Laboratory Interim Memorandum Report
 150. 1973
7. Rocchio, J., Ruth, C. and May, I. W.
 "Grain Geometry Effects on Wave Dynamics in Large
 Caliber Guns"
 Proc. 13th JANNAF Combustion Meeting. 1976
8. Horst, A. W., Smith, T. C. and Mitchell, S. E.
 "Key Design Parameters in Controlling Gun-Environment
 Pressure Wave Phenomena--Theory versus Experiment"
 Proc. 13th JANNAF Combustion Meeting 1976
9. Horst, A. W. and Gough, P. S.
 "Influence of Propellant Packaging on Performance of
 Navy Case Gun Ammunition"
 J. Ballistics, v. 1, n. 3. 1977
10. East, J. L. and McClure, D. R.
 "Projectile Motion Predicted by a Solid/Gas
 Flow Interior Ballistic Model"
 Proc. 10th JANNAF Combustion Meeting 1973

11. Krier, H., van Tassel, W. F., Rajan, S. and Vershaw, J.
"Model of Flame Spreading and Combustion Through
Packed Bed of Propellant Grains"
Tech. Rept. AAE74-1, University of Illinois at
Urbana-Champaign. 1974
12. Kuo, K. K., Koo, J. H., Davis, T. R. and Coates, G. R.
"Transient Combustion in Mobile, Gas-Permeable
Propellants"
Acta Astron., v. 3, n. 7-8, pp. 575-591. 1976
13. Gough, P. S. and Zwarts, F. J.
"Theoretical Model for Ignition of Gun Propellant"
Final Report, Part II, Contract N00174-72-C-0223. 1972
14. Gough, P. S.
"The NOVA Code: A User's Manual"
Final Report, Task I, Contract N00174-79-C-0082. 1979
15. Fisher, E. B. and Graves, K. W.
"Mathematical Model of Double Base Propellant
Ignition and Combustion in the 81-mm Mortar"
CAL Report No. DG-3029-D-1. 1972
16. Fisher, E. B. and Trippe, A. P.
"A Mathematical Model of Center Core Ignition in
the 175-mm Gun"
Calspan Report No. VQ-5163-D-2. 1974
17. Fisher, E. B.
"Propellant Ignition and Combustion in the 105-mm
Howitzer"
Calspan Report No. VQ-5524-D-1. 1975
18. Fisher, E. B. and Trippe, A. P.
"Development of a Basis for Acceptance of Continuously
Produced Propellant"
Calspan Report No. VQ-5163-D-1. 1975
19. Gough, P. S.
"Theoretical Study of Two-Phase Flow Associated
with Granular Bag Charges"
Final Report, Contract DAAK11-77-C-0028. 1978

20. Horst, A. W. and Gough, P. S.
 "Modeling Ignition and Flamespread Phenomena in
 Bagged Artillery Charges"
 Ballistic Research Laboratory Technical Report
 ARBRL-TR-02263. (AD #A091790) 1980
21. Gough, P. S.
 "The Flow of a Compressible Gas Through an Aggregate
 of Mobile, Reacting Particles"
 Ph.D. Thesis, McGill University. 1974
22. Gough, P. S. and Zwarts, F. J.
 "Modeling Heterogeneous Two-Phase Reacting Flow"
 AIAA J v. 17, n. 1, pp. 17-25. 1979
23. Gough, P. S.
 "On the Closure and Character of the Balance Equations
 for Heterogeneous Two-Phase Flow"
 Dynamics and Modelling of Reactive Systems,
 Academic Press. 1980
24. Williams, F. A.
 "The Role of Black Powder in Propelling Charges"
 Picatinny Arsenal Technical Report 4770. 1975
25. Gough, P. S.
 "Modeling of Two-Phase Flow in Guns"
 Progress in Astronautics and Aeronautics v. 66,
 edited by H. Krier and M. Summerfield. 1979
26. Krier, H., Shimpi, S. A. and Adams, M. J.
 "Interior Ballistic Predictions Using Data from
 Closed and Variable Volume Simulators"
 Univ. of Illinois at Urbana-Champaign.
 TR-AAE-73-6. 1973
27. Horst, A.
 Private Communication
28. Ergun, S.
 "Fluid Flow Through Packed Columns"
 Chem. Eng. Progr. v. 48, p. 89. 1952
29. Anderssen, K. E. B.
 "Pressure Drop in Ideal Fluidization"
 Chem. Eng. Sci. v. 15, pp. 276-297. 1961

30. Gelperin, N. I. and Einstein, V. G.
"Heat Transfer in Fluidized Beds"
Fluidization, edited by J. F. Davidson and
D. Harrison. Academic Press, NY 1971
31. MacCormack, R. W.
"The Effect of Viscosity in Hypervelocity Impact
Cratering"
AIAA Paper No. 69-354. 1969
32. Moretti, G.
"Calculation of the Three-Dimensional, Supersonic,
Inviscid, Steady Flow Past an Arrow-Winged Airframe"
POLY-AE/AM Report No. 76-8. 1976
33. Richtmyer, R. D. and Morton, K. W.
"Difference Methods for Initial Value Problems"
Interscience. 1967
34. Roache, P. J.
"Computational Fluid Dynamics"
Hermosa Publishers 1972
35. Thompson, J. F., Thames, F. C. and Mastin, C. W.
"Automatic Numerical Generation of Body-Fitted
Curvilinear Coordinate System for Field Containing
Any Number of Arbitrary Two-Dimensional Bodies"
J. Comp. Phys. 15, pp. 299-319. 1974
36. Lenchitz, C. and Hayes, E.
"An Analysis of Black Powder Ignition and Performance.
Ignition Properties of Black Powder, Phase I"
Proc. 16th JANNAF Combustion Meeting. 1979
37. Rose, J. E. and Hardt, A. P.
"Black Powder . . . A Modern Commentary . . . 1979"
Proc. 10th Symposium on Explosives and Pyrotechnics,
Franklin Research Center, Phila., PA. Feb. 14-16. 1979

NOMENCLATURE

English Symbols

A	Cross sectional area of a quasi-one-dimensional flow
a	Rate of propagation of granular disturbances
a_1	Value of a for settled bed during compression
a_2	Value of a for unloading or reloading bed when porosity is less than settling porosity
B_1	Burn rate additive constant
B_2	Burn rate pre-exponential factor
b	Covolume of gas phase
c	Speed of sound in gas phase
c_v, c_p	Specific heats at constant volume and constant pressure
D_p	Effective diameter of a grain of propellant
D_o	Initial external diameter of a grain of propellant
d	Total surface regression of a grain of propellant
\dot{d}	Rate of surface regression
d_o	Initial diameter of a perforation of a grain of propellant
E	Sum of internal and kinetic energies
e	Internal energy of gas phase
e_p	Chemical energy released in combustion of solid-phase
F_{RES}	Bore resistance
\vec{f}	Interphase drag
\hat{f}_s	Steady state interphase drag coefficient
g_o	Constant used to reconcile units of measurement
H	Parameter used to deduce propellant surface temperature by cubic profile method
h	Heat transfer coefficient
j	Mass flux
K	Friction factor for pressure drop due to mass flux through permeable section of bag
k	Thermal conductivity
L_o	Initial length of a grain of propellant

M	Projectile mass
\dot{m}	Mass production per unit volume per unit time due to propellant combustion
\dot{m}_i, \dot{m}_o	Mass fluxes to and from a region
\dot{m}_{bp}	Mass production per unit surface area per unit time due to reactive substrates of bag
N	Number of perforations of a grain of propellant
Nu_p	Nusselt number based on effective grain diameter
\vec{n}	Normal vector
n	Burn rate exponent
Pr	Prandtl number
p	Pressure
q	Heat flux
Re_p	Reynolds number based on effective particle diameter
R_i, R_o	Radii of surfaces of quasi-one-dimensional axial flow across which mass enters and exits, respectively
r	Radial coordinate
S_p	Surface area of a propellant grain
s	Streamwise coordinate in region of quasi-one-dimensional flow
S_p	Surface area of propellant per unit volume
T	Gas temperature
T_p	Surface temperature of solid phase
t	Time
\vec{u}	Gas velocity vector, components (u, v)
\vec{u}_p	Solid phase velocity vector, components (u_p, v_p)
u_T	Streamwise velocity component of gas in region of quasi-one-dimensional flow
V_p	Volume of a propellant grain
w, w_p	ζ -component of gas, solid velocity in computational plane
x, x_p	η -component of gas, solid velocity in computational plane
z	Axial coordinate

Greek Symbols

α	Characteristic coordinate
α_p	Thermal diffusivity of a grain of propellant
γ	Ratio of specific heats
ϵ	Porosity
ϵ_o	Settling porosity
ζ	Computational coordinate, corresponds to axial direction
η	Computational coordinate, corresponds to radial direction
λ	Coefficient used to render balance equations pseudo-totally hyperbolic
μ	Viscosity
ρ	Density of gas
ρ_p	Density of solid propellant, a constant
σ	$(1 - \epsilon)R$
τ	Time coordinate in computational frame
ψ	Rate of production of gas per unit volume due to igniter

Special Symbols and Subscripts

D/Dt	Convective derivative along average gas-phase streamline
D/Dt_p	Convective derivative along average solid-phase streamline
IG, p	The subscript IG is used to denote properties of the igniter and p is used to denote properties of the solid-phase. Gas-phase properties are unsubscripted.

Appendix: TDNOVA - Structure and Use

The purpose of this Appendix is to provide sufficient information to enable the reader to make use of the code TDNOVA. To that end we provide, in three successive subsections, an overview of the code macrostructure, a brief discussion of the storage arrays and the principal storage pointers, and a complete description of the code input and output files.

CODE MACROSTRUCTURE

TDNOVA is written in the Fortran IV language. Because it was developed on a 32 bit word machine (ITEL AS-6), all computations are performed in double precision. Thus, users of the code who employ a machine in which the standard word length is 60 or more bits, such as the CYBER 7600, may wish to convert the code to single precision as a measure of economy.

The code macrostructure is illustrated schematically in figure A.1. The main program TDMAIN is essentially a dummy routine. It executes a call to INPUT, to read and print the problem data, to SETUP, to initialize the problem variables, and then transfers complete control of the calculations to subroutine TDXC, which is, in fact, the principal executive routine. The code version at BRL, following the return from TDXC, also executes a call to a BRL routine called RECAP, whose purpose is to plot data accumulated in the summary tables during the evolution of the solution.

Users who wish to reduce the overall code storage may perform successive overlays onto INPUT and SETUP since these subroutines are each called just once.

The next level of code structure is defined by the principal linkages to the executive TDXC. TDXC is supported by the output routine LOGOUT which is called intermittently to prepare tables of state variables at various times. LOGOUT also stores the solution on disc, if desired, and executes optional calls to PLOTRZ which is responsible for the preparation of graphic representations of the solution. PLOTRZ may be seen to be supported by subroutines PLTLOD, PLTFLO, CONTR, and SEE. Additional output processing is performed by subroutine SUMTAB, which prepares tables of summary data, as desired. These, however, are only printed at the conclusion of the run. It is these data which are further processed by the BRL routine RECAP.

TDXC is supported by TDMESH and MAP which respectively allocate storage to the various computational regions and assure that the two-dimensional regions of ullage have boundary-fitted equipotential meshes.

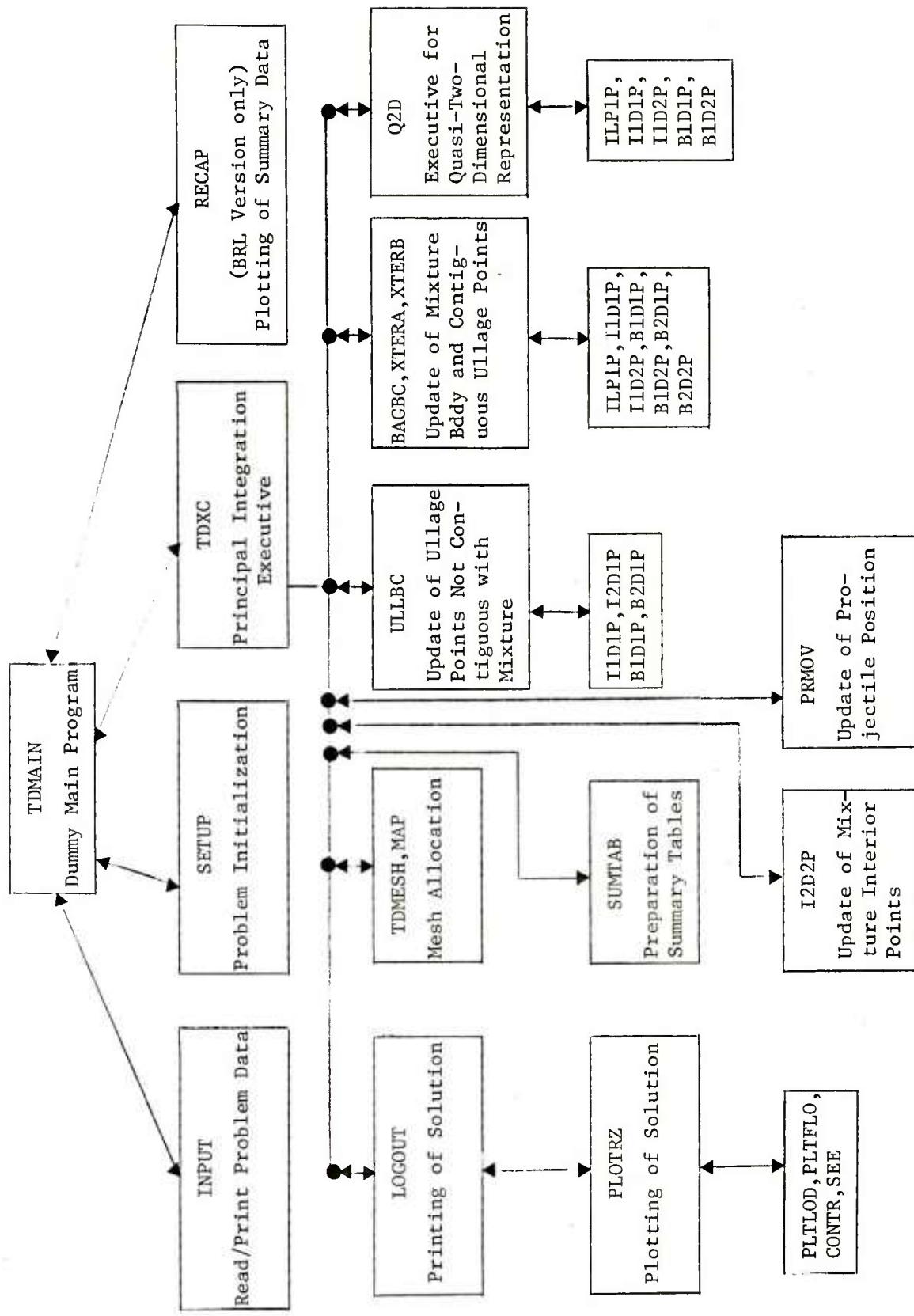


Figure A.1 Schematic Illustration of TDNOVA Macrostructure
(Only principal linkages and routines are shown. See Table A.1.)

The integration of all points interior to the mixture is performed by I2D2P. Subroutine ULLBC executes calls to I2D1P to update the solution in the interior of all fully two-dimensional regions of ullage and also performs the update of all ullage boundary points which are not contiguous with the mixture. In the latter capacity it is supported by the routines B1D1P, I1D1P and B2D1P.

Subroutine BAGBC is called by TDXC to effect the update of all points on the boundary of the mixture as well as these points in the ullage which are contiguous with the mixture. For this purpose, mesh points in a region of quasi-one-dimensional ullage adjacent to the bag are regarded as contiguous with the mixture. BAGBC itself is responsible for the implementation of all the conditions of physical compatibility at the bag boundaries contiguous with quasi-one-dimensional ullage. It is supported by the routines I1D1P, I1D2P which update points in the interior of adjacent quasi-one-dimensional regions, by B1D1P, B1D2P, and E2D2P which provide trial update values for contiguous boundary points, and by ILP1P which updates lumped parameter ullage regions. The conditions of physical compatibility at points contiguous with two-dimensional ullage are implemented by XTERA and XTERB which are called from BAGBC.

Subroutines I2D2P, ULLBC and BAGBC are called only until the flow has evolved to such a point as to be amenable to a quasi-two-dimensional analysis. Subsequently TDXC is supported entirely by the routine Q2D which acts as the integration executive for the quasi-two-dimensional representation. Q2D enforces the conditions of physical compatibility between regions and is supported by the subroutines I1D1P, I1D2P, B1D1P, B1D2P and by ILP1P.

We also note that TDXC is cycled twice per complete integration step since each step is composed of a predictor and a corrector level as discussed further in the next section when we consider the structure of the storage arrays.

TDNOVA does contain other routines than those which we have mentioned explicitly in this section. A complete summary of the various routines and their linkages to one another is contained in Table A.1. Following the entry for TDMAIN, all the routines are described in alphabetic order. Not shown in Table A.1 are the linkages to standard Fortran functions and to the standard CALCOMP software package. The use of the latter may be system-dependent, particularly with regard to the plot initialization and termination routines.

DATA STORAGE

Table A.2 provides a summary of all the program variables stored in common blocks, except those associated with the BRL program RECAP. Variables which are purely local to a given subroutine or function are not described in Table A.2.

The purpose of the present discussion is to provide a description of the principal pointers and to explain the manner in which the state variables are stored.

Each integration step consists of two levels, a predictor and a corrector. The counter NDT, initialized to zero, is bumped by unity on each predictor and each corrector level. The switch INT = MOD(NDT+1,2) is equal to 1 on a predictor level and 0 on a corrector level. At each level the variables NI, NF, NP are used to construct pointers to current, future and past storage and they cyclically run through the values 1, 2, 3.

A total of nine regions are defined at any time as illustrated by figure A.2. Each region I has attributes NDZ(I), the total number of axial mesh points; NDR(I), the total number of radial mesh points; MODL(I), an indicator of the type of flow equations to be used; and NRBIAS(I), used to construct storage pointers, as described below. The indicator MODL(I) has the following set of values.

MODL(I)	Type of Flow in Region I
1	Lumped Parameter One-Phase (LP1P)
2	Quasi-One-Dimensional One-Phase (1D1P) (Axially directed)
3	Quasi-One-Dimensional One-Phase (1D1P) (Radially directed)
4	Two-Dimensional One-Phase (2D1P)
5	Quasi-One-Dimensional Two-Phase (1D2P)
6	Two-Dimensional Two-Phase (2D2P)

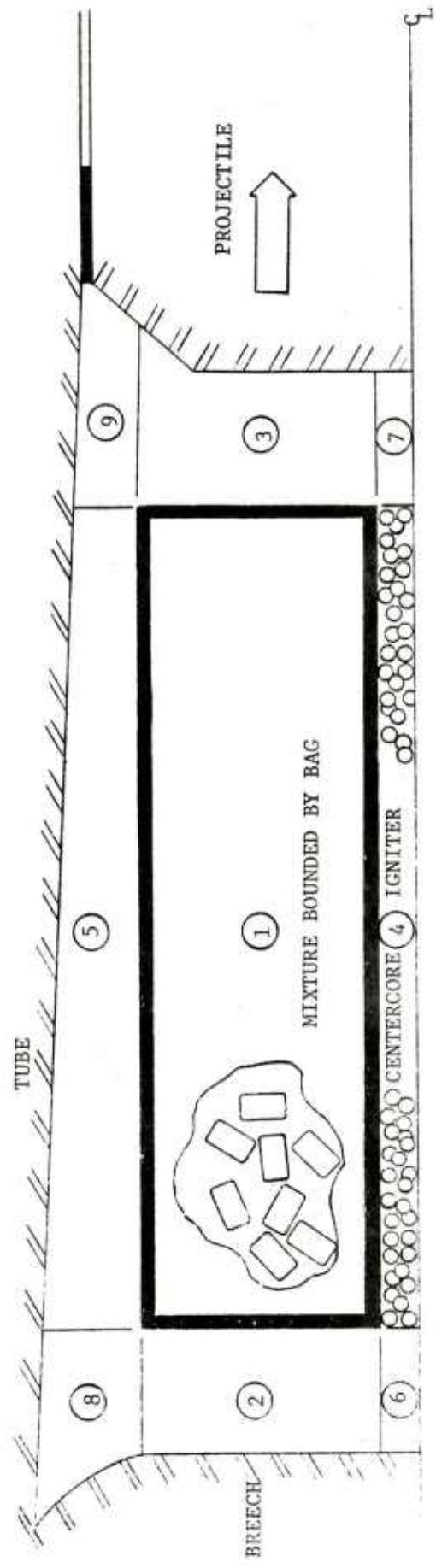


Figure A.2 Nomenclature for Region Labelling in TDNOVA

The parenthetical acronyms for each type of region are also present in the names of subroutines dedicated to the integration of each type of region with the further distinguishing characteristic of an initial letter I or B according as the routine pertains to interior or boundary mesh points. The distinction between cases MODL(I) = 2 and 3 is purely formal in the present version of the code.

The state variables are stored in singly indexed arrays. Accordingly, the values pertaining to a given mesh point at a given level of a given time step are located by construction of a suitable pointer. Consider, for example, the gas-phase density, stored in the array RHO(J).

The array RHO contains values of density in the following order. First the NDZ(1) values pertaining to the line $\eta = 0$ in region 1 (the mixture) are stored. These are followed by successive blocks of NDZ(1) values corresponding to successive increments of the coordinate η . There are, of course, a total of NDR(1) such blocks. Then there are loaded NDZ(2) values corresponding to the line $\eta = 0$ for region 2 and so on through region 9. It should be noted that NDZ and NDR are each equal to at least one for any type of region. A lumped parameter region has NDZ = NDR = 1.

Following the last value for region 9, there are loaded NDZ(1) values for the line $\eta = 0$ in region 1 corresponding to the next level of integration. Three such integration level blocks are defined.

The quantity NRBIAS(I) is defined as

$$NRBIAS(I) = \begin{cases} \sum_{J=1}^{I-1} NDZ(J)*NDR(J) & \text{for } I > 1 \\ 0 & \text{for } I = 1 \end{cases}$$

and the total number of mesh points is given by

$$NPTOT = \sum_{J=1}^9 NDZ(J)*NDR(J)$$

We also define the quantity

$$NIBIAS = (NI - 1)*NPTOT$$

and an analogous definition is given for NPBIAS, NFBIAS which are used to construct pointers to NP- and NF- integration levels respectively.

Now let $\rho_{IJ,K}^{NI}$ be the value of ρ at the ζ -mesh point I, the η -mesh point J, in region K, at level NI, then

$$\rho_{IJ,K}^{NI} = RHO(NIBIAS + NRBIAS(K) + (J - 1)*NDZ(K) + I)$$

This pattern is followed for all the independent state variables. However for dependent state variables, such as the internal energy, only current storage is maintained. Thus pointers for the array E are constructed similarly to those for RHO, but the quantities NIBIAS, NPBIAS, NFBIAS are not used.

INPUT AND OUTPUT FILES

TDNOVA is structured to run only one problem. It does not support parametric input, nor does it search for a new data set following problem termination. A given problem, however, may be stored on disc at various points during the solution, as part of the logout procedure. Subsequently, the problem may be restarted from disc at any intermediate point at which logout has been performed. The structure of the input files is described fully in Table A.3 and requires no additional comment here.

We conclude with a description of the output files. Logout may be obtained at multiples of an inputted number of integration steps and at multiples of an inputted increment of time. The logout associated with such intermediate points of the solution consists of printed text, disc storage and plotting, all in accordance with user-selectable options.

When printed logout is requested it is furnished as a table of the current storage of the state variables in the order of storage described in the preceding section. Thus the table proceeds to list the state variables region by region. Within each region, the state variables are tabulated in successive blocks of constant η (which may be thought of as approximately constant radius). The tabulated quantities are, in order: Region number as described in figure A.2, mesh axial coordinate, mesh radial coordinate, gas-phase pressure, intergranular stress, gas-phase axial velocity, gas-phase radial velocity, solid-phase axial velocity, solid-phase radial velocity, porosity, gas-phase density, gas-phase temperature, solid-phase surface temperature, and, for points on the boundary of the bag, indicators as to whether the bag is permeable and/or ruptured.

As an option, any of the state variables may be plotted as an isometric view of the surface $\phi(z,r)$ where ϕ is a state variable.

Hidden lines are normally deleted, but may be retained as an option. Further information concerning the solution may be had by requesting contour plots of the same surfaces. The isometric and contour plotting options are, however, fully independent of one another. An additional option is the preparation of flowfield plots in which the velocity fields of the gas- and solid-phases are represented, separately, as vector fields superimposed on the computational mesh.

A plot of the ignition delay, essentially a contour representation, may also be had. This is prepared just once, at the conclusion of the run. It should be noted that this map is constructed by reference to the initial configuration of the propelling charge.

In addition to the intermediate logout one may request certain summary data. These are accumulated during the run and are printed following the completion of the calculation. A table of summarized interior ballistic data is printed which contains, in order: time, breech pressure, base pressure and space mean pressure, mass fraction of unburnt propellant, mass fraction of unburnt centercore charge, projectile travel, velocity and acceleration. The pressures are all centerline quantities. Optionally, these summary data may be followed by pressure histories at user-selectable locations for comparison with experimental pressure gage records. These values of pressure may be obtained at any axial location on either the tube or the centerline. The tabulation of these histories is followed by a tabulation of the histories of pressure difference formed by subtracting the last pressure history from each of the others.

Table A.1 Summary of TDNOVA Routines and Linkages

TDMAIN	<p><u>Purpose:</u> Dummy main program. Calls INPUT to read and print data, SETUP to initialize problem and then calls TDXC, which is the principal executive routine, to integrate the solution. The BRL version also executes an optional call to RECAP to plot the summary data.</p> <p><u>Calls:</u> INPUT, (RECAP), SETUP, TDXC</p> <p><u>Called by:</u> None</p>
AP	<p><u>Purpose:</u> Function to compute rate of propagation of intergranular disturbances as a function of porosity and direction of loading.</p> <p><u>Calls:</u> SIGL</p> <p><u>Called by:</u> B1D2P, B2D2P, I1D2P, I2D2P</p>
AREA	<p><u>Purpose:</u> Function to compute area of quadrilateral defined by four mesh points.</p> <p><u>Calls:</u> None</p> <p><u>Called by:</u> BAGBC, Q2D, SETUP, SUMTAB, TDMESH, XSECT</p>
BAGBC	<p><u>Purpose:</u> Subroutine to enforce physical boundary conditions at all mesh points on the boundary of the mixture as well as contiguous points in the ullage.</p> <p><u>Calls:</u> AREA, B1D1P, B1D2P, B2D2P, CALFLO, CALPRM, DIS, EPTOR, ILP1P, I1D1P, I1D2P, LOGOUT, NAYBOR, PRTOE, XTERA, XTERB</p> <p><u>Called by:</u> TDXC</p>
BLKDAT	<p><u>Purpose:</u> Block data initialization</p> <p><u>Calls:</u> None</p> <p><u>Called by:</u> None</p>

B1D1P Purpose: Subroutine to perform trial update of boundary point of a quasi-one-dimensional single-phase region.

Calls: PSI

Called by: BAGBC, Q2D, ULLBC, XTERB

B1D2P Purpose: Subroutine to perform trial update of boundary point of a quasi-one-dimensional two-phase region.

Calls: AP, CDB, DP, PROPER, PSI, QP, RDOT, SIGL

Called by: BAGBC, Q2D, XTERB

B2D1P Purpose: Subroutine to perform trial update of boundary point of a two-dimensional, single-phase region.

Calls: LOGOUT, PSI

Called by: ULLBC, XTERA, XTERB

B2D2P Purpose: Subroutine to perform trial update of boundary point of a two-dimensional, two-phase region.

Calls: AP, CDB, DP, LOGOUT, PSI, QP, RDOT

Called by: BAGBC

CALFLO Purpose: Subroutine to calculate rate of reaction of bag substrate at a given point.

Calls: None

Called by: BAGBC, Q2D, XTERB

CALPRM Purpose: Subroutine to compute friction factor associated with bag flow resistance at a given mesh point.

Calls: None

Called by: BAGBC

CDB	<u>Purpose:</u> Function to compute friction factor associated with flow resistance through granular bed.
	<u>Calls:</u> None
	<u>Called by:</u> B1D2P, B2D2P, I1D2P, I2D2P, Q2D
CONTR	<u>Purpose:</u> Subroutine to prepare contour plots of a given state variable.
	<u>Calls:</u> None
	<u>Called by:</u> PLOTRZ
DIS	<u>Purpose:</u> Function to compute algebraic distance from a given mesh point to a given external boundary element along either a line of constant radius (external boundary given as breech or projectile) or constant axial location (external boundary given as centerline or tube).
	<u>Calls:</u> None
	<u>Called by:</u> BAGBC, PLTLOD, PRMOV, Q2D, SETUP, TDMESH TDXC, ULLBC, XSECT, XTERB
DP	<u>Purpose:</u> Function to compute ratio of volume to surface area of a propellant grain as a function of surface regression.
	<u>Calls:</u> PERF19, SPLIND
	<u>Called by:</u> B1D2P, B2D2P, I1D2P, I2D2P, Q2D
EPTOR	<u>Purpose:</u> Function to compute density of gas as a function of internal energy and pressure.
	<u>Calls:</u> None
	<u>Called by:</u> BAGBC, Q2D, SETUP, TDXC, XTERA, XTERB
ERTOP	<u>Purpose:</u> Function to compute pressure of gas as a function of internal energy and density.
	<u>Calls:</u> None
	<u>Called by:</u> TDMESH

FIT	<p><u>Purpose:</u> Subroutine which replaces NIN equally spaced data by NOUT equally spaced data using a cubic spline interpolation.</p> <p><u>Calls:</u> SPLINE</p> <p><u>Called by:</u> PLOTRZ</p>
ILP1P	<p><u>Purpose:</u> Subroutine to update state of a lumped parameter, single-phase region.</p> <p><u>Calls:</u> PSI</p> <p><u>Called by:</u> BAGBC, Q2D</p>
INPUT	<p><u>Purpose:</u> Subrcutine to read and print input data used to define problem. See Table A.3 for discussion of input data.</p> <p><u>Calls:</u> None</p> <p><u>Called by:</u> TDMAIN</p>
I1D1P	<p><u>Purpose:</u> Subroutine to update state of quasi-one-dimensional, single-phase flow at a given interior mesh point.</p> <p><u>Calls:</u> PSI</p> <p><u>Called by:</u> BAGBC, Q2D, ULLBC</p>
I1D2P	<p><u>Purpose:</u> Subroutine to update state of a quasi-one-dimensional, two-phase region at a given interior mesh point.</p> <p><u>Calls:</u> AP, CDB, DP, PROPER, PSI, QP, RDOT, SIGL</p> <p><u>Called by:</u> BAGBC, Q2D</p>
I2D1P	<p><u>Purpose:</u> Subroutine to update state of a two-dimensional, single-phase region at all interior mesh points.</p> <p><u>Calls:</u> LOGOUT, PSI</p> <p><u>Called by:</u> ULLBC</p>
I2D2P	<p><u>Purpose:</u> Subroutine to update state of a two-dimensional, two-phase region at all interior mesh points.</p> <p><u>Calls:</u> AP, CDB, DP, LOGOUT, PSI, QP, RDOT</p> <p><u>Called by:</u> TDXC</p>

LOGOUT Purpose: Subroutine to print tables of flow-field distributions and execute disc storage, plotting, as required.

Calls: PLOTRZ

Called by: BAGBC, B2D1P, B2D2P, I2D1P, I2D2P,
 SETUP, TDMESH, TDXC

MAP Purpose: Subroutine to establish mesh within a two-dimensional domain to satisfy coupled elliptic equations subject to either Dirichlet or Neumann boundary conditions.

Calls: None

Called by: SETUP, TDXC

NAYBOR Purpose: Subroutine to compute region and mesh pointers as required by BAGBC.

Calls: None

Called by: BAGBC, XSECT, XTERA

PERF19 Purpose: Subroutine to compute surface area and volume of a nineteen-perforation propellant grain following slivering.

Calls: None

Called by: DP

PLOTRZ Purpose: Principal plotting executive for preparation of CALCOMP plots of state variables (isometric, contour, flowfield) and ignition delay.

Calls: CONTR, FIT, PLTFLO, PLTLOD, SEE

Called by: LOGOUT, TDXC

PLTFLO Purpose: Subroutine to prepare CALCOMP flow-field plots.

Calls: PLTLOD

Called by: PLOTRZ

PLTLOD Purpose: Subroutine to transfer data from computational arrays into plotting arrays

Calls: DIS

Called by: PLOTRZ, PLTFLO

PRES Purpose: Function to compute gas pressure or intergranular stress or sum of both at a specified boundary location.

Calls: SIDE

Called by: PRMOV, SUMTAB, TDMESH

PRMOV Purpose: Subroutine to update motion of projectile.

Calls: DIS, PRES

Called by: TDXC

PROPER Purpose: Subroutine to move vector properties of solid phase into scalar arrays.

Calls: None

Called by: B1D2P, I1D2P, SETUP, TDXC

PRTOE Purpose: Function to compute internal energy of gas as a function of pressure and density.

Calls: None

Called by: BAGBC, Q2D, TDMESH, TDXC, XTERA, XTERB

PSI Purpose: Function to compute rate of discharge of externally injected ignition stimulus at a given point and time.

Calls: None

Called by: B1D1P, B1D2P, B2D1P, B2D2P, ILP1P, I1D1P, I1D2P, I2D1P, I2D2P

QP	<p><u>Purpose:</u> Function to compute interphase heat transfer coefficient and update solid phase surface temperature according to cubic profile approximation.</p> <p><u>Calls:</u> VIS</p> <p><u>Called by:</u> B1D2P, B2D2P, I1D2P, I2D2P</p>
Q2D	<p><u>Purpose:</u> Subroutine to effect update of solution through one integration step (predictor or corrector) when a quasi-two-dimensional representation of the propelling charge is in effect.</p> <p><u>Calls:</u> AREA, B1D1P, B1D2P, CALFLO, CDB, DIS, DP, EPTOR, ILP1P, I1D1P, I1D2P, PRTOE</p> <p><u>Called by:</u> TDXC</p>
RDOT	<p><u>Purpose:</u> Function to compute rate of surface regression of solid phase as a function of ambient pressure.</p> <p><u>Calls:</u> SPLIND</p> <p><u>Called by:</u> B1D2P, B2D2P, I1D2P, I2D2P</p>
SEE	<p><u>Purpose:</u> Subroutine to assess visibility of given line segment in preparation of isometric views of state variables at a given time.</p> <p><u>Calls:</u> None</p> <p><u>Called by:</u> PLOTRZ</p>
SETUP	<p><u>Purpose:</u> Subroutine to perform initialization of all state variables and internally set constants.</p> <p><u>Calls:</u> AREA, DIS, EPTOR, LOGOUT, MAP, PROPER, SUMTAB, TDMESH, XSECT</p> <p><u>Called by:</u> TDMAIN</p>
SIDE	<p><u>Purpose:</u> Subroutine to compute pointers to mesh storage along a given side of a given computational region.</p> <p><u>Calls:</u> None</p> <p><u>Called by:</u> PRES, TDMESH, TDXC, ULLBC</p>

SIGL	<p><u>Purpose:</u> Function to compute intergranular stress as a function of porosity on nominal loading curve.</p> <p><u>Calls:</u> None</p> <p><u>Called by:</u> AP, B1D2P, I1D2P, TDXC</p>
SPLIND	<p><u>Purpose:</u> Subroutine to prepare table of values of second derivatives for double precision cubic spline interpolation.</p> <p><u>Calls:</u> None</p> <p><u>Called by:</u> DP, RDOT</p>
SPLINE	<p><u>Purpose:</u> Subroutine to prepare table of values of second derivatives for single precision cubic spline interpolation.</p> <p><u>Calls:</u> None</p> <p><u>Called by:</u> FIT</p>
SUMTAB	<p><u>Purpose:</u> Subroutine to compile and print tables of summary data.</p> <p><u>Calls:</u> AREA, PRES</p> <p><u>Called by:</u> SETUP, TDXC</p>
TDMESH	<p><u>Purpose:</u> Subroutine to administer region representations and perform mesh point allocations.</p> <p><u>Calls:</u> AREA, DIS, ERTOP, LOGOUT, PRES, PRTOE, SIDE</p> <p><u>Called by:</u> SETUP, TDXC</p>
TDXC	<p><u>Purpose:</u> Subroutine to control overall update and logout procedures. TDXC is the principal executive routine of TDNOVA.</p> <p><u>Calls:</u> BAGBC, DIS, EPTOR, I2D2P, LOGOUT, MAP, PLOTRZ, PRMOV, PROPER, PRTOE, Q2D, SIDE, SIGL, SUMTAB, TDMESH, ULLBC, XSECT</p> <p><u>Called by:</u> TDMAIN</p>

ULLBC Purpose: Subroutine to control update of all ullage mesh points other than those contiguous with the mixture.

Calls: B1D1P, B2D1P, DIS, I1D1P, I2D1P, SIDE

Called by: TDXC

VIS Purpose: Function to compute gas viscosity as a function of temperature.

Calls: None

Called by: QP

XSECT Purpose: Subroutine to compute cross-sectional flow area of quasi-one-dimensional regions and volume of lumped parameter regions.

Calls: AREA, DIS, NAYBOR

Called by: SETUP, TDXC

XTERA Purpose: Subroutine to impose physical boundary conditions at a point on the side of the bag adjacent to a fully two-dimensional region of ullage.

Calls: B2D1P, EPTOR, NAYBOR, PRTOE

Called by: BAGBC

XTERB Purpose: Subroutine to update solution at a corner of the bag which is bounded by a fully two-dimensional flow on one or both sides.

Calls: B1D1P, B1D2P, B2D1P, CALFLO, DIS, EPTOR, PRTOE

Called by: BAGBC

Table A.2 Glossary of Fortran Variables Contained in Common Blocks

Variable	Common Block	Definition
ALFAP	C02	Thermal diffusivity of solid phase, α_p
AP1	C02	Rate of propagation of intergranular disturbances in solid phase, at settling porosity, under conditions of loading, a_1
AP2	C02	Rate of propagation of intergranular disturbances in solid phase, under conditions of unloading, a_2
AP3	C11	$a_1 \epsilon_o$
AXC	C34	Array containing cross-sectional areas of quasi-one-dimensional regions and volumes of lumped parameter regions.
BITS	C39	$\zeta_z^2 + \zeta_r^2$ if $\tau - \zeta$ characteristic and $\eta_z^2 + \eta_r^2$ if $\tau - \eta$ characteristic
BV	C02	Covolume of products of combustion of propellant, b
CFLON	C39	$\partial m / \partial u_n$
CHSO	C14	Charge standoff distance
CP	C02	Specific heat at constant pressure of products of combustion of propellant, c_p
CPF	C11	$0.4 P_r^{-2/3} \gamma R_g / (\gamma - 1)$
CV	C02	Specific heat at constant volume of products of combustion of propellant, c_v
D	C01	Array containing values of d, solid-phase surface regression
DATR	C37	Plot buffer array
DATV	C37	Plot buffer array
DATX	C18	Array used to construct plots
DATY	C18	Array used to construct plots

Variable	Common Block	Definition
DATZ	C37	Plot buffer array
DB	C34	Computational mesh increment along boundary
DEFF	C11	Effective particle diameter, D_p
DN	C34	Computational mesh increment normal to boundary
DPERF	C02	Initial diameter of grain perforation, d_o
DR	C36	$\Delta\eta$
DT	C09	Time step, $\Delta\tau$
DTLOG	C05	Time increment for logout
DTMAX	C05	Maximum time step consistent with C-F-L condition
DTSUM	C16	Time increment for storage in summary tables
DZ	C36	$\Delta\zeta$
E	C01	Array containing current values of e , gas-phase internal energy
ECH	C02	Chemical energy released during combustion of solid-phase, e_p
EDDSIG	C44	$\partial e / \partial \sigma$ in quasi-one-dimensional two-phase flow
EIG	C02	Chemical energy released by externally injected ignition stimulus, e_{IG}
EPDSIG	C36	$\partial e / \partial \sigma$ in two-dimensional two-phase flow
EPS	C01	Array containing values of porosity
EPS0	C02	Initial porosity of solid phase
ER	C30	$(1 - \varepsilon_o) / \varepsilon_o$
ERCT	C25	Array of values of chemical energy released by reactive substrates of bag
ESS	C27	Local value of ESSIG
ESSBC	C44	Energy of basepad at boundary of centerline

Variable	Common Block	Definition
ESSIG	C27	Array of values of chemical energy released by bag reactive substrates
ETAS	C34	Mesh transformation coefficient, ζ_s , for quasi-one-dimensional regions
E0	C02	Settling porosity of solid phase, ε_o
EOR	C11	$1/\varepsilon_o$
E1	C30	$1/(1 + 0.02(1 - \varepsilon_o)/\varepsilon_o)$
FAC	C20	Scale factor used in plotting
FBRES	C26	Array of values of bore resistance
FLOIG	C27	Array of values of rate of reactivity of bag substrates
FLOLP	C41	Array of values of m for transfer between quasi-one-dimensional and lumped parameter regions
FOLPC	C41	Array of values of $\partial m / \partial u$ for transfers between quasi-one-dimensional and lumped parameter regions
FLON	C34	Rate of mass flow normal to boundary, positive exiting mixture
FLRCT	C25	Array of values of rate of bag reactivity
FLOSBC	C44	Rate of reactivity of basepad at boundary of centercore
FLOSS	C27	Local value of FLOIG
FR	C42	Plotting parameter
FS	C20	Length of axis corresponding to state variable being plotted
FZ	C42	Plotting parameter
G	C04	Constant used to reconcile units, g_o
GAM	C02	Ratio of specific heats of products of combustion of propellant, γ

Variable	Common Block	Definition
GAM1	C02	$\gamma - 1$
GLEN	C02	Initial length of a grain, L_o
GMOL	C02	Molecular weight of products of combustion of propellant, M_w
H	C01	Array containing values of state variable H used in cubic profile solution of solid-phase surface temperature
HIDEDR	C42	Plotting parameter
HIDEDZ	C42	Plotting parameter
I	C35	Counter used to enumerate side and corners of a two-dimensional region during update of boundary values
ICA	C17	Switch used in hidden line algorithm
ICB	C17	Switch used in hidden line algorithm
ICL	C17	Switch used in hidden line algorithm
IHL	C17	Counter used in hidden line algorithm
INDIMR	C07	Number of mesh points allocated to η -coordinate in representation of propelling charge
INDIMZ	C07	Number of mesh points allocated to ζ -coordinate in representation of propelling charge
INT	C07	Switch used to indicate whether step is predictor or corrector
IPLTV	C13	Array of switches used to determine whether or not to create isometric plots of various state variables during logout
ISWP	C17	Counter used in hidden line algorithm
ITYP	C31	Pointer to type of solid phase (propellant or centercore) under consideration

Variable	Common Block	Definition
J	C35	Loop counter enumerating points on a side of a two-dimensional region
JDB	C35	Storage increment in direction tangential to boundary
JDN	C35	Storage increment in direction normal to boundary
JF	C35	Pointer to future storage level of a point on the boundary of a two-dimensional region
JP	C35	Pointer to past storage level of a point on the boundary of a two-dimensional region
JPLTV	C13	Array of switches used to determine whether or not to create contour plots of various state variables during logout
JRCT	C25	Number of entries in tables of bag reactivity rates
JRP	C03	Number of entries in array RPHI
JTP	C03	Number of entries in array TPHI
JZP	C03	Number of entries in array ZPHI
J1	C35	Loop delimiter used in update of side of boundary
J2	C35	Loop delimiter used in update of side of boundary
J3	C35	Storage increment along side of two-dimensional region
J4	C35	Pointer to current storage level of a point on the boundary of a two-dimensional region
KDIMR	C42	Number of radial points in plot field
KDIMRM	C42	KDIMR - 1
KDIMZ	C42	Number of axial points in plot field
KDIMZM	C42	KDIMZ - 1

Variable	Common Block	Definition
KDR	C38	Array of values of NDR, a subset
KDZ	C38	Array of values of NDZ, a subset
KP	C02	Thermal conductivity of solid-phase, k_p
KPT	C42	Number of points in plot field
LOC	C16	Array of switches indicating whether stations for pressure history summaries are on tube or centerline
MAPIT	C15	Maximum allowable number of iterations for convergence of SOR algorithm for equipotential mesh
MODL	C29	Array of values indicating type of flow in each region
NABRB	C35	Pointer to mesh point adjacent to side $\eta = \text{constant}$ at corner of mixture
NABRBF	C41	Pointer to future storage level of side $\eta = \text{constant}$ at corner of mixture
NABRC	C35	Pointer to mesh point adjacent to corner of mixture, in corner region of physical domain
NABRCF	C41	Pointer to future storage level of point of physical corner region adjacent to corner of mixture
NABRN	C35	Pointer to mesh point adjacent to first point on a given side of a two-dimensional region
NABRND	C35	Storage increment between points adjacent to a given side of a two-dimensional region
NABRNF	C41	Pointer to future storage level of mesh point adjacent to boundary of two-dimensional region. Pertains to $\zeta = \text{constant}$ side of corner of mixture

Variable	Common Block	Definition
NBASIC	C25	Pointer to reactivity data set associated with breech end of centercore
NBH1	C17	Counter used in hidden line algorithm
NBH2	C17	Counter used in hidden line algorithm
NBH11	C17	Counter used in hidden line algorithm
NBRES	C26	Number of entries in bore resistance arrays
NBY	C14	Array containing number of points used to specify bag boundaries initially
NBYE	C22	Array of number of entries in tables of points used to define external boundaries
NCCORE	C25	Switch to determine whether or not a centercore ignition charge is present
NCHAR	C35	Switch used to indicate whether characteristic is $\tau - \zeta$ or $\tau - \eta$
NCYCL	C35	Switch used to indicate whether characteristic direction has been altered in call to B2D2P
NDIMR	C35	Number of η -mesh points in a region
NDIMRM	C35	NDIMR - 1
NDIMZ	C35	Number of ζ -mesh points in a region
NDIMZM	C35	NDIMZ - 1
NDR	C29	Array of values of η -mesh points allocated to regions
NDSKR	C06	Switch used to determine whether or not solution is to be initialized by disc read
NDSKW	C06	Switch used to determine whether or not solutions are to be stored on disc during logout
NDT	C07	Counter, initialized to zero, bumped by unity on each predictor and each corrector level of each integration step
NDTSKP	C32	Switch used to bypass tests of C-F-L criterion four steps out of five

Variable	Common Block	Definition
NDZ	C29	Array of values of number of ζ -mesh points allocated to regions
NEW	C17	Counter used in hidden line algorithm
NF	C07	Pointer to future storage
NFBIAS	C12	Quantity used to construct pointer to future storage location in state variable arrays
NH	C17	Number of points on horizon of visibility in isometric plotting
NI	C07	Pointer to current storage
NIBIAS	C12	Quantity used to construct pointer to current storage location in state variable arrays
NMPT	C23	Maximum number of mesh points to be used in dynamic allocation mode
NMSH	C23	Switch used to determine strategy for mesh allocation
NOC	C17	Switch used in hidden line algorithm
NOR	C14	Array of switches indicating whether initial mesh in mixture satisfies Dirichlet or Neumann boundary conditions
NP	C07	Pointer to past storage
NPBIAS	C12	Quantity used to construct pointer to past storage location in state variable arrays
NPERF	C02	Total number of perforations in a grain, N
NPERM	C24	Array of pointers to bag permeability data sets
NPLCON	C06	Switch used to determine whether or not contour plots are required on logout
NPLFLM	C06	Switch used to determine whether flame-spread map is to be plotted at conclusion of run
NPLFLO	C06	Switch used to determine whether or not flow field plots are required on logout

Variable	Common Block	Definition
NPLOT	C06	Switch used to determine whether or not isometric plots are required on logout
NPRINT	C06	Switch used to determine whether or not printed output is required on logout
NPRM	C25	Number of bag permeability data sets
NPT	C35	Total number of mesh points in a region
NPTBY	C14	Array indicating numbers of points pre-allocated to various segments of boundaries of bag
NPTOL	C29	Switch used to indicate whether or not quasi-two-dimensional analysis is in effect
NPTOT	C07	Total number of mesh points allocated at any time
NRBIAS	C29	Array of values used to construct storage pointers
NRCT	C25	Number of bag reactivity data sets
NREACT	C24	Array of pointers to bag reactivity data sets
NREGB	C35	At a corner of the mixture, NREGB points to the region adjacent to the $\eta =$ constant side
NREGC	C35	At a corner of the mixture, NREGC points to a corner region of the physical domain
NREGN	C35	Pointer to region adjacent to boundary point of two-dimensional region. At a corner, NREGN points to the $\zeta =$ constant side
NSTEP	C06	Number of integration steps for logout
NSTOP	C06	Number of integration steps for termination of solution
NSUBSK	C27	Array of pointers to bag permeability data sets

Variable	Common Block	Definition
NSUBSM	C27	Array of pointers to bag reactivity data sets
NSUM	C16	Number of stations at which pressure histories are to be summarized
NSUMRY	C06	Switch used to determine whether summary tables are to be prepared for printing at the conclusion of the run
NTABIG	C25	Switch to determine whether or not an externally injected ignition stimulus is present
NTB	C21	Array of number of entries in burn rate tables
NVHL	C20	Switch used to determine whether or not to delete hidden lines from isometric plots
OD	C02	Initial diameter of grain, D_0
OREL	C15	Overrelaxation factor used to establish equipotential mesh
P	C01	Array containing values of p, gas-phase pressure
PDUN	C36	$\partial p / \partial u_n$
PERM	C27	Array of values of bag friction factor
PFAC1	C39	$\partial p / \partial m$ for quasi-one-dimensional region
PFAC2	C41	Array of values of $\partial p / \partial u_T$ for boundaries of quasi-one-dimensional regions
PFACLP	C41	$\partial p / \partial m$ for lumped parameter region
PHI	C03	Array of values used to describe rate of injection of external ignition stimulus, ψ
PI	C04	π
PR	C04	Prandtl number, Pr

Variable	Common Block	Definition
PR3	C04	$Pr^{1/3}$
PRM	C25	Array of values of initial bag friction factor
PRMASS	C26	Projectile mass
PST	C02	Initial pressure of gas phase
PTOL	C23	Fractional pressure difference below which quasi-two-dimensional solution is implemented
QFLON	C45	Array of values of transverse mass fluxes used in quasi-two-dimensional analysis
QPFACT1	C45	Array of values of $\partial p / \partial m$ used in quasi-two-dimensional analysis
QRFACT1	C45	Array of values of $\partial p / \partial m$ used in quasi-two-dimensional analysis
QUFACT1	C45	Array of values of $\partial u / \partial m$ used in quasi-two-dimensional analysis
R	C04	Universal gas constant, R
RBY	C14	Array of radial coordinates of points on boundaries of bag
RBYE	C22	Array of values of radial coordinate of points on external boundaries
RFAC1	C39	$\partial p / \partial m$ for quasi-one-dimensional region
RFAC2	C41	Array of values of $\partial p / \partial u_T$ for quasi-one-dimensional region
RFACLP	C41	$\partial p / \partial m$ for lumped parameter region
RFRAC	C23	Radial spatial resolution factor
RG	C04	Gas constant for products of combustion of solid-phase, R_G
RHO	C01	Array containing values of ρ , gas-phase density

Variable	Common Block	Definition
RHODP	C36	$\partial \rho / \partial p$
RHOP	C02	Solid-phase density, ρ_p
RM	C01	Array containing values of r_m , radial component of mesh point
RMO	C43	Array of initial values of r_m
ROZR	C39	η_r if $\tau - \zeta$ characteristic and ζ_r if $\tau - \eta$ characteristic
ROZZ	C39	η_z if $\tau - \zeta$ characteristic and ζ_z if $\tau - \eta$ characteristic
RPHI	C03	Array of radial positions used to describe externally injected ignition stimulus
RRA	C39	r_η
RS	C20	Length of r-axis in plots
RUPINT	C25	Array of values of interval over which bag rupture is completed once rupture strength is exceeded
RUPSTR	C25	Array of values of bag rupture strength
RUPT	C27	Array of values of time at which bag rupture is complete locally
RZA	C39	r_ζ
SAFE	C05	Safety factor used to divide time step allowable by C-F-L criterion
SDUPN	C36	$\partial \sigma / \partial \hat{u}_n$
SDVP	C44	$\partial \sigma / \partial V_n$ where σ is in a quasi-one-dimensional region and V_n is normal component of velocity of contiguous region

Variable	Common Block	Definition
SGB	C36	Equal to ± 1 depending on side of region at which boundary point is located
SGN	C36	Equal to ± 1 depending on side of region at which boundary point is located
SIG	C01	Array containing values of σ , intergranular stress (N.B. This is a partial stress)
SIGLC	C11	$\rho_p a_1^2 \epsilon_o^2 / g_o$
SQUDOT	C11	$[(u - u_p)^2 + (v - v_p)^2]^{1/2}$
SSK	C27	Local value of PERM
TBN	C21	Array of values of burn rate exponents
TB1	C21	Array of values of burn rate additive constants
TB2	C21	Array of values of burn rate pre-exponential coefficients
TDR	C36	$2\Delta\eta$
TDZ	C36	$2\Delta\zeta$
TEMST	C02	Initial temperature of gas phase
TIG	C02	Ignition temperature of solid-phase, T_{ig}
TIME	C02	Time, τ
TIMIG	C43	Array of values of time at which ignition occurs
TITLE	C08	Array containing problem title
TKPP	C11	$3k_p^2$
TMAXP	C21	Array of values of maximum pressure for which burn rate coefficients are to be used
TMAXSM	C33	Pending time for data storage in summary table

Variable	Common Block	Definition
TOL	C15	Maximum allowable fractional displacement of mesh to satisfy equipotential equations
TP	C01	Array containing current values of T_p , solid-phase surface temperature
TPHI	C03	Array of times used to describe externally injected ignition stimulus
TRCT	C25	Array of values of times used to define rate of bag reactivity
TSTOP	C05	Time for termination of solution
U	C01	Array containing values of u , axial component of gas-phase velocity
UDUN	C36	$\partial u / \partial \hat{u}_n$
UDUT	C36	$\partial u / \partial \hat{u}_t$
UDOTN	C41	Array of values of $\dot{\hat{u}}_n$ (not in physical units)
UFAC1	C39	$\partial u_T / \partial m$ for quasi-one-dimensional region
UN	C34	Gas-phase velocity component normal to boundary (not in physical units)
UOLD	C41	Array of trial boundary values of u_T in quasi-one-dimensional regions
UP	C01	Array containing values of u_p , axial component of solid-phase velocity
UPDOTN	C41	Array of values of $\dot{\hat{u}}_{p_n}$ (not in physical units)
UPN	C36	Component of solid-phase velocity normal to boundary (not in physical units)
UPR	C01	Array containing values of v_p , radial component of solid-phase velocity
UPT	C36	Component of solid-phase velocity tangential to boundary (not in physical units)
UR	C01	Array containing values of v , radial component of gas-phase velocity

Variable	Common Block	Definition
URDUN	C36	$\partial v / \partial \hat{u}_n$
URDUT	C36	$\partial v / \partial \hat{u}_t$
UT	C34	Gas-phase velocity component parallel to boundary (not in physical units)
UTC	C40	Coefficient to convert \hat{u}_n into physical units
V	C34	Array containing current local state variables at boundary point in mixture
VE	C34	Current local value of e at boundary point in mixture
VFRA	C40	$1 + \frac{f \overline{\Delta\tau}}{\epsilon \rho u - u_p } \text{ where } \overline{\Delta\tau} = \Delta\tau$ on predictor level and $\overline{\Delta\tau} = \Delta\tau/2$ on corrector level
VPR	C26	Projectile velocity
VPRDOT	C26	Projectile acceleration
VRM	C34	Current local value of r_m at boundary point in mixture
VUM	C34	Mesh velocity in quasi-one-dimensional region
XA	C17	Coordinate of endpoint of segment to be plotted isometrically
XALFAP	C28	Array of values of ALFAP
XAP1	C28	Array of values of AP1
XAP2	C28	Array of values of AP2
XAP3	C28	Array of values of AP3
XB	C17	Coordinate of endpoint of segment to be plotted isometrically
XCHWT	C28	Array of values of initial mass of solid phase
XDPERF	C28	Array of values of DPERF

Variable	Common Block	Definition
XDTA	C34	Rate of change of cross-sectional area or of volume
XDTU	C34	Rate of change of gas-phase velocity at boundary of quasi-one-dimensional region
XDTUP	C44	$\partial u_p / \partial t$ in quasi-one-dimensional two-phase flow
XECH	C28	Array of values of ECH
XEPS0	C28	Array of values of EPS0
XER	C30	Array of values of ER
XE0	C28	Array of values of E0
XEOR	C28	Array of values of EOR
XE1	C30	Array of values of E1
XGLEN	C28	Array of values of GLEN
XH	C19	Array of abscissae of visibility horizon in hidden line algorithm
XKP	C28	Array of values of KP
XNPERF	C28	Array of values of NPERF
XOD	C28	Array of values of OD
XPR	C26	Projectile displacement
XRHOP	C28	Array of values of RHOP
XSIGLC	C28	Array of values of SIGLC
XTIG	C28	Array of values of TIG
XTKPP	C28	Array of values of TKPP
YA	C17	Coordinate of endpoint of segment to be plotted isometrically
YB	C17	Coordinate of endpoint of segment to be plotted isometrically
YH	C19	Array of ordinates of visibility horizon in hidden line algorithm

Variable	Common Block	Definition
ZBRES	C26	Array of projectile displacements used to define bore resistance
ZBY	C14	Array of axial coordinates of points on boundaries of bag
ZBYE	C22	Array of axial coordinates of points on external boundaries
ZFRAC	C23	Axial spatial resolution factor
ZM	C01	Array containing values of z_m , axial coordinate of mesh point
ZMO	C43	Array of initial values of z_m
ZORR	C39	ζ_r if $\tau - \zeta$ characteristic and η_r if $\tau - \eta$ characteristic
ZORZ	C39	ζ_z if $\tau - \zeta$ characteristic and η_z if $\tau - \eta$ characteristic
ZPHI	C03	Array of axial positions used to describe externally injected ignition stimulus
ZRA	C39	z_η
ZS	C20	Length of z-axis in plots
ZSTOP	C05	Projectile displacement for termination of solution
ZSUM	C16	Array of axial locations of stations at which histories of gas pressure are to be tabulated at conclusion of run
ZZA	C39	z_ζ

Table A.3 Description of TDNOVA Input Files

<u>File 1: One Card (20A4) Problem Title</u>	
TITLE	Problem title, up to 80 alphanumeric characters.
<u>File 2: Two Cards (9I5,4X,11I1,4X,11I1/4F10.1) Control Parameters</u>	
NPRINT	0 - Tables of state variables are not printed. 1 - Tables of the state variables are printed on a logout schedule determined by NSTEP and DTLOG as described in File 3.
NSUMRY	0 - No summary tables are produced at the conclusion of the run. 1 - Summary tables are provided of the histories of the conventional interior ballistic variables and, if NSUM (File 3) is greater than zero, of the histories of pressure at selected positions in the tube. 2 - The summary data are not only tabulated at the end of the run but are also plotted by the BRL plot package (RECAP). This option applies only to the code version at BRL.
NPLOT	0 - No isometric plots produced on logout. 1 - CALCOMP plots of state variables produced on logout. These plots are isometric views of the state variables as selected in accordance with the values of the array IPLTV defined below.
NVHL	0 - Hidden lines are removed from CALCOMP plots. 1 - If not zero, hidden lines are retained and plots are faired with a cubic spline interpolator.
NPLCON	0 - No CALCOMP contour plots produced on logout. 1 - Contour plots will be produced in accordance with the values of JPLTV defined below.
NPLFLO	0 - No CALCOMP plots of flow field on logout. 1 - Plots are produced of the velocity fields of both the gas and solid phases.

NPLFLM 0 - No summary plot of flamespreading.
 1 - A summary plot is produced at the conclusion of the run to illustrate the path of flamespreading by reference to contours of the ignition boundary at various times.

NDSKW 0 - No disc storage on logout.
 1 - Solution saved on disc (Unit 8) on logout.

NDSKR 0 - Initial distributions are constructed from input data.
 >0 - If not zero, initial distributions are read from Unit 8 and correspond to time step equal to NDSKR.

IPLTV(I), I=1,...,11 - If IPLTV(I) = 1, the quantity tabulated below will be plotted as an isometric view. Otherwise not.

I	QUANTITY PLOTTED IF IPLTV(I)=1
1	Mesh
2	Porosity
3	Granular Stress
4	Pressure
5	Density
6	Gas Axial Velocity
7	Solid Axial Velocity
8	Gas Radial Velocity
9	Solid Radial Velocity
10	Gas Temperature
11	Particle Surface Temperature

JPLTV(I), I=1,...,11 - As per IPLTV but pertaining to the contour plots. It should be noted that if JPLTV(1) is set equal to one, the result is identical to that produced if IPLTV(1) = 1.

FAC - Scale factor for CALCOMP plots. (Begin second card).

ZS - Length of Z-axis in CALCOMP plots (in).

RS - Length of R-axis in CALCOMP plots (in).

FS - Length of ordinate axis in isometric plots (in).

File 3: One Card (I5,F10.0,I5,F10.0) Logout Parameters

NSTEP >0 - Number of integration steps before logout.
 0 - Logout will occur on every predictor and
 every corrector level.

DTLOG >0 - Time increment at which logout will occur
 (msec).
 ≤0 - Logout will occur only in accordance with
 the value of NSTEP.

NSUM - Number of stations for storage of pressure
 summary data, maximum of eight.
 Note: If NSUM is greater than zero, File
 34 is required.

DTSUM - Desired time interval for summary table
 storage (msec). Automatically increased
 if table overflow about to occur during
 execution.

File 4: One Card (I5,2F10.0) Termination Parameters

NSTOP - Number of integration steps before termination.
 If problem involves a disc start, NSTOP is
 taken to include all steps up to the point of
 restart.

TSTOP - Time for termination of solution (msec).

ZSTOP - Projectile displacement for termination of
 solution (cm).

File 5: Two Cards (5I5/6F10.0) Mesh Parameters

NMSH 0 - The propelling charge is initially
 represented by means of INDIMZ axial mesh
 points and INDIMR radial mesh points. The
 propelling charge will continue to be given
 a fully two-dimensional representation
 until the PTOL criterion is satisfied as
 defined below. Moreover, in this case the
 ullage contiguous with each side of the
 charge will be represented as quasi-one-
 dimensional for that period in which the
 charge is treated as two-dimensional.

1 - The treatment of the propelling charge will be the same as in the case when NMSH = 0. However, the mesh will be allocated to the ullage regions dynamically in such a fashion as to constrain the total number of storage points to a value less than or equal to NMPT defined below, and so that no region has an axial mesh spacing less than ZFRAC times the distance between the breech face and the base of the projectile or a radial mesh spacing less than RFRAC times the radius of the bore, where ZFRAC and RFRAC are input quantities as defined below. Thus, in this case, the ullage may be treated as either quasi-one-dimensional or as fully two-dimensional accordingly as its geometry dictates.

- | | |
|--------|---|
| NMPT | - Maximum number of storage points to be used in dynamic allocation of mesh as occurs when NMSH is equal to one and PTOL criterion has not been satisfied. It should be noted that NMPT is a grand total and includes the points allocated to the propelling charge as well as those to be allocated dynamically to the ullage. |
| INDIMZ | - Number of axial mesh points used to represent the propelling charge in both the fully two-dimensional and quasi-one-dimensional modes. |
| INDIMR | - Number of radial mesh points used to represent the propelling charge in the fully two-dimensional mode. |
| MAPIT | - Maximum number of iterations to be used in determining initial mesh distribution by successive over-relaxation. See also Files 12-15 for discussion of boundary conditions on initial mesh. |
| SAFE | - Safety factor to be applied to CFL stability criterion. Must be greater than or equal to 1. |
| TOL | - Maximum fractional displacement of mesh coordinates for initial configuration to be accepted as converged. |

OREL	- Over-relaxation factor. Must be between 1 and 2.
PTOL	- Quantity used to determine point in solution at which a quasi-two-dimensional representation of the flow is adequate to complete the solution. The value of PTOL is inspected only after the completion of flamespreading and when the bag rupture is complete. If the maximum value of pressure difference in each cross-section of the tube does not exceed PTOL times the pressure at the centerline, the solution is continued according to a quasi-two-dimensional representation until all radial ullage has disappeared or until burnout occurs and according to a quasi-one-dimensional representation thereafter.
ZFRAC	- Dimensionless quantity used to allocate axial distribution of mesh to individual regions when NMSH is equal to one.
RFRAC	- Dimensionless quantity used to allocate radial distribution of mesh to individual regions when NMSH is equal to one.

File 6: One Card (3F10.0) Ambient Conditions

TEMST	- Initial temperature of both phases ($^{\circ}$ K).
PST	- Initial pressure of gas phase (MPa).
CHSO	- Charge standoff distance (cm). This input datum may be used to effect axial translations of the propelling charge and it is understood to be a quantity which is added to the axial coordinate of every point used to define the geometry of the bag. If the description of the bag (see Files 12-15) represents it as already having a standoff with respect to the breech face then CHSO may be given a negative value provided that that this does not result in a rearward translation of such a magnitude as actually to move the charge out of the gun chamber.

File 7: One Card (8F10.0) Solid Phase Constitutive Data

XCHWT - Initial mass of granular bed (kg).
XEPSO - Initial porosity of granular bed (-).
XEO - Settling porosity of bed (-).
XAP1 - Rate of propagation of compressive wave
in settled bed (m/sec).
XAP2 - Rate of propagation of unloading wave
(m/sec).
XRHOP - Density of solid phase (gm/cc).
XKP - Thermal conductivity of solid phase
(J/cm-sec-°K).
XALFAP - Thermal diffusivity of solid phase (cm**2/sec).
Note: If XCHWT is entered as zero, a value is computed from
XEPSO and is printed following the tabulation of all the
input data.
If a non-zero value of XCHWT is entered, the value of
XEPSO will be replaced by a value which is consistent
with the entered value of XCHWT.
If XEO is entered as zero, it will automatically be
replaced by the value of XEPSON, following the preceding
test of consistency of XEPSON with XCHWT.
Internally revised values of XEPSON and XEO are printed
following the tabulation of all input data.

File 8: One Card (3F10.0) Gas Phase Constitutive Data

GAM - Ratio of specific heats.
GMOL - Molecular Weight (gm/gm-mol).
BV - Covolume (cc/gm).

File 9: Two or More Cards (2F10.0,I5/(8F10.0))
Solid Phase Combustion Characteristics

XTIG	- Ignition temperature of solid phase (°K).
XECH	- Chemical energy released in combustion (J/gm).
NTB	- Number of tabular data to define burn rate. Maximum of 10.
TMAXP(1)	- Maximum pressure for which corresponding coefficients are applicable in the law $RDOT=TB1(1)+TB2(1)*P**TBN(1)$ where P is pressure and RDOT is regression rate. This quantity starts a new card.
TB1(1)	- Burn rate additive constant (cm/sec).
TB2(1)	- Burn rate pre-exponential factor (cm/sec-MPa**TBN(1)).
TBN(1)	- Burn rate exponent (-).
.	.
.	.
TMAXP(NTB)	- Maximum pressure for which corresponding coefficients are applicable in the law $RDOT=TB1(NTB)+TB2(NTB)*P**TBN(NTB)$ where P is pressure and RDOT is regression rate.
TB1(NTB)	- Burn rate additive constant (cm/sec).
TB2(NTB)	- Burn rate pre-exponential factor (cm/sec-MPa**TBN(NTB)).
TBN(NTB)	- Burn rate exponent (-).

- Notes:
- (1) A new card is started for TMAXP(1),TMAXP(3) etc., but not for TMAXP(2),TMAXP(4) etc.
 - (2) If the pressure exceeds TMAXP(NTB), the corresponding data are used as default values.

File 10: One Card (4F10.0) Grain Geometry

XOD - External diameter (cm).
XGLEN - Length (cm).
XDPERF - Diameter of perforation (cm).

XNPERF - Number of perforations (-).

Note: XNPERF may be 1, 7, or 19 when the file refers to the propelling charge, as it does in this location. However, the similar File 24, used to describe the centercore igniter, only uses the value of XOD(2) to describe the geometry of the powder since it is taken to consist of spherical grains.

File 11: One Card (4I5) Boundary File Counters

NBY(1) - Number of entries in file for tabular description of rear of bag, maximum of fifty.
NBY(2) - Number of entries in file for tabular description of front of bag, maximum of fifty.
NBY(3) - Number of entries in file for tabular description of properties of internal circumferential boundary of bag, maximum of fifty.
NBY(4) - Number of entries in file for tabular description of properties of external circumferential boundary of bag, maximum of fifty.

File 12: NBY(1) Cards (2F10.0,4I5) Properties of Rear of Bag

ZBY(1,1) - Axial location of first point on rear (cm).
RBY(1,1) - Corresponding radial location (cm).
NPERM(1,1) - Pointer to data set (File 32) to describe the flow resistance of a section of the bag wall defined by (ZBY(1,1),RBY(1,1)) and (ZBY(2,1),RBY(2,1)). May take any integer value from zero to ten.

NREACT(1,1)	- Pointer to data set (File 33) to describe the reactivity of the same segment. May take any integer value from zero to ten.
NPTBY(1,1)	- Number of points pre-allocated to interior of line segment defined by (ZBY(1,1),RBY(1,1)) and (ZBY(2,1),RBY(2,1)).
NOR(1,1)	<ul style="list-style-type: none"> - If NOR(1,1) = 0, Dirichlet data will be assumed for the initial distribution of mesh points on the line segment defined by (ZBY(1,1),RBY(1,1)) and (ZBY(2,1),RBY(2,1)). - If NOR(1,1) = 1, Neumann data will be assumed for the initial distribution of mesh points on the line segment defined by (ZBY(1,1),RBY(1,1)) and (ZBY(2,1),RBY(2,1)). The mesh will be made orthogonal on the boundary segment.
ZBY(NBY(1),1)	- Axial location of last point on rear (cm).
RBY(NBY(1),1)	- Corresponding radial location (cm).

File 13: NBY(2) Cards (2F10.0,4I5) Properties of Front of Bag	
ZBY(1,2)	- Axial location of first point on front (cm).
RBY(1,2)	- Corresponding radial location (cm).
NPERM(1,2)	- Pointer to data set (File 32) to describe the flow resistance of a section of the bag wall defined by (ZBY(1,2),RBY(1,2)) and (ZBY(2,2),RBY(2,2)). May take any integer value from zero to ten.
NREACT(1,2)	- Pointer to data set (File 33) to describe the reactivity of the same segment. May take any integer value from zero to ten.
NPTBY(1,2)	- Number of points pre-allocated to interior of line segment defined by (ZBY(1,2),RBY(1,2)) and (ZBY(2,2),RBY(2,2)).

NOR(1,2)	0 - Dirichlet data will be assumed for the initial distribution of mesh points on the line segment defined by (ZBY(1,2), RBY(1,2)) and (ZBY(2,2),RBY(2,2)). 1 - Neumann data will be assumed for the initial distribution of mesh points on the line segment defined by (ZBY(1,2), RBY(1,2)) and (ZBY(2,2),RBY(2,2)). The mesh will be made orthogonal on the boundary segment.
ZBY(NBY(2),2)	- Axial location of last point on front (cm).
RBY(NBY(2),2)	- Corresponding radial location (cm).
<hr/>	
File 14: NBY(3) Cards (2F10.0,4I5)	Properties of Internal Circumferential Boundary of Bag
ZBY(1,3)	- Axial location of first point on internal boundary of bag (cm).
RBY(1,3)	- Corresponding radial location (cm).
NPERM(1,3)	- Pointer to data set (File 32) to describe the flow resistance of a section of the bag wall defined by (ZBY(1,3),RBY(1,3)) and (ZBY(2,3),RBY(2,3)). May take any integer value from zero to ten.
NREACT(1,3)	- Pointer to data set (File 33) to describe the reactivity of the same segment. May take any integer value from zero to ten.
NPTBY(1,3)	- Number of points pre-allocated to interior of line segment defined by (ZBY(1,3),RBY(1,3)) and (ZBY(2,3),RBY(2,3)).
NOR(1,3)	0 - Dirichlet data will be assumed for the initial distribution of mesh points on the line segment defined by (ZBY(1,3),RBY(1,3)) and (ZBY(2,3),RBY(2,3)). 1 - Neumann data will be assumed for the initial distribution of mesh points on the line segment defined by (ZBY(1,3),RBY(1,3)) and (ZBY(2,3),RBY(2,3)). The mesh will be made orthogonal on the boundary segment.
.	

ZBY(NBY(3),3) - Axial location of last point (cm).
RBY(NBY(3),3) - Corresponding radial location (cm).

File 15: NBY(4) Cards (2F10.0,4I5) Properties of External
Circumferential Boundary of Bag

ZBY(1,4) - Axial location of first point on external boundary of bag (cm).
RBY(1,4) - Corresponding radial location (cm).
NPERM(1,4) - Pointer to data set (File 32) to describe the flow resistance of a section of the bag wall defined by (ZBY(1,4),RBY(1,4)) and (ZBY(2,4),RBY(2,4)). May take any integer value from zero to ten.
NREACT(1,4) - Pointer to data set (File 33) to describe the reactivity of the same segment. May take any integer value from zero to ten.
NPTBY(1,4) - Number of points pre-allocated to interior of line segment defined by (ZBY(1,4),RBY(1,4)) and (ZBY(2,4),RBY(2,4)).
NOR(1,4) 0 - Dirichlet data will be assumed for the initial distribution of mesh points on the line segment defined by (ZBY(1,4),RBY(1,4)) and (ZBY(2,4),RBY(2,4)).
1 - Neumann data will be assumed for the initial distribution of mesh points on the line segment defined by (ZBY(1,4),RBY(1,4)) and (ZBY(2,4),RBY(2,4)). The mesh will be made orthogonal on the boundary segment.
ZBY(NBY(4),4) - Axial location of last point (cm).
RBY(NBY(4),4) - Corresponding radial location (cm).

Notes on Files 12 through 15:

- (1) Note that a new card is started for each value of ZBY(I,K), all I and K.
- (2) Values of NPTBY and NOR are only required for the first NBY-1 cards of each boundary set, at most.
- (3) Files 12-15 must be consistent with each other in the sense that the end points must match to define a continuous closed boundary for the computational domain.
- (4) In Files 12 and 13, the first point must correspond to the internal boundary of the domain and the last point must correspond to the external boundary.
- (5) In Files 14 and 15, the first point must correspond to the rear and the last must correspond to the front of the bag.
- (6) Only endpoints of Files 12-15 are treated as explicit corners of the computational domain. All other corners, defined implicitly by the tabular data within a given file are treated as though they lay on a continuously differentiable curve.
- (7) A mesh point is always located at the initial location defined by ZBY(I,K), RBY(I,K), all I and K.
- (8) If NPERM is set equal to zero for any line segment, the segment in question is assumed to be fully permeable to the gas phase. A similar convention applies to NREACT for which a zero value implies that the segment in question is non-reactive.
- (9) With regard to the initial description of the properties of the bag, it should be noted that a fully independent analysis is not made of the permeability and reactivity of the corners. Instead, values of flow resistance and surface mass generation are established by extrapolation of either the source terms or of the state variables themselves along each side of the bag boundary.

- (10) For a given segment of the bag, the designated resistance and reactivity models are applied to all mesh points in the interior of the segment and to the mesh point at the start of the segment, but not to the mesh point at the end of the segment.
- (11) It is assumed that if flow resistance and reactivity models are specified, then the initial distribution of boundary points is to be determined by Dirichlet data.

File 16: One Card (4I5) External (Breech, Tube and Projectile)
Boundary File Counters

- NBYE(1) - Number of entries in file for tabular description of breech geometry, maximum of fifty.
- NBYE(2) - Number of entries in file for tabular description of geometry of projectile base, maximum of fifty.
- NBYE(3) - Number of entries in file for tabular description of geometry of internal circumferential boundary of tube (normally centerline), maximum of fifty.
- NBYE(4) - Number of entries in file for tabular description of geometry of external circumferential boundary of tube, maximum of fifty.

File 17: NBYE(1) Cards (2F10.0) Geometry of Breech

- ZBYE(1,1) - Axial location of first point on breech (cm).
- RBYE(1,1) - Corresponding radial location (cm).
- ZBYE (2,1) - Axial location of second point. Starts a new card.
-
- ZBYE(NBYE(1),1) - Axial location of last point on breech (cm).
- RBYE(NBYE(1),1) - Corresponding radial location (cm).

File 18: NBYE(2) Cards (2F10.0) Geometry of Projectile Base

ZBYE(1,2) - Axial location of first point on projectile base (cm).
RBYE(1,2) - Corresponding radial location (cm).
.
.
ZBYE(NBYE(2),2) - Axial location of last point on projectile base (cm).
RBYE(NBYE(2),2) - Corresponding radial location (cm).

File 19: NBYE(3) Cards (2F10.0) Geometry of Internal Circumferential Boundary

ZBYE(1,3) - Axial location of first point on internal boundary (cm).
RBYE(1,3) - Corresponding radial location (cm).
.
.
ZBYE(NBYE(3),3) - Axial location of last point (cm).
RBYE(NBYE(3),3) - Corresponding radial location (cm).

File 20: NBYE(4) Cards (2F10.0) Geometry of External Circumferential Boundary

ZBYE(1,4) - Axial location of first point on external boundary (cm).
RBYE(1,4) - Corresponding radial location (cm).
.
.
ZBYE(NBYE(4),4) - Axial location of last point (cm).
RBYE(NBYE(4),4) - Corresponding radial location (cm).

File 21: One Card (6I5) Igniter Discharge Table Counters and Options

NCCORE	0 - A centercore igniter is not considered. 1 - A centercore igniter is assumed to occupy the region interior to the bag, namely that defined by Files 14 and 19 over the axial extent of the charge. Files 22, 23 and 24 are required in this case.
NBASIG	- When NCCORE is equal to one, NBASIG is a pointer to a reactivity data set in the same sense as NREACT (File 12) and defines the discharge characteristics of that part of a basepad which overlaps the rear section of the centercore igniter tube.
NTABIG	0 - A tabular representation of an ignition stimulus viewed as an externally injected source is not considered. 1 - An externally injected ignition source is considered. Values of JZP, JRP and JTP must be specified and Files 25, 26, 27, 28 and 29 must be included.
JZP	- Number of axial stations in discharge table for case when NTABIG equals one. JZP must not exceed eight.
JRP	- Number of radial stations in discharge table for case when NTABIG equals one. JRP must not exceed eight.
JTP	- Number of time levels in discharge table for case when NTABIG equals one. JTP must not exceed eight.

File 22: One Card (8F10.0) Igniter Solid Phase Constitutive Data

Note: This file is required if and only if NCCORE is equal to one. Its contents are identical with those of File 7. Properties of the propellant are distinguished from those of the igniter internally to the program.

File 23: Two or More Cards (2F10.0,I5/(8F10.0))
Igniter Solid Phase Combustion Characteristics

Note: This file is required if and only if NCCORE is equal to one.
Its contents are identical with those of File 9.

File 24: One Card (4F10.0) Igniter Grain Geometry

Note: This file is required if and only if NCCORE is equal to one.
Its contents are identical with those of File 10. However,
as noted in the discussion of File 10, the centercore is
assumed to consist of spherical grains in the present version
of the code. Therefore, only the external diameter need be
specified in this file.

File 25: One Card (F10.0) Energy of External Ignition Source

Note: This file is required if and only if NTABIG is equal to one.

EIG - Energy of igniter gas (J/gm).

File 26: One Card (8F10.0) Axial Positions for Discharge Table

Note: This file is required if and only if NTABIG is equal to one.

ZPHI(I), I=1,JZP - Axial positions (cm).

File 27: One Card (8F10.0) Radial Positions for Discharge Table

Note: This file is required if and only if NTABIG is equal to one.

RPHI(I), I=1,JRP - Radial positions (cm).

File 28: One Card (8F10.0) Time Levels for Discharge Table

Note: This file is required if and only if NTABIG is equal to one.

TPHI(I), I=1,JTP - Time levels (msec).

File 29: JRP*JTP Cards (8F10.0) Discharge Table

Note: This file is required if and only if NTABIG is equal to one.

- PHI(1,1,1) - First value of rate of discharge per unit volume (gm/cc-sec).
- PHI(2,1,1) - Second value
- .
- PHI(JZP,1,1) - Value at last axial position, first radial position and first time.
- PHI(1,2,1) - Value at first axial, second radial position. This entry starts a new card.
- .
- PHI(JZP,JRP,JTP) - Last value.

File 30: One Card (F10.0,I5) Projectile Mass and Bore Resistance Counter

- PRMASS - Projectile mass (kg).
- NBRES - Number of entries in tabular description of bore resistance. Must not exceed 10.

File 31: One to Three Cards (8F10.0) Bore Resistance Table

- ZBRES(1) - First value of projectile displacement at which bore resistance is specified (cm).
- FBRES(1) - Corresponding value of bore resistance (MPa).
- .
- ZBRES(NBRES) - Last value of displacement.
- FBRES(NBRES) - Corresponding value of bore resistance.

NPRM	- Total number of bag resistance data sets. May take any integer value from zero to ten.
PRM(1)	- Initial friction factor for normal flux through bag element (-).
RUPSTR(1)	- Pressure difference supportable by bag element before rupture commences (MPa).
RUPINT(1)	- Time interval over which bag flow resistance decreases to zero in a linear fashion (msec). May have any non-negative value, including zero.
PRM(2)	- (New Card).
.	
.	
RUPINT(NPRM)	

Note: The impedance to gas flow is controlled by the friction factor. However, the motion of the solid phase at the external circumferential boundary is also influenced by the state of integrity of the bag. Dilatation of the bag beyond its initial radius will not occur until it is completely ruptured. Thus by setting PRM = 0 and RUPSTR equal to some large number (or RUPINT equal to some period which exceeds the firing interval) one may characterize a bag segment as impeding the motion of the solid phase alone.

A similar consideration applies at the internal circumferential boundary which embeds the structural characteristics of the centercore igniter tube. No radial displacement will occur in either the positive or the negative direction until the igniter tube is locally ruptured. The rupture pressure of the tube is assumed to be the same for bursting as for compression.

File 33: 1+NRCT*(2 or 3) Cards (I5/(I5,F10.0/(8F10.0)))
Bag Reactivity Data

NRCT - Total number of reactivity data sets. May take any integer value from zero to ten.

JRCT(1) - Number of pairs of data in tabular description of mass generation rate for element Type 1. (New card). Maximum of eight.

ERCT(1) - Chemical energy released by reaction of bag material (J/gm). Positive if reaction is exothermic.

TRCT(1,1) - Value of time (msec). (New Card).

FLORCT(1,1) - Corresponding rate of reaction of bag element (gm/cm**2-sec).

.

.

.

FLORCT(JRCT(1),1)

JRCT(2) - (New Card).

.

.

.

.

FLORCT(JRCT(NRCT),NRCT)

File 34: Two Cards (8F10.0/8I5) Pressure Summary Table Locations

Note: This file is required if and only if NSUM is not zero (See File 3).

ZSUM(1) - Axial location of first station (cm).

.

.

ZSUM(NSUM) - Axial location of last station (cm).

LOC(1) 0 - First station is assumed to be on the tube wall.
1 - First station is assumed to be on the centerline of the tube.

.

.

LOC(NSUM) - Location of the last station.

DISTRIBUTION LIST

<u>No. of Copies</u>	<u>Organization</u>	<u>No. of Copies</u>	<u>Organization</u>
12	Commander Defense Technical Info Center ATTN: DDC-DDA Cameron Station Alexandria, VA 22314	1	Director US Army ARRADCOM Benet Weapons Laboratory ATTN: DRDAR-LCB-TL Watervliet, NY 12189
1	Commander US Army Materiel Development and Readiness Command ATTN: DRCDMD-ST 5001 Eisenhower Avenue Alexandria, VA 22333	1	Commander US Army Watervliet Arsenal ATTN: SARWV-RD, R. Thierry Watervliet, NY 12189
1	Commander US Army Materiel Development and Readiness Command ATTN: DRCDE-DW 5001 Eisenhower Avenue Alexandria, VA 22333	1	Commander US Army Aviation Research and Development Command ATTN: DRSAV-E P. O. Box 209 St. Louis, MO 63166
10	Commander US Army Armament Research and Development Command ATTN: DRDAR-TSS (2 cys) DRDAR-LCA H. Fair S. Bernstein S. Einstein P. Kemmey D. Downs L. Schlosberg DRDAR-LCE, R. Walker DRDAR-SCA, L. Stiefel Dover, NJ 07801	1	Director US Army Air Mobility Research and Development Laboratory Ames Research Center Moffett Field, CA 94035
1	Commander US Army Armament Materiel Readiness Command ATTN: DRDAR-LEP-L, Tech Lib Rock Island, IL 61299	1	Commander US Army Communications Rsch and Development Command ATTN: DRDCO-PPA-SA Fort Monmouth, NJ 07703
1	Commander US Army Electronics Research and Development Command Technical Support Activity ATTN: DELSD-L Fort Monmouth, NJ 07703	1	Commander US Army Missile Command ATTN: DRSMI-R Redstone Arsenal, AL 35809

DISTRIBUTION LIST

<u>No. of Copies</u>	<u>Organization</u>	<u>No. of Copies</u>	<u>Organization</u>
1	Commander US Army Missile Command ATTN: DRSMI-YDL Redstone Arsenal, AL 35809	1	Commander Naval Sea Systems Command ATTN: SEA-62R2, J. Murrin National Center, Bldg. 2 Room 6E08 Washington, DC 20360
1	Commander US Army Natick Research and Development Command ATTN: DRXRE, D. Sieling Natick, MA 01762	5	Commander Naval Surface Weapons Center ATTN: Code G33, J. East D. McClure W. Burrell J. Johndrow Code DX-21, Tech Lib Dahlgren, VA 22448
1	Commander US Army Tank Automotive Research & Development Cmd ATTN: DRDTA-UL Warren, MI 48090	3	Commander Naval Surface Weapons Center ATTN: S. Jacobs, Code 240 Code 730 K. Kim, Code R-13 Silver Spring, MD 20910
2	Commander US Army Materiels and Mechanics Research Center ATTN: DRXMR-ATL Tech Lib Watertown, MA 02172	1	Commander Naval Underwater Systems Center Energy Conversion Dept. ATTN: Code 5B331, R. Lazar Newport, RI 02840
1	Commander US Army Research Office ATTN: Tech Lib P. O. Box 12211 Research Triangle Park NC 27706	2	Commander Naval Weapons Center ATTN: Code 388, R. Derr C. Price China Lake, CA 93555
1	Director US Army TRADOC Systems Analysis Activity ATTN: ATAA-SL, Tech Lib White Sands Missile Range NM 88002	1	Superintendent Naval Postgraduate School Dept of Mechanical Engineering ATTN: A. Fuhs Monterey, CA 93940
1	Chief of Naval Research ATTN: Code 473, R. Miller 800 N. Quincy Street Arlington, VA 22217		

DISTRIBUTION LIST

No. of Copies	<u>Organization</u>	No. of Copies	<u>Organization</u>
2	Commander Naval Ordnance Station ATTN: P. Stang C. Smith Indian Head, MD 20640	1	Foster Miller Associates, Inc. ATTN: A. Erickson 135 Second Avenue Waltham, MA 02154
1	AFOSR (L. Caveny) Bolling AFB, DC 20332	1	General Applied Sciences Labs ATTN: J. Erdos Merrick & Stewart Avenues Westbury Long Island, NY 11590
2	AFRPL/DYSC (D. George, J. Levine) Edwards AFB, CA 93523	1	General Electric Company Armament Systems Dept. ATTN: M. Bulman, Rm. 1311 Lakeside Avenue Burlington, VT 05402
1	AFATL/DSDL (O. Heiney) Eglin AFB, FL 32542	1	Hercules, Inc. Allegany Ballistics Laboratory ATTN: R. Miller P. O. Box 210 Cumberland, MD 21502
1	Aerojet Solid Propulsion Co. ATTN: P. Micheli Sacramento, CA 95813	1	Hercules, Inc. Bacchus Works ATTN: K. McCarty P. O. Box 98 Magna, UT 84044
1	ARO Incorporated ATTN: N. Dougherty Arnold AFS, TN 37389	1	Hercules, Inc. Eglin Operations AFATL/DSDL ATTN: R. Simmons Eglin AFB, FL 32542
1	Atlantic Research Corporation ATTN: M. King 5390 Cherokee Avenue Alexandria, VA 22314	1	IITRI ATTN: M. J. Klein 10 W. 35th Street Chicago, IL 60615
1	AVCO Corporation AVCO Everett Rsch Lab Div ATTN: D. Stickler 2385 Revere Beach Parkway Everett, MA 02149	1	Lawrence Livermore Laboratory ATTN: M.S. L-355, A. Buckingham P. O. Box 808 Livermore, CA 94550
1	Calspan Corporation ATTN: E. Fisher P. O. Box 400 Buffalo, NY 14221		
1	Foster Miller Assoc., Inc. ATTN: A. Erickson 135 Second Avenue Waltham, MA 02154		

DISTRIBUTION LIST

<u>No. of Copies</u>	<u>Organization</u>	<u>No. of Copies</u>	<u>Organization</u>
1	Olin Corporation Badger Army Ammunition Plant ATTN: R. Thiede Baraboo, WI 53913	1	Shock Hydrodynamics, Inc. ATTN: W. Anderson 4710-16 Vineland Avenue North Hollywood, CA 91602
1	Olin Corporation Smokeless Powder Operations ATTN: R. Cook P. O. Box 222 St. Marks, FL 32355	3	Thiokol Corporation Huntsville Division ATTN: D. Flanigan R. Glick Tech Library Huntsville, AL 35807
1	Paul Gough Associates, Inc. ATTN: P. Gough P. O. Box 1614 Portsmouth, NH 03801	2	Thiokol Corporation Wasatch Division ATTN: John Peterson Tech Library P. O. Box 524 Brigham City, UT 84302
1	Physics International Company 2700 Merced Street Leandro, CA 94577	2	United Technology Center ATTN: R. Brown Tech Library P. O. Box 358 Sunnyvale, CA 94088
1	Princeton Combustion Research Lab., Inc. ATTN: M. Summerfield 1041 US Highway One North Princeton, NJ 08540	1	Universal Propulsion Company ATTN: H. McSpadden 1800 W. Deer Valley Road Phoenix, AZ 85027
1	Pulsepower Systems, Inc. ATTN: L. Elmore 815 American Street San Carlos, CA 94070	1	Battelle Memorial Institute ATTN: Tech Library 505 King Avenue Columbus, OH 43201
1	Rockwell International Corp. Rocketdyne Division ATTN: BA08, J. Flanagan 6633 Canoga Avenue Canoga Park, CA 91304	1	Brigham Young University Dept. of Chemical Engineering ATTN: R. Coates Provo, UT 84601
1	Science Applications, Inc. ATTN: R. Edelman 23146 Cumorah Crest Woodland Hills, CA 91364	1	California Institute of Tech 204 Karman Lab Mail Stop 301-46 ATTN: F.E.C. Culick 1201 E. California Street Pasadena, CA 91125
1	Scientific Research Assoc., Inc. ATTN: H. McDonald P. O. Box 498 Glastonbury, CT 06033		

DISTRIBUTION LIST

<u>No. of Copies</u>	<u>Organization</u>	<u>No. of Copies</u>	<u>Organization</u>
1	California Institute of Technology Jet Propulsion Laboratory ATTN: L. Strand 4800 Oak Grove Drive Pasadena, CA 91103	1	Pennsylvania State University Dept of Mechanical Engineering ATTN: K. Kuo University Park, PA 16802
1	Case Western Reserve University Division of Aerospace Sciences ATTN: J. Tien Cleveland, OH 44135	1	Purdue University School of Mechanical Engineering ATTN: J. Osborn TSPC Chaffee Hall West Lafayette, IN 47906
3	Georgia Institute of Tech School of Aerospace Eng. ATTN: B. Zinn E. Price W. Strahle Atlanta, GA 30332	1	Rutgers State University Dept. of Mechanical and Aerospace Engineering ATTN: S. Temkin University Heights Campus New Brunswick, NJ 08903
1	Institute of Gas Technology ATTN: D. Gidaspow 3424 S. State Street Chicago, IL 60616	1	Rensselaer Polytechnic Inst. Department of Mathematics ATTN: D. Drew Troy, NY 12181
1	Johns Hopkins University Applied Physics Laboratory Chemical Propulsion Information Agency ATTN: T. Christian Johns Hopkins Road Laurel, MD 20810	1	SRI International Propulsion Sciences Division ATTN: Tech Library 333 Ravenswood Avenue Menlo Park, CA 94024
1	Massachusetts Institute of Technology Dept. of Mechanical Engineering ATTN: T. Toong Cambridge, MA 02139	1	Stevens Institute of Technology Davidson Laboratory ATTN: R. McAlevy, III Hoboken, NJ 07030
1	Pennsylvania State University Applied Research Lab ATTN: G. Faeth P. O. Box 30 State College, PA 16801	1	University of California Los Alamos Scientific Lab ATTN: T3, D. Butler Los Alamos, NM 87554

DISTRIBUTION LIST

<u>No. of Copies</u>	<u>Organization</u>	<u>No. of Copies</u>	<u>Organization</u>
1	University of Southern California Mechanical Engineering Dept. ATTN: OHE200, M. Gerstein Los Angeles, CA 90007		Aberdeen Proving Ground Dir, USAMSAA ATTN: DRXSY-D DRXSY-MP, H. Cohen
1	University of California, San Diego AMES Department ATTN: F. Williams P. O. Box 109 La Jolla, CA 92037		Cdr, USATECOM ATTN: DRSTE-TO-F Dir, USACSL, Bldg. E3516, EA ATTN: DRDAR-CLB-PA
1	University of Illinois AAE Department ATTN: H. Krier Transportation Bldg. Rm 105 Urbana, IL 61801		
1	University of Massachusetts Dept. of Mechanical Engineering ATTN: K. Jakus Amherst, MA 01002		
1	University of Minnesota Dept. of Mechanical Engineering ATTN: E. Fletcher Minneapolis, MN 55455		
2	University of Utah Dept. of Chemical Engineering ATTN: A. Baer G. Flandro Salt Lake City, UT 84112		
1	Washington State University Dept. of Mechanical Engineering ATTN: C. Crowe Pullman, WA 99163		

USER EVALUATION OF REPORT

Please take a few minutes to answer the questions below; tear out this sheet, fold as indicated, staple or tape closed, and place in the mail. Your comments will provide us with information for improving future reports.

1. BRL Report Number _____

2. Does this report satisfy a need? (Comment on purpose, related project, or other area of interest for which report will be used.)

3. How, specifically, is the report being used? (Information source, design data or procedure, management procedure, source of ideas, etc.)

4. Has the information in this report led to any quantitative savings as far as man-hours/contract dollars saved, operating costs avoided, efficiencies achieved, etc.? If so, please elaborate.

5. General Comments (Indicate what you think should be changed to make this report and future reports of this type more responsive to your needs, more usable, improve readability, etc.)

6. If you would like to be contacted by the personnel who prepared this report to raise specific questions or discuss the topic, please fill in the following information.

Name: _____

Telephone Number: _____

Organization Address: _____

